

**PREFRONTAL-THALAMO-HIPPOCAMPAL CIRCUIT CONTRIBUTIONS
TO SPATIAL WORKING MEMORY**

by

Henry L. Hallock

A dissertation submitted to the Faculty of the University of Delaware in partial fulfillment of the requirements for the degree of Doctor of Philosophy in Psychology

Summer 2015

© 2015 Henry L. Hallock
All Rights Reserved

ProQuest Number: 3730246

All rights reserved

INFORMATION TO ALL USERS

The quality of this reproduction is dependent upon the quality of the copy submitted.

In the unlikely event that the author did not send a complete manuscript and there are missing pages, these will be noted. Also, if material had to be removed, a note will indicate the deletion.



ProQuest 3730246

Published by ProQuest LLC (2015). Copyright of the Dissertation is held by the Author.

All rights reserved.

This work is protected against unauthorized copying under Title 17, United States Code
Microform Edition © ProQuest LLC.

ProQuest LLC.
789 East Eisenhower Parkway
P.O. Box 1346
Ann Arbor, MI 48106 - 1346

**PREFRONTAL-THALAMO-HIPPOCAMPAL CIRCUIT CONTRIBUTIONS
TO SPATIAL WORKING MEMORY**

by

Henry L. Hallock

Approved: _____
Robert F. Simons, Ph.D.
Chair of the Department of Psychological and Brain Sciences

Approved: _____
George H. Watson, Ph.D.
Dean of the College of Arts and Sciences

Approved: _____
James G. Richards, Ph.D.
Vice Provost for Graduate and Professional Education

I certify that I have read this dissertation and that in my opinion it meets the academic and professional standard required by the University as a dissertation for the degree of Doctor of Philosophy.

Signed:

Amy L. Griffin, Ph.D.
Professor in charge of dissertation

I certify that I have read this dissertation and that in my opinion it meets the academic and professional standard required by the University as a dissertation for the degree of Doctor of Philosophy.

Signed:

Mark E. Stanton, Ph.D.
Member of dissertation committee

I certify that I have read this dissertation and that in my opinion it meets the academic and professional standard required by the University as a dissertation for the degree of Doctor of Philosophy.

Signed:

Dayan Knox, Ph.D.
Member of dissertation committee

I certify that I have read this dissertation and that in my opinion it meets the academic and professional standard required by the University as a dissertation for the degree of Doctor of Philosophy.

Signed:

Chad E. Forbes, Ph.D.
Member of dissertation committee

I certify that I have read this dissertation and that in my opinion it meets the academic and professional standard required by the University as a dissertation for the degree of Doctor of Philosophy.

Signed:

David M. Smith, Ph.D.
Member of dissertation committee

ACKNOWLEDGMENTS

To my mentor, Amy, for helping me grow as a scientist – I will always be grateful that she chose me to go on this journey with her.

To my wife, Abbey, and son, Oscar, for helping me grow as a husband and father in the face of my relationship with science – I will always be grateful that they chose me as their partner in life.

This dissertation is a testament to the countless hours put in by other members of the Griffin lab, my dissertation committee and other members of the University of Delaware department of Psychological and Brain Sciences, my fellow graduate students, my mother and father, and others whom I have surely forgotten to mention. None of this could have been possible without the selfless help, lab related or otherwise, of these people. I am grateful to them all.

TABLE OF CONTENTS

LIST OF TABLES	x
LIST OF FIGURES	xi
ABSTRACT	xix

Chapter

1	SPATIAL WORKING MEMORY ACROSS SPECIES	1
1.1	Introduction	1
1.2	Non-Human Primates	5
1.2.1:	Electrophysiology and Behavior	5
1.2.2:	Role of Dopamine in Working Memory	11
1.2.3:	Conclusion.....	13
1.3	Humans.....	13
1.4	Rodents.....	20
2	ANATOMY AND PHYSIOLOGY OF THE RODENT HIPPOCAMPUS AND THE HIPPOCAMPAL-MEDIAL PREFRONTAL CIRCUIT	27
2.1	Hippocampal Anatomy.....	27
2.2	Hippocampal Physiology: Relationship to Behavior	31
2.3	Anatomy of the Hippocampal-Medial Prefrontal Circuit.....	37
2.4	Summary.....	42
3	SPECIFIC AIMS OF THE DISSERTATION	44
3.1	Introduction	44
3.2	Aim 1	45
3.3	Aim 2	48
3.4	Aim 3	52
4	DETAILED METHODS	54
4.1	Subjects.....	54

4.2	Handling	54
4.3	Behavioral Apparatus and Testing Room.....	55
4.4	Pre-Training.....	56
	4.4.1 Goal Box Training.....	56
	4.4.2 Forced Run Training.....	58
4.5	Behavioral Training.....	58
	4.5.1 Experiments 1 & 3.....	58
	4.5.2 Experiment 2	59
4.6	Surgical Procedures	60
4.7	Microdrive Arrays and Recording System.....	62
4.8	Infusion Protocol	64
4.9	Perfusion and Histology	66
4.10	Analysis of Electrophysiological Data	67
	4.10.1 Identification of Single Units in mPFC	67
	4.10.2 Analysis of Position Data	68
	4.10.3 Quality Control of Continuously Sampled Data	68
	4.10.4 Firing Rate Analyses	70
	4.10.5 Entrainment of mPFC Single Units to the Hippocampal Theta Oscillation	71
	4.10.6 Power Spectral Density	75
	4.10.7 Phase Coherence.....	78
	4.10.8 Phase-Amplitude Coupling	80
	4.10.9 Analysis of Dependent Variables at Different Points Along the Maze Stem	82
4.11	Summary Analysis of Data.....	83
5	EXPERIMENT 1: EFFECTS OF RE/RH INACTIVATION ON DELAYED SPATIAL ALTERNATION PERFORMANCE	84
	5.1 Introduction	84
	5.2 Materials and Methods	84

5.2.1	Experimental Design	85
5.2.2	Data Analysis.....	85
5.3	Results	86
5.3.1	Behavior	86
5.3.2	Histology	86
5.4	Discussion.....	89
6	EXPERIMENT 2: HIPPOCAMPAL-PREFRONTAL SYNCHRONY AND SPATIAL WORKING MEMORY	91
6.1	Introduction	91
6.2	Materials and Methods	94
6.2.1	Subjects.....	94
6.2.2	Pre-Training and Behavioral Training.....	95
6.2.3	Experimental Design	95
6.2.4	Data Analysis.....	96
6.3	Results	98
6.3.1	Behavior	98
6.3.2	Firing Rate.....	101
6.3.3	Entrainment	104
6.3.4	Coherence	104
6.3.5	Phase-Amplitude Coupling	108
6.4	Discussion.....	108
7	EXPERIMENT 3: ROLE OF RE/RH IN HIPPOCAMPAL-PREFRONTAL SYNCHRONY AND SPATIAL WORKING MEMORY	116
7.1	Introduction	116
7.2	Materials and Methods	119
7.2.1	Experimental Design	119

7.2.2	Data Analysis.....	121
7.3	Results	128
7.3.1	Behavior	128
7.3.2	Prefrontal Firing Rates	129
7.3.3	Single Unit Entrainment	137
7.3.4	Phase Coherence.....	140
7.3.5	Phase-Amplitude Coupling	146
7.3.6	Power, Coherence, and Phase-Amplitude Coupling as a Function of Stem Position	153
7.4	Discussion.....	155
8	CONCLUSIONS	161
	REFERENCES	171
Appendix		
A	LIST OF CODE.....	197
B	INSTITUTIONAL ANIMAL CARE AND USE COMMITTEE APPROVAL FORM.....	233

LIST OF TABLES

Table 6.1	Distribution of Pyramidal Neurons Across Rats and Session Types.....	115
Table 7.1	Distribution of mPFC Pyramidal Neurons Across Rats.....	160
Table 7.2	Number of mPFC Pyramidal Neurons Included in Entrainment Analyses Across Rats.....	160

LIST OF FIGURES

- Figure 4.1 Schematic of the DA and CD T-Maze Tasks. The non-working memory-dependent CD task (top), and the working memory-dependent DA task (bottom). During the CD task, the texture of the wood insert cue is pseudorandomly presented from trial to trial – the location of the food reward is based on the texture of the cue. During the DA task, the rat must alternate between the left and right goal arms on successive trials. Both tasks feature a 30-second inter-trial period, during which the rat waits on the “start box” which is occluded from the maze with a large wooden blocker. During both tasks, the rat runs up the central stem, chooses a goal arm, and returns to the start box via the modified return arms.....57
- Figure 4.2 Bundle Configuration and Cluster Cutting Schematic. (A) Picture of the two bundles that house tetrodes which target the mPFC and hippocampus simultaneously. (B) Depiction of the “cluster-cutting” software that is used for isolating individual units (putative neurons) from activity recorded from a single tetrode. Each color represents an individual unit (signal) that has been separated from other activity (noise) picked up by the tetrode. Each colored dot represents a spike (action potential) emitted by that particular neuron. Individual units are identified based on differences in waveform peak, valley, and energy between all four channels on the tetrode, and included for analysis based on published mathematical criteria (i.e., isolation distance and L-ratio) (Schmitzer-Torbert et al., 2005).....65
- Figure 4.3 Quantification of Cluster Stability. Identification of cluster stability between task epochs from an example single unit in the mPFC from Experiment 2. Peak wavelength is plotted across time, and each color represents a separate task epoch (red = DA, blue = CD, and green = second DA). Peak wavelength did not change during the recording session, indicating that the single unit remained stable across the recording session.....69
- Figure 4.4. Representations of Entrainment, Coherence, and Phase-Amplitude Coupling (A) Representative schematic of single unit entrainment to the hippocampal theta oscillation. Individual spikes from one neuron are represented as red tick marks on the bottom, and theta (red) is superimposed over the raw LFP from the hippocampus. (B) Schematic of phase coherence between simultaneously recorded theta oscillations (red traces) recorded

	from the hippocampus (top) and mPFC (bottom). Notice that lines drawn between peaks are roughly parallel across cycles. (C) Schematic of phase-amplitude coupling between hippocampal theta (top-most red trace) and mPFC slow gamma (bottom-most red trace).....72
Figure 5.1	RE/Rh Inactivation Disrupts DA Task Performance. Muscimol infusions into RE/Rh significantly impaired DA task performance at all three doses as compared to saline infusion sessions. ** $p < .01$. Error bars = SEM.....87
Figure 5.2	Placement of Internal Cannulas in RE/Rh. Compiled histology showing placements of internal cannula tips in the ventral midline thalamus for all rats included in the experiment.....88
Figure 6.1	Maze Behavior Across Task Epochs. Top: Time spent at the choice point is not significantly different between good performance (> 75% correct choices) or bad performance (< 75% correct choices) epochs. Bottom: Stem velocity is not significantly different between task epochs.....99
Figure 6.2	Tetrode Placements in mPFC and Hippocampus. (A) Representative nissl-stained coronal sections from one rat showing placement of tetrode tips in the mPFC (top) and dorsal hippocampus (bottom). (B) Coronal sections showing placement of tetrode tips in mPFC (left panel; different colors are equal to individual rats), and dorsal hippocampus (right panel) for all animals.....100
Figure 6.3	Delay Period Firing Rates of mPFC Neurons are Task-Sensitive. Representative example of an mPFC single unit that is sensitive to task. Raster plots represent individual spikes emitted over time during start box occupancy for a DA epoch (top panel), a CD epoch (middle panel), and a second DA epoch (bottom panel) within a single recording session. The bottom firing rate plot shows trial-averaged firing rate as a function of time for DA epochs (blue) and the CD epoch (red). This single unit dramatically decreased its firing rate during the CD epoch. The 0 on the far right of the x-axis represents termination of the delay period.....102
Figure 6.4	Single Unit Entrainment and Firing Rate Across Epochs. (A) Rayleigh's z-statistic was normalized within neurons and compared across sessions in which the rat performed poorly and sessions in which the rat performed

well. Rayleigh's z-statistic dropped significantly from DA to CD epochs in which the rat performed well, but not epochs in which the rat performed poorly. $** p < .01$. Error bars = 95% confidence intervals. (B) Mean resultant vector length (MRL) dropped significantly from good DA epochs to good CD epochs. MRL also increased significantly from good DA epochs to bad CD epochs. $** p < .01$. Error bars = 95% confidence intervals. (C) Firing rate on the start box dropped significantly from good DA epochs to good CD epochs. $** p < .01$. Error bars = 95% confidence intervals.....103

Figure 6.5 Theta Coherence During Choice Point Traversals. Theta coherence as the rat moves through the choice point is higher during good DA epochs (black line), as compared to good CD epochs (blue-grey), bad DA epochs (orange), and bad CD epochs (purple). Dashed line indicates choice point entry (time 0).....106

Figure 6.6 Choice Point Coherence Across Frequency Bands. Theta coherence at the maze choice point is significantly higher during good DA epochs than during good CD epochs. Coherence differences between epochs are specific to the theta frequency band. $** p < .01$. Error bars = SEM..... 107

Figure 6.7 Theta Coherence Across Maze Locations. Theta coherence differences are not seen on the maze stem (top) or start box (bottom).....109

Figure 6.8 Phase-Amplitude Coupling at the Choice Point. Theta-gamma coupling at the choice point within the mPFC (middle panel) and between the hippocampus and mPFC (bottom panel) is significantly higher during good DA epochs as compared to good CD epochs. Theta-gamma coupling within the hippocampus (top panel) does not significantly differ between epochs. $** p < .01$. Error bars = SEM.....111

Figure 7.1 Histology. (A) Example histology from one rat. Coronal sections stained with cresyl-violet show the locations of tetrode tips in the mPFC (middle) and dorsal hippocampal fissure (left; black arrows). A coronal section that was counter-stained with DAPI shows the spread of fluorescent muscimol from the tip of the internal cannula in the ventral midline thalamus (right). (B) Coronal sections showing placements of tetrode tips in the mPFC (left panel; each color represents an individual rat), placements of internal

	cannula tips in the ventral midline thalamus (middle panel), and placements of tetrode tips in the dorsal hippocampus (right panel) for all rats.....	120
Figure 7.2	Choice Accuracy During the DA Task. Muscimol infusions into RE/Rh significantly impaired choice accuracy on the DA task, as compared to no infusion and saline sessions (individual dots are equal to individual rats).....	123
Figure 7.3	Behavior Across Sessions. (A) Normalized choice accuracy (testing epoch score – baseline epoch score) was significantly lower than zero for muscimol sessions only (** $p < .01$). (B) Normalized time spent in choice point (seconds) was not significantly different from zero for any of the three sessions. (C) Normalized stem velocity (cm/sec) was not significantly different from zero for any of the three sessions.....	126
Figure 7.4	Delay Period Firing Rates Across Sessions. RE/Rh inactivation significantly decreased the firing rates of putative pyramidal neurons in the mPFC during the delay period. Each dot represents an individual pyramidal neuron. Black bars represent median firing rate (Hz). Grey dots represent baseline epochs, colored dots (green, blue, and red) represent testing epochs for the three sessions. ** $p < .01$, Wilcoxon’s rank-sum test.....	127
Figure 7.5	mPFC Firing Rates Across Maze Locations. Mean firing rates of mPFC pyramidal neurons as a function of epoch and maze location. Muscimol infusions significantly reduced mean firing rate across all maze locations. Grey lines represent baseline epochs, colored lines represent testing epochs. Errors bars = SEM.....	130
Figure 7.6	Firing Rate Over Time During the Delay Period. Example raster and trial-averaged firing rate plots for three pyramidal neurons during the delay period. For all three plots, time 0 at the far right of the x-axis represents start box exit. The top-most panel shows a representative neuron that did not display “ramping” or “decay” activity during the delay period, but rather showed a sustained firing rate throughout the duration of the delay. The majority of pyramidal neurons exhibited this type of delay period activity. The middle panel shows an example of a “ramping” neuron that significantly increased its firing rate as a function of time throughout the delay. The bottom-most panel shows a “decay” neuron that significantly	

	decreased its firing rate as a function of time. “Ramping” and “decay” neurons were relatively rare in the recorded population of mPFC pyramidal neurons. Individual squares on raster plots are equal to individual spikes, shaded lines in rate plots equal SEM.....	132
Figure 7.7	Entrainment of mPFC Single Units to Hippocampal Theta. (A) Rose plot from a representative pyramidal neuron recorded during a muscimol baseline epoch in mPFC showing significant entrainment to the hippocampal theta oscillation. Numbers on circumference are equal to theta phase (degrees), and bin height (blue bars) is equal to proportion of total spikes emitted by that neuron. The red line extending from the center of the plot is the mean resultant vector. Its direction indicates the neuron’s preferred spiking phase (~205 degrees), and its length indicates magnitude of entrainment. (B) Linearized distribution of preferred spiking phases for all mPFC pyramidal neurons recorded during muscimol baseline (grey bars) and testing (red bars) epochs. Two theta cycles are included in black for reference. Y-axis represents the number of pyramidal neurons that showed a preference for each theta phase bin (x-axis). Darker colors equal significantly entrained neurons, lighter colors equal neurons that were not significantly entrained. mPFC neurons showed phase-locking that was modulated by theta peaks during baseline epochs. This phase-locking relationship was diminished following RE/Rh inactivation.....	135
Figure 7.8	Rayleigh’s Z-Statistic Distributions Across Sessions. Cumulative density plots of Rayleigh’s z-statistic values (the higher the z-statistic, the higher the entrainment) for all three sessions. Distributions between baseline and testing epochs did not significantly differ for no infusion and saline sessions, but did significantly differ for muscimol session.....	138
Figure 7.9	Mean-Resultant Vector Lengths Across Sessions. Subsampled mean resultant vector length (MRL) values for all sessions. RE/Rh inactivation significantly decreased MRL scores as compared to the pre-muscimol baseline epoch. ** $p < .01$, error bars = SEM.....	139
Figure 7.10	Phase Coherence at the Maze Choice Point. Phase coherence between the hippocampus and mPFC in the theta frequency band is lowered at the maze choice point following RE/Rh inactivation. Grey lines are equal to baseline epochs, colored lines are equal to testing epochs (top panel = no infusion	

	session, middle panel = saline session, bottom panel = muscimol session). Shaded lines = SEM.....	141
Figure 7.11	Coherence Across Time During Choice Point Traversals. Averaged coherograms show coherence across frequency bands as a function of time as rats move through the choice point. Top coherogram = muscimol baseline epochs, bottom coherogram = muscimol testing epochs. Dashed line indicates choice point entry. Note the prominent band of high coherence in the theta frequency range that appears directly following choice point entry during baseline epochs. This band of coherence is not present during muscimol testing epochs. (Bottom panel) Theta coherence across time during choice point entry for muscimol sessions. Grey equals baseline epoch, red equals testing epoch. Shaded lines = SEM.....	142
Figure 7.12	Theta Coherence Across Maze Locations and Sessions. (A) Normalized coherence (testing – baseline) across frequency bands for muscimol sessions during choice point occupancy. Normalized theta coherence is significantly different from zero. $** p < .01$. Error bars equal 95% confidence intervals. (B) Decrease in theta coherence following RE/Rh inactivation is specific to the maze choice point. Normalized theta coherence is significantly lower than zero only for choice point occupancy during muscimol sessions. $** p < .01$. Error bars equal 95% confidence intervals. (C) Normalized theta coherence at the maze choice point is significantly lower than zero only during muscimol sessions. $** p < .01$. Error bars equal 95% confidence intervals.....	145
Figure 7.13	Single-Trial Schematic of Phase-Amplitude Coupling. Example of phase-amplitude coupling from one trial during choice point entry from a muscimol baseline epoch. Periods of high amplitude gamma (bottom blue trace) tend to coincide with the ascending phase of hippocampal theta peaks (middle grey and red traces). Slow mPFC gamma power is represented as heat in the top spectrogram.....	147
Figure 7.14	Theta-Gamma Coupling Across Phases and Frequencies. (A) Co-modulograms showing preferred phase-amplitude pairs between hippocampal theta and mPFC gamma during muscimol baseline (left panel) and muscimol testing (right panel) sessions while the rat occupies the maze choice point. During baseline sessions, mPFC slow gamma (~60 – 80 Hz) is	

	modulated by the ascending phase of hippocampal theta peaks (~120 degrees). Phase-amplitude coupling between hippocampal theta and mPFC slow gamma is diminished during testing sessions. (B) Normalized modulation index (MI) scores for hippocampal-prefrontal theta-gamma coupling at the maze choice point across a range of gamma frequencies. Green = no infusion, blue = saline, and red = muscimol sessions. Note the drop in theta-gamma coupling for slow gamma (~40 – 80 Hz) frequencies during muscimol sessions.....	148
Figure 7.15	Theta-Gamma Coupling at the Maze Choice Point. Normalized MI scores across sessions for hippocampal-prefrontal theta-gamma coupling (top panel), mPFC theta-gamma coupling (middle panel), and hippocampal theta-gamma coupling (bottom panel) during choice point occupancy. Choice point theta-gamma coupling was severely decreased between the hippocampus and mPFC, and within the mPFC, following RE/Rh inactivation. ** $p < .01$. Error bars equal 95% confidence intervals.....	151
Figure 7.16	Coherence and Theta-Gamma Coupling Along the Maze. (A) Theta coherence as a function of maze location during muscimol sessions. Theta coherence is selectively disrupted at the maze choice point following RE/Rh inactivation. (B) Hippocampal-prefrontal theta-gamma coupling as a function of maze location during muscimol sessions. Theta-gamma coupling is disrupted as the rat moves closer to the choice point following RE/Rh inactivation. Note the timeline of theta-gamma coupling deficits as compared to the timeline of coherence deficits. Grey = baseline, red = testing.....	154
Figure 7.17	Theta Power Along the Maze. Theta power in the hippocampus (top panel) and mPFC (bottom panel) as a function of maze location. RE/Rh inactivation does not cause a significant decrease in theta power in either brain region at any section of the maze.....	160

ABSTRACT

A growing body of evidence suggests that different types of learning and memory processes are distributed across specialized neural circuits consisting of two or more anatomically- and functionally-connected brain areas. One such neural circuit consists of the dorsal hippocampus (dHC) and the medial prefrontal cortex (mPFC). This circuit is thought to be critically important for spatial working memory (the ability to flexibly maintain and use trial-specific spatial information within a testing session). dHC-mPFC interactions have been shown to correlate with spatial working memory-guided task performance in rodents; however, there are no direct anatomical connections between the dHC and mPFC. The reuniens and rhomboid (RE/Rh) nuclei of the ventral midline thalamus are bi-directionally connected with the infralimbic, prelimbic, and anterior cingulate sub-regions of the mPFC, as well as the CA1 subfield of dHC. The efferent and afferent connections of the RE/Rh suggest that these thalamic nuclei may support working memory by modulating interactions between the dHC and mPFC. This prediction was directly tested by simultaneously recording single units and local field potentials (LFPs) from CA1 of the dHC and the mPFC while rats performed a working memory-dependent delayed spatial alternation (DA) task in a T-maze. The DA task is dependent on the functional integrity of RE/Rh (Experiment 1), and increased hippocampal-prefrontal synchrony is seen during good performance of the DA task, as compared to a control task (CD; Experiment 2). Prior to the recording session, RE/Rh were functionally inactivated by an intracranial infusion of the GABA_A receptor agonist muscimol. Our results show that RE/Rh inactivation caused severe performance impairments that were accompanied by

decreases in hippocampal-prefrontal synchrony on the maze (Experiment 3). These results provide a novel characterization of the mechanisms underlying memory-guided decision making by directly examining the relationship between thalamic gating of cortico-limbic interactions and spatial working memory performance.

Chapter 1

SPATIAL WORKING MEMORY ACROSS SPECIES

1.1 Introduction

One of the many contributions of Donald Olding Hebb to theories on the neurobiological bases of learning and memory was his recognition that short-term memory and long-term memory are separate processes that are likely mediated by distinct neural mechanisms. Hebb proposed that long-term memory (the long-term storage of information) is supported by neuronal growth, whereas short-term memory (the short-term maintenance of information, on the order of tens of seconds) is facilitated by temporary electrical activation (Hebb, 1949). This proposal, along with his famous postulate that the temporally-proximate activation of neuronal networks strengthens the connections within those networks, serves to illustrate his incredible prescience in the absence of any substantial empirical support. Hebb's theoretical contributions to the field of learning and memory have produced multiple experiments and theories that have refined his original hypothesis that short-term memory and long-term memory have distinct neural underpinnings, but the basic idea remains the same. We now know that memory, far from enjoying a unitary representation in the brain, can be divided into a number of different sub-categories, each of which is sub-served by distinct neuroanatomical loci (Sherry and Schacter, 1987; Squire, 1992; Squire, 2004).

Since Hebb's theories were put forth, our understanding of short-term memory has increased considerably. A unitary storage site in the brain for short-term memory was proposed in the 1960's (Atkinson & Shiffrin, 1968), but considerable evidence since then has supported the theory that short-term memory is further segregated into different sub-components that are characterized by the nature of each respective component's preferred memorandum. The term "working memory" was also coined to reflect the transient nature of the short-term information maintenance process (Miller et al., 1960). The definition of "working memory" has since been expanded to describe a process whereby a limited amount of information is held "online" for a limited amount of time, during which the information in question is available for manipulation (Baddeley, 1992).

The most famous model of working memory has been the three-component model (later amended to include a fourth component (Baddeley, 2000)) put forth by Baddeley and Hitch (1974), which challenged the assertion that a unitary storage system in the brain was responsible for all of short-term memory. Evidence for a multi-component model of working memory came largely from neuropsychological studies in which patients with damage to specific areas of the brain showed impaired short-term memory for verbal information, but were able to retrieve the same verbal information from long-term memory some time later. These findings contradicted the hypothesis that a single brain area supported the transfer of information from short-term memory to long-term memory (Shallice & Warrington, 1970; Vallar & Papagno, 2002). Baddeley and Hitch proposed that

working memory is mediated by three distinct systems. The first system, dubbed the phonological loop, was proposed to support working memory for phonemes by allowing articulatory rehearsal for remembered items to take place (the mental repetition of to-be-remembered sounds) (Baddeley, 1998). The code for the phonological loop is acoustic, as evidenced by the fact that lists of similar-sounding letters are more easily remembered than lists of letters that sound dissimilar (Conrad, 1964; Conrad & Hull, 1964). The second system, the visuospatial sketch pad, supports working memory for visual features of objects, such as color, shape, and location (Baddeley, 2003). The third system, known as the central executive, exerts attentional control over the other two “slave” systems, flexibly routing sensory information to one or the other (Baddeley, 1986). The fourth component, known as the “episodic buffer”, interfaces with long-term memory stores to bind information from long-term memory and the two slave systems in working memory (Baddeley, 2000). The multi-component model of working memory continues to be an influential theory of how humans compartmentalize and temporarily store sensory information after the presentation of a sensory stimulus has been terminated.

Since the proposal of the multi-component model, the next logical step has been to conduct experiments with the aim of uncovering “how” (or “if”) the theoretical components of the model map onto what we have since discovered about the relationship between brain function and working memory (the issue that lies at the heart of this thesis). One further fractionation of visual working memory

that has gained acceptance, largely through single-unit recording studies in non-human primates, is that between “spatial working memory” (memory for the spatial location of an object), and “non-spatial working memory” (memory for other non-spatial features of an object (i.e., color, shape, etc.)) (Wilson et al., 1993; Della Sala et al., 1999). A large body of literature has now been amassed that addresses the brain-working memory relationship, with experiments having been conducted in a range of species, including humans, non-human primates, rats, and mice.

Data from the molecular level of analysis to the systems level of analysis have been collected that implicate different brain regions and neurobiological processes within those brain regions in different types of working memory (auditory/verbal, object, spatial, etc.). While not intended to be a comprehensive review of every study related to the neural correlates of working memory, the aim of this chapter is to provide a summary of some of the more influential studies that are germane to the topic at hand. As such, this chapter will focus on what we know about the relationship between the nervous system and working memory in (1.2) non-human primates, (1.3) humans, and (1.4) rodents, with an emphasis on spatial working memory.

1.2 Non-Human Primates

1.2.1 Electrophysiology and Behavior

Seminal *in vivo* recording studies in non-human primates paved the way for an understanding of the relationships between working memory and neural activity at the cellular level. Working memory in these studies was probed with delayed-match to sample (DMS) or delayed-match to position (DMP) tasks that required the animal to attend to a presented stimulus, and then recall either certain features of the stimulus or the location of the stimulus following a brief delay in which the stimulus was not present. Reminiscent of Hebb's earlier theory that short-term memory was supported by "sustained bouts of electrical activity", these studies found that certain neurons throughout the primate brain in several disparate regions increased and sustained their firing rates during the brief delay period between termination of the stimulus and the recall period; these cells were termed "delay cells", and were thought to be the neural correlate of information maintenance in working memory (Fuster & Alexander, 1971; Goldman-Rakic, 1995).

One prediction of multi-component models of working memory is that patterns of neural activation should be dependent on the attributes of the stimulus that is being held in mind. In support of this prediction, areas within visual processing pathways of the primate brain exhibit neural activity that is linked to working memory for visual stimuli. Specifically, single units (putative individual

neurons) in the primate inferotemporal cortex (IT) (a brain area in the ventral visual stream that is important for processing complex shapes), as well as single units in area V4, show elevations in firing rate when monkeys are trained to remember information about the color or shape of an object (Miyashita & Chang, 1988; Fuster, 1990; Miller et al., 1993; Motter, 1994). Neurons in area MT, an area of the brain in the dorsal visual stream that is responsible for processing motion, also display elevated firing rates during the delay period of working memory tasks in which the stimulus moves in a specific direction (Bisley et al., 2004). Lesions of IT also produce performance impairments in delayed non-match to sample (DNMS) tasks that require the animal to maintain information about the visual features of an object over a delay (Fuster et al., 1981; Fuster et al., 1985). These data support the conclusion that visual working memory for an object's location is correlated with activity in the dorsal visual stream (area MT, posterior parietal cortex), and visual working memory for other features of an object (i.e., color, shape) is correlated with activity in the ventral visual stream (area IT and V4), indicating that spatial working memory and object working memory are dissociable processes in both the psychological and neurobiological domains.

Working memory for other sensory modalities is also linked with activity in each modality's representative neuroanatomical association region. Firing rates of individual neurons in the somatosensory association cortex (SII) are elevated during the delay period of a task in which a monkey is trained to discriminate

between different frequencies of mechanical flutter applied to the monkey's fingertips (Hernandez et al., 2000; Romo & Salinas, 2001; Romo et al., 2002). Neurons in the auditory cortex increase their firing rate when two tones, separated by a delay, match each other in frequency (Gottlieb et al., 1989). Finally, single units in the parietal cortex (area 7a and the lateral intraparietal cortex) exhibit sustained elevations in firing rate during the delay period of working memory tasks in which monkeys are trained to remember the spatial locations of objects (Ferrera et al., 1994; Constantinidis & Steinmetz, 1996). These data support the conclusion that the original distinctions between auditory working memory and visual working memory by Baddeley and Hitch are further supported by non-human primate recording studies demonstrating that auditory and visual working memory differentially engage areas of the brain broadly responsible for auditory and visual processing, respectively.

Although the brain has the ability to process different sensory features of a stimulus separately, it also has the ability to combine those features and process them in parallel, as evidenced by our ability to form integrated mental representations of objects and experiences. Experimental attempts to define the neuroanatomical locations responsible for the maintenance of integrated information in working memory have largely converged on one key area: The prefrontal cortex (PFC). Fuster et al. (1982) trained monkeys on two tasks. The first task was a delayed match-to-sample task which required the animal to attend to the color of a light (either red or green), which was extinguished after the

monkey touched it. Following a 20-second delay, both red and green lights were presented, and the monkey was required to touch the previously-presented light. This task required visual working memory for color. The monkeys were trained on another task in which a light cue was presented in a specific location (left or right). Following a 20-second delay, lights were presented in both positions and the animal had to touch the light that was in the position previously occupied by the cue. This delayed match-to-position task required visual working memory for spatial location. Recordings from the lateral PFC revealed a population of cells that responded to the delay period of the object working memory task. These cells were largely localized to the inferior convexity, an area of the lateral PFC that receives major input from brain areas in the ventral visual pathway (Ungerleider & Mishkin, 1982). Other recorded cells responded preferentially to the delay period of the spatial working memory task, and these cells were spread throughout the extent of the recorded area in the lateral PFC, including some cells that were located in the inferior convexity. This study provided support for the hypothesis that the lateral PFC integrates information about object features and spatial location in working memory.

Subsequent studies have demonstrated that individual neurons in the lateral PFC can dynamically represent different types of information in tasks that tax working memory for multiple features. In a task in which monkeys must make a saccade to a previously presented *object* following a delay (object delay), and then make another saccade to the *location* of the previously identified object following

another delay (spatial delay), the majority of recorded neurons in the lateral PFC showed object delay-specificity (increasing their firing rates during the delay period following presentation of a specific object), as well as spatial delay-specificity (responding during the delay period following the presentation of an object in a specific spatial location) (Rao et al., 1997). In another study, monkeys were trained to attend to a “target” object (a visual cue), then shown an array of three objects which contained the target object, and then had to press a button if another array of three objects presented following a delay also contained the target object (Rainer et al., 1998). Neurons in the lateral PFC responded both to the identity of the target object (firing during the presentation of a specific visual cue), and to the spatial location of the target object (firing during the delay period if the target object was in a specific spatial location within the array). The major finding from these studies was that neurons in the prefrontal cortex are capable of modulating their firing rates to represent both object identity and object location in working memory.

The studies outlined above used recordings from a range of areas within the lateral PFC. One question in the field that is currently debated is whether a functional segregation exists between sub-regions that are mainly important for visual working memory for object location and sub-regions that are mainly important for visual working memory for object features within the lateral PFC. Neuroanatomical studies have revealed dense inter-connectivity between the dorsolateral PFC and areas in the dorsal visual stream (Cavada & Goldman-Rakic,

1989), as well as connections between the ventrolateral PFC and areas in the ventral visual stream (Ungerleider & Mishkin, 1982). In support of the hypothesis that the dorsolateral PFC is part of a circuit that is critical for spatial working memory, simultaneously recorded posterior parietal and dorsolateral prefrontal neurons show strikingly similar patterns of activation during an oculomotor delayed-response task, in which a monkey is rewarded for making a saccade to an area of a screen that was previously occupied by an object following a delay period (Chafee & Goldman-Rakic, 1998). Funahashi et al. (1989) showed that neurons in the dorsolateral PFC elevated their firing rates only during the delay period of trials in which the cue was presented in a specific location. The delay-specific spatial tuning curves of these neurons were referred to as “memory fields”, and have been proposed to represent the neural substrate of spatial information maintenance in the dorsolateral PFC (Funahashi et al., 1990; Funahashi, et al. 1991; Goldman-Rakic, 1995). The hypothesis that the dorsolateral PFC is selectively important for spatial working memory, and the ventrolateral PFC is selectively important for object working memory, has been further supported by single unit recording studies that have demonstrated dissociable patterns of neural activity in dorsolateral PFC and more ventral portions of the lateral PFC during spatial and object working memory tasks, respectively (Wilson et al., 1993). Although the idea of a dorsal-ventral subdivision of spatial and non-spatial visual working memory within the lateral PFC has been debated (e.g., Fuster, 2001), the evidence suggests that neurons in

the lateral PFC can selectively code for an object's spatial location or the visual features of an object, functionally compartmentalizing spatial and non-spatial visual information when required by the behavioral context. Putatively identical neurons within the lateral PFC also appear able to integrate “what” and “where” information across delays, but studies that have demonstrated this have been less clear with regard to the precise neuroanatomical location of these neurons within the lateral PFC (Rao et al., 1997; Rainer et al., 1998). Even if a spatial/non-spatial distinction exists between the dorsal- and ventral-lateral PFC, it is likely that the dorsolateral and ventrolateral PFC exchange information via their direct anatomical connections with one another (Barbas & Pandya, 1989).

1.2.2 Role of Dopamine in Working Memory

At the molecular level, dopamine receptors in the lateral PFC are thought to play a key role in the modulation of prefrontal neuron firing rates during working memory tasks. The lateral PFC is the recipient of dopaminergic afferents that pass through the mesocortical pathway from the substantia nigra (Williams & Goldman-Rakic, 1993; Williams & Goldman-Rakic, 1998), and a dense concentration of D1 receptors exists mainly on the dendritic shafts and spines of both pyramidal neurons and interneurons (basket cells and chandelier cells) (Goldman-Rakic et al., 1989; Smiley & Goldman-Rakic, 1993). Down-regulation of D1 receptor mRNA and protein in the primate lateral PFC by chronic exposure to low doses of amphetamine impairs performance in working memory tasks

(Castner & Goldman-Rakic, 1999). Several studies have now shown that administration of a D1 receptor agonist produces an “inverted-U” dose-response effect on working memory performance (Arnsten & Goldman-Rakic, 1998; Cai & Arnsten, 1999), and a similar inverted-U dose-response curve exists for D1 receptor activation and the tuning specificity of prefrontal “memory fields” (Sawaguchi et al., 1990; Williams & Goldman-Rakic, 1995). The effects of excessive (non-optimal) D1 receptor activation on memory field suppression are mediated by cyclic-AMP (cAMP) (Vijayraghavan et al., 2007), which is a second messenger that is important for intracellular signal transduction. cAMP binds to and activates the hyper-polarization induced cyclic nucleotide-gated cation channel HCN1, leading to persistently elevated firing rates and increased neuronal excitability (Poolos et al., 2002; Day et al., 2005). Tonically-active interneurons that provide peri-somatic and peri-dendritic inhibition to pyramidal neurons (putative “delay cells”) could disrupt memory field-specificity by prohibiting the location-specific input from oculomotor regions that sculpts delay-specific tuning curves in the lateral PFC (Goldman-Rakic, 2000). Noradrenaline in the lateral PFC exerts similar influences on working memory and memory fields via α 2A-adrenoreceptors (Wang et al., 2007), and 5-HT receptor agonists also affect working memory and delay period activity in the lateral PFC, likely exerting their effects by increasing cortical dopamine levels (Williams et al., 1999). In sum, D1 receptors in the PFC appear to play a critical role in sculpting the delay-specific

firing rate profiles of prefrontal neurons, which are thought to represent the neural substrate of working memory in mammals.

1.2.3 Conclusion

In summary, the primate lateral prefrontal cortex is critically important for maintenance of visual information in working memory, likely integrating converging signals from upstream sensory association areas in the dorsal and ventral visual pathways. The presumed neural substrate of information maintenance in the lateral PFC is the delay cell, which has memory fields that are influenced by D1 receptor activation within the local architecture of the structure.

1.3 Humans

In agreement with studies in non-human primates, early studies in human patients with frontal lobe lesions revealed robust deficits in tasks designed to tax spatial working memory (Petrides & Milner, 1982; Owen et al., 1990). With the inventions of positron-emission tomography (PET) scanning and functional magnetic-resonance imaging (fMRI), and the application of these technologies to the scientific realm, a more precise understanding of the links between neural activity and cognition became possible. A logical first step was to uncover whether the brain areas thought to support working memory in non-human primates were also associated with working memory in humans. Several studies using PET scanning showed that regional cerebral blood flow (rCBF) near the posterior-inferior bank of the Sylvian fissure, directly adjacent to Wernicke's area, increased

during verbal working memory tasks (Paulesu et al., 1993; Paulesu et al., 1996; Salmon et al., 1996). These studies provided a possible neuroanatomical location for the phonological loop of the multi-component model, and further demonstrated that a region of the brain known to be critically involved in language comprehension seemed also to be important for maintaining that information in working memory. Participants that performed a visual working memory task for object location (spatial working memory) showed increased activity in the posterior parietal cortex (Jonides et al., 1993), which is in agreement with non-human primate studies of single units in this brain region. The posterior parietal cortex may therefore house the visuospatial sketch pad system of the multi-component model. These findings are generally in agreement with non-human primate studies (outlined in the previous section) that have repeatedly demonstrated that the cortical areas responsible for processing the specific sensory features of a stimulus are the same areas that are responsible for maintaining a mental representation of those features in working memory.

A number of imaging studies in the 1990's were undertaken with the goal of elucidating the role of the human lateral PFC in working memory. The first study to use PET scanning in an attempt to identify a spatial working memory network in the human brain found that activity in the right dorsolateral PFC increased during the delay period of a spatial working memory task. In this task, participants fixated on the center point of a screen while three dots briefly appeared in the periphery. Following a brief delay, a circle appeared on the screen,

and participants pressed one button if the circle was in the location of one of the previously presented dots, and another button if it was not. (Jonides et al., 1993). A subsequent study using fMRI showed that activation in the right middle-frontal gyrus, an area that includes the dorsolateral PFC, increased during a working memory task for item location, as compared to a working memory task for item color (McCarthy et al., 1994). A further demonstration of this dissociation occurred in a study where participants were shown three faces in a grid, and were asked to identify if a face subsequently presented after a delay was either identical to a face shown previously (non-spatial), or in the same location as a face shown previously (spatial) (Courtney et al., 1996). In addition, the length of the delay period was increased or decreased in order to parametrically manipulate the memory load of either version of the task. During the spatial working memory version of the task, increased blood flow was detected in the posterior parietal cortex and right superior frontal sulcus. In contrast, during the non-spatial working memory version of the task, increased blood flow was observed in the fusiform gyrus and inferior frontal lobe. These results support the hypothesis that spatial and non-spatial working memory are supported by distinct prefrontal sub-regions in humans.

Courtney et al. (1996) further found that the extrastriate regions associated with working memory were transiently activated during the beginning of the delay period, with blood flow increasing directly after the cued stimulus set disappeared,

and quickly decreasing as a function of time. This negative correlation between delay length and cerebral blood flow in extrastriate areas was not evident in the PFC, as blood flow in prefrontal areas increased directly after stimulus offset and remained elevated throughout the delay period, regardless of delay length. This result suggested that sensory association areas involved in working memory may be primarily involved in aspects of perceptual processing, while the PFC may be the primary site of information maintenance. Another study replicated these results, additionally demonstrating that increased activation in dorsolateral PFC was not due to task difficulty, as evidenced by the fact that increasing the difficulty of a non-working memory task (stimulus degradation) did not result in a corresponding increase in PFC activation by the same subjects that had performed the working memory task (Cohen et al., 1997). Additional work has revealed that a functional spectrum of feature-selectivity in working memory exists, and is governed by a neuroanatomical hierarchy, such that earlier structures in the visual processing streams are transiently activated by the presentation of visual stimuli, later structures in the visual processing streams show more persistent delay-period activity to preferred visual stimuli (i.e., the fusiform face gyrus in working memory tasks for faces), and prefrontal structures show persistent delay-period activity that is non-specific for stimulus features (i.e., ventrolateral PFC shows sustained activity for item color, shape, identity, etc.) (Courtney et al., 1997).

Other imaging studies have found that spatial and non-spatial working memory are functionally lateralized in the human brain. During the performance of

a spatial working memory task in which participants must match the location of a circle on a screen to the previous location of a dot following a delay, activation in the right lateral PFC and right superior parietal cortex is increased. In contrast, activation in Broca's area and the left inferior parietal cortex (adjacent to Wernicke's area) increases during the performance of a verbal working memory task in which participants must indicate whether a letter presented on the screen was previously shown in an array of four letters following a delay (Smith et al., 1996). Other studies have replicated this effect (D'Esposito et al., 1998; Wager & Smith, 2003), using this result to argue that a hemispheric lateralization of spatial and non-spatial working memory better accounts for the data than a dorsal-ventral sub-division.

The human dorsolateral PFC may be more involved in response selection than in information maintenance during working memory tasks. To separate these two processes, Rowe et al. (2000) asked participants to fixate on the center point of a screen while three dots briefly flashed in the periphery. After a brief delay (information maintenance), a line was drawn through the center of screen. This line intersected with the position of one of the three dots that was previously shown. After the line disappeared, participants had to move a dot with their finger to the location on the screen that was previously occupied by the dot that the line had transected (response selection). Activity in the dorsolateral PFC was higher during the response selection portion of the trial than during the information maintenance portion, indicating that one important role of the dorsolateral PFC

may be the selection of appropriate representations. In contrast, another distinct area of the PFC was activated during the information maintenance portion of the task. This region (Brodmann's area 8), located in the superior frontal sulcus, is directly anterior to the human frontal eye fields (FEF). In non-human primates, the dorsolateral PFC is also located directly anterior to the FEF, raising the possibility that the dorsolateral PFC in non-human primates may be more functionally homologous with the human superior frontal sulcus. If this is the case, the prediction would be that the human superior frontal sulcus would show delay-period activity that is specific to spatial working memory tasks. Courtney et al. (1998) directly tested this prediction by using fMRI to detect fluctuations in BOLD signaling while participants completed a working memory task for face identity, as well as a working memory task for face location. Their results confirmed this prediction, as increases in BOLD signaling in the superior frontal sulcus were strikingly selective for the delay period of the face location task, indicating that a dorsal-ventral fractionation of spatial and non-spatial working memory in human PFC may indeed exist, but that variations in cortical anatomy between humans and non-human primates must be taken into account when comparisons are made across species.

The human PFC appears to be a brain region that is critically involved in working memory, but the PFC does not work in isolation. Several studies in humans have investigated how communication between the PFC and other areas of the brain may contribute to working memory. In particular, several studies have

shown that interactions between the hippocampus and PFC are correlated with the performance of working memory tasks in humans. Experiments using scalp EEG recordings have demonstrated that phase synchronization (discussed in greater detail in chapter 4 of the thesis) in the theta frequency band is increased between the PFC and temporal lobe during the delay period of a working memory task (Sarnthein et al., 1998; Serrien et al., 2004). Scalp EEG studies have also shown that fronto-temporal theta phase synchronization increases when the memory load of a task is also increased by lengthening the delay period (Payne & Kounious, 2009). Levels of fronto-temporal theta phase synchronization also predict individual differences in working memory performance (Kopp et al., 2006). Taken together, these results suggest that interactions between the hippocampus and PFC play an important role in human spatial working memory.

In summary, the human data are largely in agreement with non-human primate data showing that specific cortical association areas are involved in the transient maintenance of preferred sensory information in working memory, and that areas of the lateral PFC are responsible for maintaining an integrated representation over a temporal gap when comparisons must be made between temporally non-contiguous stimulus presentations. Results from imaging studies also demonstrate that spatial and non-spatial working memory are differentially represented in the human brain, although whether spatial and non-spatial working memory are sub-divided between hemispheres or between dorsal and ventral portions of the lateral PFC is still a matter of debate. Further studies have shown

that the PFC may interact with the hippocampus during delayed non-match to sample tasks, forming a neural circuit that is important for working memory.

1.4 Rodents

While spatial working memory studies in humans and non-human primates have largely required subjects to focus visual attention on the spatial location of a stimulus, spatial working memory studies in rodents have required that subjects physically navigate to a location on a maze, and then use that information following a delay period to navigate to a previously non-visited maze location (delayed non-match to position; DNMP). One theoretical question that looms in the field is whether the type of memory being tested with DNMP tasks in rodents is the same type of memory that is being tested with delayed-response tasks in primates (Baddeley, 1998). Olton (1979) did not make a distinction between working memory and short-term memory in rodents, defining working memory as “useful for retaining information required for only a short period of time” (pg. 587). This operational definition has since been expanded by Dudchenko (2004) to describe “a type of short term memory for stimuli or spatial locations that is typically used within a testing session, but not between testing sessions” (pg. 708). Working memory in humans centers around the active maintenance of trial-related information, which presents a key problem with regard to generalizing this definition of working memory to non-human species because it is difficult, if not impossible, to know whether non-human mammals actively hold information in

mind from trial to trial, or consolidate trial-specific information and retrieve it directly before a behavioral choice is made.

The assertion that spatial working memory tasks in rodents and humans rely on different cognitive processes (Baddeley, 1998) is supported by the fact that DNMP tasks rely heavily on the function of the hippocampus (Olton, 1980; Aggleton et al., 1986; Dudchenko et al., 2000; Ainge et al., 2007; Czerniawski et al., 2009; Hallock et al., 2013a), a brain area not typically associated with spatial working memory in non-human primates. The hippocampus is also associated with the formation of internal representations of allocentric space (cognitive mapping; O'Keefe & Dostrovsky, 1971; O'Keefe & Nadel, 1978; Morris et al., 1982), raising the possibility that the hippocampus is critically involved in rodent DNMP tasks because these tasks require the animal to navigate around a maze by assessing distal cue configurations, as evidenced by the fact that task performance is disrupted when distal cue configurations are changed, or the maze is shifted relative to distal cues in the testing room (Olton & Collison, 1979; Walker & Olton, 1979; Dudchenko, 2001; Dudchenko & Davidson, 2002). However, lesions of the fimbria-fornix (a major output center of the hippocampus) disrupt performance on a DNMP task even when extra-maze cues are occluded and the topological relationship between intra-maze cues shifts from trial to trial, indicating that the hippocampus is important for working memory tasks that do not require an allothetic strategy (Olton, 1980). The hippocampus has therefore

become a brain area of interest with regard to the performance of spatial working memory tasks in rodents.

One example of a spatial working memory task is the win-shift task, in which animals are placed in the center of a radial arm maze with food rewards placed at the ends of goal arms that radiate outwards from the central platform. Optimal performance of this task requires that the animal visits each goal arm only once during a behavioral session, as repetitive visits to previously occupied goal arms will not result in a reward. This task requires that the animal remembers which goal arms were visited earlier in the session, and uses that information to guide ongoing behavioral choices. Performance of this task is reliably impaired by both lesions and pharmacological inactivation of the hippocampus (Becker et al., 1978; Olton et al., 1978; Churchwell et al., 2011). Another task commonly used to probe spatial working memory in rodents is spatial delayed alternation, which normally takes place in a T-maze. During spatial delayed alternation, the animal is rewarded for alternating between the left and right goal arms of the T-maze. In one variant of this task (discrete-trials delayed alternation, or forced-choice alternation), one trial consists of a forced run phase, during which the animal is “forced” (meaning one goal arm is physically blocked, making it inaccessible) to go down one goal arm of the maze, and a choice run phase, during which both goal arms are accessible, and the animal is rewarded for choosing the goal arm that was not visited during the forced run phase. The forced run and choice run phases of each trial are separated by a delay period. During this task, the animal must use

information about where it was during the forced run phase in order to make an appropriate behavioral choice during the choice run phase. Performance of this task is also disrupted by hippocampal lesions (Racine & Kimble, 1965). In another variant of this task, both goal arms are always accessible, and the animal is rewarded for continuously alternating between them from trial to trial.

Performance of this task becomes dependent on hippocampal function only after a delay (as brief as 2 seconds) is introduced between trials, requiring the animal to retain trial-specific information over a temporal gap (Ainge et al., 2007; Hallock et al., 2013a).

Although the hippocampus appears to be critically involved in the successful performance of DNMP tasks in rodents, it is not the only brain area that participates in rodent spatial working memory. The rodent medial prefrontal cortex (mPFC) has been proposed to be homologous to the primate dorsolateral PFC, based in part on its anatomical connections with limbic regions (Vertes, 2006). Lesions of the mPFC also produce profound performance deficits in spatial working memory tasks in rodents (Brito & Brito, 1990; Seamans et al., 1995; Delatour & Gisquet-Verrier, 1996; Dalley et al., 2004), which is in agreement with studies that have demonstrated spatial working memory deficits following lesions of the dorsolateral PFC in primates (Kolb, 1984; Goldman-Rakic, 1987). The rodent mPFC receives both direct and indirect projections from the hippocampus (direct via axo-dendritic synapses from pyramidal neurons in temporal CA1 (Swanson, 1981; Ferino et al., 1987); indirect via the subiculum

(Jay & Witter, 1991) and ventral midline thalamus (Herkenham, 1971; Vertes et al., 2007)). The anatomical connections between the hippocampus and prefrontal cortex, combined with lesion studies implicating both brain regions in the performance of DNMP tasks, suggests that communication between the two structures may be important for spatial working memory in rodents. In support of this idea, pharmacological disconnection studies in which the hippocampus and mPFC are rendered unable to communicate with one another have shown that hippocampal-prefrontal communication is necessary for spatial working memory tasks when memory load is increased (memory load was manipulated by increasing the length of the delay period between trials; Lee & Kesner, 2003; Churchwell et al., 2011).

In vivo recording studies in rodents have further implicated the hippocampal-prefrontal circuit in spatial working memory by showing that single units in each individual brain region, as well as physiological interactions between the two brain regions, are correlated with behavior during the performance of DNMP tasks. During the performance of a discrete-trials spatial delayed alternation task, populations of hippocampal neurons dynamically distinguish between the forced-run and choice-run phases of each trial by showing patterns of activation that are selective for one of the two trial phases while the rat runs up the center arm of the T-maze (Griffin et al., 2007). During the continuous version of the spatial delayed alternation task, single units show variations in firing rate that predict the future trajectory of the animal while the animal occupies the delay

pedestal in between trials (Ainge et al., 2007; Pastalkova et al., 2008; Hallock & Griffin, 2013). Recordings in the rat mPFC have also revealed that neuronal populations in this brain region represent the future choice of the animal during a spatial delayed alternation task, and that population-wide activity patterns better predict the future behavioral choice of the animal as a function of how well the animal performs the task (Baeg et al., 2003).

Simultaneous recordings from the rodent mPFC and hippocampus have revealed that the two brain regions functionally interact with one another, and that increased synchrony in the hippocampal-prefrontal circuit is correlated with performance in DNMP tasks (see chapter 4 for a detailed description of phase synchrony). Single units in the mPFC fire action potentials on the same phase of hippocampal theta oscillations over multiple cycles, becoming functionally “entrained” to hippocampal network activity (Siapas et al., 2005; Hyman et al., 2005). Single unit entrainment to hippocampal theta increases during the choice phase of a discrete-trials delayed alternation task in rats (Jones & Wilson, 2005; Hyman et al., 2010), and mice (Sigurdsson et al., 2010; O’Neill et al., 2013). Single-unit entrainment is also positively correlated with learning rate in mice that are trained on a discrete-trials delayed alternation task (Sigurdsson et al., 2010). These results provide further evidence for the theory that hippocampal-prefrontal communication in rodents is critical for spatial working memory. These results are also in agreement with human studies that have shown increased phase synchronization between the prefrontal cortex and medial temporal lobe during

working memory tasks (Sarnthein et al., 1998; Serrien et al., 2004; Kopp et al., 2006; Payne & Kounious, 2009), indicating that hippocampal-prefrontal synchrony is a property that underlies spatial working memory across mammalian species.

In summary, working memory in rodents may be a distinct process from working memory in non-human primates, as evidenced by the fact that the hippocampus is implicated in rodent working memory, but not primate working memory. However, the involvement of the dorsolateral PFC and its rodent homologue, the mPFC, in spatial working memory across mammalian species indicates that similarities in the brain-working memory relationship between rodents and primates do exist. Hippocampal-prefrontal interactions are correlated with working memory performance in rodents, non-human primates, and humans, suggesting that one key to understanding how the brain represents working memory across species is to understand how the hippocampus and prefrontal cortex communicate with one another. In any case, further research needs to be done in order to elucidate how results from rodent spatial working memory experiments can be compared to results from primate spatial working memory experiments, and vice versa.

Chapter 2

ANATOMY AND PHYSIOLOGY OF THE RODENT HIPPOCAMPUS AND THE HIPPOCAMPAL-MEDIAL PREFRONTAL CIRCUIT

2.1 Hippocampal Anatomy

The rodent hippocampus is a large subcortical structure that is composed of a “C”- shaped layer of cell bodies. The term “hippocampus” will be used throughout this chapter to describe the hippocampus proper, which comprises a portion of the hippocampal formation. The hippocampus can be sub-divided into three regions (subfields) based on unique efferent and afferent connections within each region. The ventral-most half of the most superficial cell layer (the CA3 subfield) contains pyramidal neurons that receive input from the dentate gyrus (DG) via the mossy fiber pathway, as well as collateral input from the axons of neighboring CA3 neurons. The dorsal-most half of the most superficial cell layer (the CA1 subfield) contains pyramidal neurons that receive input from the CA3 subfield via the Schaffer collateral pathway. The CA2 subfield, interposed between the CA3 and CA1 subfields, contains large pyramidal neurons that do not receive mossy fiber input (Lorente de No, 1934).

The hippocampal formation further consists of a second “C”-shaped layer of cell bodies (the CA4 subfield, more commonly referred to as the dentate gyrus),

which contains granule cells that receive input from the entorhinal cortex via the perforant pathway. The hippocampal formation also consists of several other structures that are directly connected with the hippocampus proper, namely the subiculum, presubiculum, parasubiculum, and entorhinal cortex. The entorhinal cortex provides the major neocortical interface with the hippocampus, and sends projections to CA3 and the dentate gyrus via axons originating from layer II, and projections to CA1 via axons originating from layer III. Projections within the hippocampus proper are unidirectional and output-specific, such that the mossy fiber pathway projects only to CA3, and the Schaffer collateral pathway projects only to CA1. Because of this anatomical layout, the hippocampus is often referred to as the tri-synaptic pathway, with the first synapse being perforant pathway input to the dentate gyrus. The hippocampus can be further subdivided into dorsal (septal) and ventral (temporal) regions, based on distinct patterns of efferent and afferent connections with other brain areas (Swanson & Cowan, 1977), as well as differences in each respective portion's functional relevance to behavior; for example, functional inactivation of the dorsal hippocampus impairs spatial working memory, while functional inactivation of the ventral hippocampus impairs trace-fear conditioning (Moser et al., 1995; Czerniawski et al., 2009; Fanselow and Dong, 2010; Moser et al., 2014). CA1 can be further subdivided along its transverse axis, as pyramidal neurons most proximal to CA3 receive major input from the medial entorhinal cortex, while pyramidal neurons most

distal to CA3 (toward the subiculum) receive major input from the lateral entorhinal cortex (Steward, 1976; Witter et al., 1989; Tamamaki & Nojyo, 1995).

The hippocampus has a laminar cytoarchitecture that can be further divided into different molecular layers. The principal layer of the hippocampus is the pyramidal cell layer (stratum pyramidale), which contains the somata of densely packed pyramidal neurons in CA1, CA2, and CA3. The layer directly lateral to stratum pyramidale is called stratum oriens, and contains the basal dendrites from pyramidal neurons in stratum pyramidale, as well as several classes of interneurons. Axons of inhibitory (GABA-synthesizing) basket cells in stratum oriens form synapses near pyramidal cell somata and proximal dendrites. In turn, axons arising from pyramidal neurons form both asymmetrical and symmetrical excitatory synapses on the spines of basket cells in stratum oriens. One special class of inhibitory basket cells, located in stratum oriens-lacunosum-moleculare (and hence called O-LM interneurons), provide input to the distal apical dendrites of pyramidal neurons (Lacaille et al., 1987). Distal dendrites in stratum lacunosum-moleculare also receive axons from glutamatergic principal cells in layer III of the entorhinal cortex, as well as inputs from putatively glutamatergic neurons in the ventral midline thalamus (Vertes et al., 2006; 2007). Stratum radiatum contains CA3-CA3 associational connections, as well as Schaffer collateral inputs, and stratum lucidum contains mossy fibers that arise from granule cells in the dentate gyrus.

The medial septum, specifically, the nucleus of the diagonal band of Broca, is a major source of input to the hippocampus, with GABAergic axons terminating mainly near interneurons in the portion of stratum oriens that is closest to CA3 (Kohler et al., 1984; Freund & Antal, 1988). Pyramidal neurons in CA3 send direct projections back to the lateral septum, and these projections are topographically organized, such that neurons in more dorsal portions of CA3 project to more dorsal portions of the lateral septum (Manseau et al., 2008). GABAergic and cholinergic efferents from the medial septum are thought to be a major pacemaker of the prominent hippocampal theta oscillation (Petsche et al., 1962; Stewart & Fox, 1990; Brandon et al., 2011). CA2 receives input from the supramammillary area and the tuberomammillary nucleus of the posterior hypothalamus, which terminates mainly in stratum pyramidale (Magloczky et al., 1994). Inputs from the ventral midline thalamus (reuniens and rhomboid nuclei) course through the cingulum bundle and terminate near dendritic shafts of pyramidal neurons in stratum lacunosum-moleculare (Herkenham, 1978; Dolleman-Van der Weel & Witter, 2000). The brain stem raphe nuclei send sparse serotonergic fibers that contact peri-dendritically targeting interneurons in CA3 stratum oriens, and noradrenergic inputs from the locus coeruleus form synapses near mossy fiber inputs to CA3 in stratum lucidum. The caudomedial portion of the parvocellular division of the basal nucleus of the amygdala projects to stratum oriens and stratum radiatum near both CA1 and CA3, as well as the subiculum (Pikkarainen et al., 1999; Pitkanen et al., 2000). The perirhinal cortex is reciprocally connected

to the distal portion of CA1, which overlaps with the projection arising from the lateral entorhinal cortex. The distal portion of CA1 in the ventral-most two-thirds of the hippocampus is also the site of the heaviest reciprocal connections with the basal nucleus of the amygdala. Axons from pyramidal neurons in ventral portions of CA1 also directly contact various areas of the rodent prefrontal cortex.

2.2 Hippocampal Physiology – Relationship to Behavior

The most well-known behavioral correlate of hippocampal principal neurons is the spatially specific firing patterns that they produce. These place cells, as first described by O'Keefe & Dostrovsky (1971), fire maximally when an animal occupies a discrete spatial location within its environment. The preferred spatial location of a place cell is that cell's "place field". The discovery of place cells led to the famous theory that the hippocampus functions as a cognitive map, allowing an organism to form internal representations of space (O'Keefe & Nadel, 1979). Much research in the past half of a century has been conducted in an attempt to uncover the links between the spatially specific firing patterns of hippocampal neurons and the types of memory for which the hippocampus is necessary (Eichenbaum, 2000; Leutgeb et al. 2005a; Smith & Mizumori, 2006a; Griffin & Hallock, 2013). One main finding that has emerged from this body of research is that the location-specific firing rates of place cells are also modulated by the contextually-based elements of experiences, shifting the location of their firing fields during learning (Mehta et al., 1997; Moita et al., 2004; Lee et al.,

2006; Singer et al., 2010; McKenzie et al., 2013), demonstrating firing rate differences between distinct experiences that take place in the same location (Wood et al., 2000; Frank et al., 2000; Ferbinteanu & Shapiro, 2003; Leutgeb et al., 2005b; Smith & Mizumori, 2006b; Griffin et al., 2007; Ainge et al., 2007; Ferbinteanu et al., 2011; Griffin et al., 2012; Hallock & Griffin, 2013), forming new place fields when conjunctive item-context associations are learned (Manns et al., 2007; Komorowski et al., 2010; Komorowski et al., 2013), and signaling the passage of time through sequentially activated elevations in firing rate (Pastalkova et al., 2008; Gill et al., 2011; MacDonald et al., 2011; MacDonald et al., 2013; Kraus et al., 2013). Place cells can radically alter their firing rate properties with changes in the spatial layout of an environment (“remapping”; see Colgin et al., 2008), and place fields recorded from different subfields show different patterns of activity when the physical structure of the recording environment is altered. When distal cues are rotated relative to local cues in a recording environment, place fields in CA1 show robust changes in firing rate and place field location while place fields in CA3 maintain a relatively coherent representation of the environment (Lee et al., 2004). Mature principal cells in the dentate gyrus have place fields that resemble those recorded from CA1 and CA3 (Neunuebel & Knierim, 2012), and population recordings from granule cells in the dentate gyrus have revealed that place cells in this area are sensitive to cue rotation in the recording environment (Neunuebel & Knierim, 2014), supporting one longstanding theory that the dentate gyrus maintains orthogonal representations of

multiple experiences with similar features (pattern separation), while reciprocal connections within CA3 allow a mental representation of an experience to take place in the face of degraded input via sparse mossy fiber projections from the dentate gyrus (pattern completion) (Yassa & Stark, 2011; Santoro, 2013).

A separate, but related, line of research has examined the relationship between the spiking of individual hippocampal neurons and oscillatory activity in the hippocampal local field potential (LFP), resulting in the discovery of hippocampal phase precession to local theta oscillations in hippocampal pyramidal neurons (O'Keefe and Recce, 1993; Skaggs et al., 1996), the segregation of place field firing rates by hippocampal theta cycles (Jezek et al., 2011; Gupta et al., 2012; Winkenhiser & Redish, 2015), and the “replay” of place field sequences across ripple oscillations during large irregular amplitude (LIA) activity (Wilson and McNaughton 1994, Skaggs and McNaughton 1996, Foster and Wilson 2006, Diba and Buzsaki 2007, Davidson et al. 2009, Singer and Frank 2009, Gupta et al. 2010). Theta oscillations are rhythmic slow oscillations with a frequency between 4 and 12 Hz. In the rat, theta oscillations are most prominent in the hippocampus proper, where they dominate the local field potential (LFP) during periods of movement or alertness, as well as during REM sleep (Buzsaki, 2002). Theta oscillations are thought to reflect the dipole between peri-somatic currents in stratum pyramidale and peri-dendritic currents in stratum radiatum (Buzsaki, 2002). Theta oscillations in the rat hippocampus have been associated with a wide variety of behavioral and cognitive phenomena, such as arousal (1940's), attention

and orienting to a stimulus (1950's), voluntary movement and motivation (1960's), memory and habituation (1980's), and now are a key component in various computational models of episodic memory and navigation (see Buzsaki, 2005; Hasselmo, 2012 for review). When a rodent runs along a linear track or takes a specific path between two points in an open field, place cells fire sequentially as the animal passes through each cell's place field. This sequential activation is compressed in time so that it can occur over the course of a theta cycle (roughly 250 milliseconds) (Gupta et al., 2012; Pfeiffer & Foster, 2013; Wikenheiser & Redish, 2015), suggesting that the theta oscillation functionally organizes spiking patterns of hippocampal neurons while an animal is actively engaged in the performance of a specific task. Various computational models have suggested that encoding and retrieval occur during specific phases of the hippocampal theta oscillation (Hasselmo, 2002; Hasselmo, 2005; Colgin & Moser, 2010), and a multitude of experimental findings have lent support for the theory that distinct mnemonic processes are partitioned across different phases of a theta cycle (Douchamps et al., 2013; Newman et al., 2013; Siegle & Wilson, 2014).

During periods of slow-wave sleep or wakeful quiescence, the dominant pattern of activity in the hippocampal LFP is LIA, which manifests as a sharply de-synchronized signal consisting of broadband voltage fluctuations within the hippocampus. It is during periods of LIA that sharp-wave ripple (SPW-R) events (super-fast oscillations >150 Hz) can be observed within the hippocampal LFP (Buzsaki, 1986; Buzsaki & Lopes da Silva, 2012). Ripple oscillations co-occur

with sharp-waves, which are large deflections in the hippocampal LFP that reflect the synchronous firing of a large sub-population (10-18%) of neurons in the CA3 subfield (Csicsvari et al., 1999). The synchronous population bursts in CA3 create a dipole between peri-dendritic EPSPs in stratum radiatum and peri-somatic IPSPs via basket cells in stratum oriens, which manifests as a fast “ripple” oscillation that appears in the LFP when recording from stratum pyramidale of the CA1 subfield (Ylinen et al., 1995; Stark et al., 2014). Although ripple oscillations and sharp-waves occur simultaneously, they are dissociable events that are reflections of different network-level processes in the hippocampus. Sharp-waves are one of the first patterns of activity that can be recorded from the neonatal rat hippocampus, while ripple oscillations do not appear in the hippocampal LFP until much later during development (Buhl & Buzsaki, 2005). Wilson and McNaughton (1994) initially found that hippocampal neurons that have overlapping place fields are significantly more likely to be temporally co-activated during periods of slow-wave sleep than hippocampal neurons with place fields that are far apart from one another. The temporal co-activation of overlapping place fields during slow-wave sleep coincides with the occurrence of SPW-R events in the LFP, suggesting that ripple oscillations may serve the purpose of re-activating specific neuronal ensembles that were previously tagged during active experience. During SPW-R events, the temporal order in which hippocampal neurons are re-activated recapitulates the spatial order in which they are activated during awake exploration. For example, when a rat traverses a linear track in one direction, a

given set of hippocampal neurons will fire in sequence as the rat moves through each one of those neuron's place fields. During epochs of slow-wave sleep directly following experience on the linear track, that same set of hippocampal neurons will be re-activated during SPW-R events, with the order in which those neurons were activated during a run on the track being preserved in time (Skaggs & McNaughton, 1996). Since the discovery of this "replay" phenomenon, a number of studies have correlated replay events with behavioral performance in hippocampal-dependent tasks (Diba & Buzsaki, 2007; Nakashiba et al., 2009; Gupta et al., 2010; Singer et al., 2013). The selective disruption of SPW-R events in the hippocampal LFP also leads to performance impairments during the acquisition of tasks that require the functional integrity of the hippocampus (Ego-Stengel & Wilson, 2010; Jadhav et al., 2013).

Both spiking activity of individual neurons and oscillatory activity, in a number of brain areas functionally synchronizes with the hippocampal theta oscillation during awake behavior, including the medial prefrontal cortex (Siapas et al., 2005; Hyman et al., 2005; Jones & Wilson, 2005; Hyman et al., 2010; Benchenane et al., 2010; Sigurdsson et al., 2010; Kim et al., 2011; O'Neill et al., 2013), orbitofrontal cortex (Young & Shapiro, 2011), ventral striatum (van der Meer & Redish, 2011; Lansink et al., 2012), and amygdala (Seidenbecher et al., 2003). The hippocampal theta oscillation may therefore be important for organizing neural activity in downstream brain areas during memory-guided behavior. During LIA, patterns of activity in cortical areas known to be important

for long-term memory consolidation become synchronized with SPW-R events in the hippocampal LFP (Battaglia et al., 2004; Peyrache et al., 2009), suggesting that “replay” events in the hippocampus may be important for the transfer of information from short-term memory to long-term memory following spatial experience. Oscillatory synchronization between disparate brain areas may therefore be important for neural communication during memory encoding, consolidation, and retrieval (Fell & Axmacher, 2011). Phase synchronization between oscillations in different brain areas may facilitate spike-timing dependent plasticity in those brain areas (Axmacher et al., 2006; Jutras & Buffalo, 2010), supporting the role of the Hebbian synapse in learning and memory.

2.3 Anatomy of the Hippocampal-Medial Prefrontal Circuit

In the rat, as in all mammalian non-primates, the prefrontal cortex is defined as that area of the neocortex that is innervated by the mediodorsal nucleus of the thalamus (Ferino et al., 1987). The medial prefrontal cortex (mPFC) comprises the rostral half of the medial wall of the prefrontal cortex, and lies roughly 2 – 4 mm anterior to bregma. Within the mPFC, three distinct sub-regions can be identified along its dorso-ventral axis. The dorsal-most sub-region is the anterior cingulate cortex (ACC), which sits adjacent to the retrosplenial cortex. The prelimbic cortex (PL) lies directly ventral to the ACC, and the infralimbic cortex (IL) comprises the ventral-most portion of the structure.

Early anatomical studies revealed that projections from the hippocampus to the mPFC arise primarily from the axons of pyramidal neurons in the temporal

portion of the CA1 subfield. One experiment demonstrated that the injection of a retrograde tracer (True blue) into the IL sub-region of the mPFC labeled roughly 20% of cells in temporal CA1 (Swanson, 1981). The location of the tracer injection influenced the location of the hippocampal cells that were labeled, with injections in layer I of the IL labeling cells in the dorsal-most regions of the temporal hippocampus, and injections in layer V labeling cells in the ventral-most regions. Injections of horseradish peroxidase into the PL and ACC also labeled cells in temporal CA1, as well as neurons in both the dorsal and ventral subiculum. Hippocampal-prefrontal fibers terminate mainly in layers I, V, and VI of the PL and IL, and layer I of the ACC (Ferino et al., 1987). Projections from the hippocampus to the prefrontal cortex also terminate differentially along the rostro-caudal axis of the mPFC, with caudal portions of the structure receiving more input than rostral portions (Jay et al., 1989). Anti-dromic stimulation of the mPFC has shown that the hippocampal-prefrontal pathway is monosynaptic, and hippocampal-prefrontal fibers synapse in the mPFC on the hemisphere ipsilateral to their origin (Ferino et al., 1987). Axons from pyramidal neurons in temporal CA1 course through the nucleus accumbens (NAcc) shell via the fimbria, and directly contact the IL, PL, and ACC. The density of hippocampal-prefrontal fibers is graded along the dorso-ventral axis of the mPFC, with the most ventral portions (IL, ventral PL) containing the densest proportion of fibers, and the most dorsal portions (ACC, dorsal PL) maintaining the least fiber density (Thierry et al., 2000).

Hippocampal-prefrontal synapses exhibit plasticity, as evidenced by the fact that LTP can be induced at those synapses following paired-pulse stimulation of temporal CA1 in a hippocampal-prefrontal slice preparation (Thierry et al., 2000). Evoked firing of single neurons in the mPFC can also be induced following a single pulse in temporal CA1. This evoked firing is abolished when either CNQX (an AMPA receptor antagonist) or APV (a NMDA receptor antagonist) is added to the preparation, and the addition of either an AMPA receptor or NMDA receptor agonist increases the firing rate of individual neurons following hippocampal stimulation (Jay et al., 1992). The effects of paired-pulse stimulation on LTP at hippocampal-prefrontal synapses are blocked by CNQX, but not APV. Anatomical studies have also shown that hippocampal-prefrontal synapses are asymmetrical, suggesting that they are excitatory (Thierry et al., 2000). These results suggest that the hippocampal-prefrontal pathway is glutamatergic, and that LTP at these synapses is facilitated by AMPA receptor-mediated membrane depolarization. The PL also projects to the NAcc core, and has reciprocal connections with the ventral tegmental area (VTA), which then sends efferent fibers back to the CA1 subfield of the hippocampus. Dopaminergic terminals in the PL that arise from the VTA lie in apposition to glutamatergic synapses that originate in the hippocampus, indicating that dopamine might modulate the effects of hippocampal activity on mPFC neurons. In support of this claim, stimulation of the mesocortical dopamine pathway inhibits the excitatory effects of hippocampal stimulation on prefrontal neurons, suggesting that

dopaminergic transmission plays a critical role in dampening the prefrontal network's response to hippocampal excitation (Jay et al., 1995). In anesthetized rats, the local administration of dopamine increases phase coherence between theta oscillations in the hippocampus and mPFC, indicating that dopaminergic signaling within the PFC is important for functionally synchronizing the two structures (Benchenane et al., 2010).

Although the temporal portion of the hippocampus sends direct projections to the mPFC, there is no direct reciprocal connection between the mPFC and the hippocampus; however, the mPFC does indirectly project to the hippocampus via direct connections with other brain regions. One such area that has received increased attention over the last decade is the group of nuclei that comprise the ventral midline section of the thalamus. Of this group, the reuniens nucleus (RE) and rhomboid nucleus (Rh) have been the subject of heightened investigation due to their direct anatomical connections with both the mPFC and the hippocampus. Early studies using anterograde tracing (titrated amino acids) demonstrated that RE heavily projects to both the septal and temporal portions of the hippocampus, with fibers originating in RE almost exclusively terminating near proximal dendrites in stratum lacunosum-moleculare (Herkenham, 1979). RE also projects to the mPFC, with the densest connections in layers I, V, and VI of the medial wall of the IL and PL, and with sparser projections to layer I of the ACC (Vertes et al., 2006). The PL, IL, and ACC all send fibers directly back to RE, and these axons directly contact the dendrites of neurons that project back to the hippocampus. A

combination of anterograde tracing (PHAL virus) in the mPFC and retrograde (gold) labeling in the hippocampus, coupled with visualization of RE slices with electron microscopy, verified that axons originating from the mPFC form asymmetric peri-dendritic synapses on hippocampal-projecting neurons, indicating that glutamatergic transmission at these cortico-thalamic synapses directly modulates thalamo-hippocampal transmission (Vertes et al., 2007). A subset of neurons within RE/Rh also send efferent projections to both the mPFC and hippocampus, raising the possibility that this subpopulation of neurons in the ventral midline thalamus is particularly important for orchestrating hippocampal-prefrontal interactions (Varela et al., 2014). Stimulation of RE produces strong evoked potentials in more ventral portions of the mPFC (IL and PL), as well as weaker evoked potentials in the ACC (Viana di Prisco and Vertes, 2006). RE stimulation also creates evoked responses in both the septal and temporal portions of CA1 stratum pyramidale, which are similar in strength to CA1 evoked potentials following stimulation of the Schaffer collateral pathway (Bertram & Zhang, 1999). Although Rh also projects to both mPFC and the hippocampus, the efferent projections from this nucleus are more widely distributed throughout the brain, contacting somatosensory cortex, posterior parietal cortex, occipital cortex, retrosplenial cortex, as well as the basolateral complex of the amygdala (Vertes et al., 2006). The anatomical connections between the mPFC, RE and Rh nuclei, and the hippocampus suggest that the ventral midline thalamus may be well-situated to modulate hippocampal-prefrontal interactions. The prelimbic area of the mPFC

also indirectly projects to the hippocampus via direct projections from the lateral entorhinal cortex, providing another potential avenue of communication between the prefrontal cortex and hippocampal formation.

2.4 Summary

Hippocampal networks may support memory encoding and retrieval via interactions between individual hippocampal neurons and the hippocampal LFP, which is thought to reflect the activity of large subpopulations of neurons within a given brain area (Buzsaki et al., 2012). The hippocampal LFP shifts between two “states”; one state (while the animal is moving or in REM sleep) is dominated by the hippocampal theta (4 – 12 Hz) oscillation, while the other state (while the animal is still or in slow-wave sleep) is dominated by large irregular amplitude (LIA) activity, during which sharp-wave ripple (SPW-R) complexes are observed. Individual hippocampal neurons spike during earlier phases of successive theta cycles, and sequentially activated place cell sequences are temporally compressed to fit within one theta cycle, suggesting that the theta oscillation functionally organizes cellular assemblies in the hippocampus during memory-guided behavior. Separate theta phases may facilitate encoding and retrieval, effectively reducing interference between encoded and retrieved information (Hasselmo, 2005). During SPW-R events, place cell sequences that occurred during waking behavior are temporally re-activated, indicating that the LIA network state may be important for memory consolidation.

Patterns of cellular activity in the mPFC are functionally synchronized with the hippocampus during both theta and LIA states, indicating that communication between these two structures may be critical for memory-guided behavior. The mPFC receives direct projections from the ventral hippocampus, and the mPFC and hippocampus are reciprocally connected via the ventral midline thalamic reuniens and rhomboid nuclei. Although the anatomy and physiology of the hippocampus, mPFC, and ventral midline thalamus have been thoroughly studied, much less is known about how these brain regions interact with one another to promote memory-guided decision making.

Chapter 3

SPECIFIC AIMS OF THE DISSERTATION

3.1 Introduction

The broad aim of the dissertation is to characterize the relationships between a targeted neural circuit consisting of the medial prefrontal cortex (mPFC), dorsal hippocampus, and thalamic reuniens and rhomboid nuclei (RE/Rh), and working memory-dependent task performance. Although previous research has established that the rat dorsal hippocampus (Ainge et al. 2007, Czerniawski et al. 2009, Hallock et al. 2013a), mPFC (Kesner et al. 1996, Porter and Mair 1997), and RE/Rh (Hembrook and Mair 2011, Hembrook et al. 2012, Hallock et al. 2013b) are all necessary for working memory-dependent delayed non-match to position tasks, the nature of the interaction between these anatomically connected brain areas (Herkenham 1979, Swanson 1981, Ferino et al. 1987, Vertes et al. 2007) during working memory-dependent task performance is not well-known. Although axons from pyramidal neurons in the CA1 subfield of the hippocampus directly synapse onto dendrites of pyramidal neurons in the infralimbic (IL), prelimbic (PrL), and anterior cingulate (ACC) sub-regions of the mPFC in the rat, these axons originate solely from pyramidal neurons in the ventral/intermediate hippocampus (Swanson 1981, Ferino et al. 1987, Jay and Witter 1991). Despite this fact, neurophysiological interactions are observed in vivo between the dorsal hippocampus and the mPFC (Siapas et al. 2005, Hyman et

al. 2005). The anatomical connections that mediate these interactions remain unknown. Two candidate brain areas are the reuniens (RE) and rhomboid (Rh) nuclei, which are situated along the ventral midline of the thalamus. These thalamic nuclei send afferent and receive efferent connections from both the mPFC and dorsal hippocampus in the rat (Herkenham 1978, Vertes et al. 2006, Viana di Prisco and Vertes 2006, Vertes et al. 2007). These anatomical data suggest that these nuclei may be well-situated to modulate communication between the hippocampus and mPFC, and therefore may be important for the performance of tasks that depend upon hippocampal and medial prefrontal functional integrity. Despite the fact that the disruption of neuronal function in RE/Rh impairs task performance in delayed non-match to place tasks (Hembrook & Mair, 2011; Hembrook et al., 2012; Hallock et al., 2013b), it is not known if these disruptions in task performance are accompanied by reductions in neural activity in the dorsal hippocampus and mPFC. The main goal of the dissertation, therefore, is to characterize the relationships between RE/Rh function, hippocampal-prefrontal oscillatory synchrony, and delayed non-match to place task performance. The results of the experiments in this dissertation will elucidate the relationships between the anatomically-connected hippocampal-RE/Rh-prefrontal network in the brain and spatial working memory.

3.2 Aim 1

RE/Rh are anatomically connected with both the mPFC and hippocampus, and so are well-positioned to orchestrate hippocampal-prefrontal synchrony. If

hippocampal-prefrontal synchrony in rodents is necessary for spatial working memory, then RE/Rh should also be necessary for spatial working memory. The first aim of the dissertation, therefore, is to establish that functional integrity of RE/Rh is a requirement for successful performance of the working memory-dependent delayed spatial alternation (DA) task that is used for electrophysiological experiments in the thesis (chapters 6 & 7). Previous experiments have shown that excitotoxic lesions of RE/Rh disrupt win-shift radial arm maze performance (Hembrook and Mair 2011), and transient inactivation of RE/Rh with muscimol disrupts the performance of a delayed non-match to position bar pressing task in an operant chamber (Hembrook et al. 2012). Recent work from our laboratory has added to this line of research by showing that muscimol infusions into RE/Rh impair the performance of a working memory-dependent tactile-visual conditional discrimination (CDWM) task, but not performance on a standard non-working memory-dependent tactile-visual conditional discrimination (CD) task (Hallock et al. 2013b), suggesting that RE/Rh serve a working memory-specific function, independently of the known contributions of the two thalamic nuclei to non-mnemonic components of other memory tasks (e.g., Dolleman-van der Weel et al. 2009, Prasad et al. 2013). **Experiment 1** (detailed in chapter 5) extends these findings by showing that infusions of muscimol into RE/Rh disrupt the performance of a 30-second delayed spatial alternation (DA) task. Successful performance of the DA task depends on spatial working memory, as the rat must flexibly use information from a previous trial in order to make a correct goal arm

choice on the upcoming trial. The 30-second DA task is useful for two reasons. The first reason is that the relatively long 30-second inter-trial delay period makes it more likely that the hippocampus and mPFC functionally interact to support memory-guided behavior (Lee and Kesner 2003; Churchwell and Kesner 2011). The second reason is that the task design lends itself well to in vivo extracellular recording, allowing for the examination and comparison of neural activity between locations on the T-maze and the start box which the rat occupies prior to entering the maze stem; differences in hippocampal rate coding between epochs in which the rat waits on the start box and epochs in which the rat ambulates down the maze stem have previously been reported in this task (Ainge et al. 2007), rendering the same comparison for hippocampal-prefrontal communication an interesting avenue of exploration. Previous work from our laboratory has shown that muscimol infusions into the dorsal hippocampus reliably disrupt performance on this task, while muscimol infusions into the dorsal striatum, a brain region typically associated with instrumental learning and habit-like memory, but not spatial working memory, do not significantly impair DA task performance (Hallock et al., 2013a). Conversely, muscimol infusions into RE/Rh do not impair the performance of a non-working memory-dependent conditional discrimination (CD) task (Hallock et al., 2013b). Our lab has also shown that CD performance is not disrupted by muscimol infusions into the dorsal hippocampus, but muscimol infusions into the dorsal striatum cause robust performance impairments in this task (Hallock et al., 2013a). These results demonstrate a dissociable role for RE/Rh

in spatial delayed alternation and conditional discrimination tasks, further supporting the hypothesis that RE/Rh is an important component of a cortico- limbic circuit that supports spatial working memory in rodents.

3.3 Aim 2

If the hippocampal-prefrontal circuit is necessary for spatial working memory, then increased synchrony between the hippocampus and mPFC should be observed during the performance of a spatial working memory-dependent task.

The second aim of the dissertation is to demonstrate that hippocampal-prefrontal synchrony is increased when a spatial working memory-guided strategy is

necessary for successful task performance. Previous findings that putative

individual pyramidal neurons in the mPFC entrain (fire action potentials on the same phase of successive oscillatory cycles) to the hippocampal theta oscillation

(Siapas et al. 2005, Hyman et al. 2005) provided one potential signature of in vivo

communication within the anatomically-connected hippocampal-prefrontal

pathway (Swanson 1981, Ferino et al. 1987, Jay and Witter 1991). Further

research showed that the strength of hippocampal theta entrainment in mPFC

neurons is positively correlated with performance in spatial alternation tasks

(Jones and Wilson 2005, Hyman et al. 2010, Sigurdsson et al. 2010). The same

studies showed that phase coherence (the degree to which the phase of one

oscillation consistently cycles during the same phase of a second oscillation within

the same frequency band) between theta oscillations in the mPFC and

hippocampus is also observed and is positively correlated with spatial alternation

task performance (Jones and Wilson 2005, Sigurdsson et al. 2010), suggesting that synchronous activity in the hippocampal-prefrontal network is important for memory-guided behavior, a finding that is supported by studies that have used fMRI to examine co-activation in the prefrontal cortex and hippocampus during memory tasks in humans (e.g., Kirchoff et al. 2000). Individual putative pyramidal neurons in both the mPFC (Jung et al. 1998) and hippocampus (Wood et al. 2000, Lee et al. 2006, Griffin et al. 2007, Ainge et al. 2007, Pastalkova et al. 2008, Hallock and Griffin 2013) also demonstrate firing rate differences that can be linked to behavior during spatial alternation and win-shift radial arm maze task performance, indicating that both rate coding in individual neurons and oscillatory activity in neuronal networks both within and between the hippocampus and mPFC might support memory-guided behavior in these tasks.

Despite these findings, a systematic examination of the relationship between neuronal activity in the hippocampal-prefrontal circuit and spatial delayed alternation performance has been lacking. Firing rate differences that appear to predict the future behavior of an animal in both hippocampal (Bower et al. 2005) and medial prefrontal (Cowen and McNaughton 2007) neurons during spatial memory tasks can be accounted for by variations in behavior (such as the trajectory taken by the animal through the environment and slight changes in head direction) rather than the mnemonic demands of the task per se. Furthermore, rate coding in hippocampal neurons is observed during tasks that are not dependent on hippocampal function (Wood et al. 2000, Ferbinteanu et al. 2011), casting doubt

on the hypothesis that firing rate differences in individual neurons are a necessary component of memory-guided task performance (Griffin and Hallock 2013). Theta phase entrainment and theta phase coherence in the hippocampal-prefrontal network may be possible mechanisms by which networks of neurons are assembled in discrete brain regions that interact to support memory-guided behavior; however, it is not known whether either the hippocampus or mPFC is necessary for the performance of the tasks in which hippocampal-prefrontal theta entrainment and coherence have been measured (Jones and Wilson 2005, Hyman et al. 2010, Sigurdsson et al. 2010, O'Neill et al. 2013). Dynamic coupling between oscillations of different frequencies has also been linked to memory performance in the human (Cohen et al. 2009), monkey (Siegel et al. 2009), and rodent (O'Neill et al. 2013) prefrontal cortices. Phase-amplitude coupling (the extent to which the phase of a low-frequency oscillation, such as theta, predicts the amplitude of a high-frequency oscillation, such as gamma) is also observed both within the hippocampus (Bragin et al. 1995, Belluscio et al. 2012) and between the hippocampus and striatum (Tort et al. 2008), suggesting that oscillations of different frequencies might dynamically interact during memory-guided tasks to support the temporal segregation and synchronization of specific cell assemblies in neural networks that are important for the coding of memory-specific information (Jensen and Lisman 1996, Lisman 2005).

In **Experiment 2** (detailed in chapter 6) of the dissertation, the relationship between hippocampal-prefrontal synchrony and spatial working memory is

directly tested by using *in vivo* electrophysiology to record from populations of hippocampal and medial prefrontal neurons simultaneously while rats switch between performance of the DA task and performance of the CD task within a single recording session. This dual-task approach allows for the direct comparison of activity in the hippocampus and mPFC between tasks that take place on the same T-maze, but differ in working memory demand. Results from Experiment 2 show that spiking of individual neurons (single units) in the mPFC is more highly modulated by the hippocampal theta oscillation (entrainment) during the DA task when compared to the CD task. Entrainment during the DA task is seen while the rat waits on the start box in between trials, and higher DA entrainment is only observed when the rat performs both the DA and CD tasks well ($> 75\%$ correct for both tasks). When the rat performs either the CD task, DA task, or both tasks poorly ($< 75\%$ correct), no significant difference in entrainment is observed between the two tasks. This result indicates that the entrainment of individual neurons to hippocampal theta is high when the rat is using a working memory-guided strategy to solve the DA task, and a non-working memory-guided strategy to solve the CD task. Phase coherence between theta oscillations in the mPFC and hippocampus, as well as hippocampal-prefrontal phase-amplitude coupling, are also increased during successful DA task performance, as compared to successful CD performance and poor DA performance. Phase coherence and phase-amplitude coupling increases are seen while the rat traverses the T-intersection of the maze (choice point). These results support the hypothesis that hippocampal-prefrontal

interactions are important for spatial working memory by showing that levels of hippocampal-prefrontal synchrony are correlated with the memory strategy that is being used to perform a task, independently of the physical attributes of the behavioral apparatus or the recording environment.

3.4 Aim 3

Due to their reciprocal connections with both the hippocampus and mPFC, one hypothesis is that RE/Rh contribute to spatial working memory-guided behavior by modulating hippocampal-prefrontal interactions (Vertes, 2006). The third aim of the dissertation is to provide evidence for this hypothesis, which has heretofore not been directly tested.

In **Experiment 3** (detailed in chapter 7), rats were trained on the 30-second DA task and then implanted with a guide cannula targeting RE/Rh, as well as a tetrode-containing microdrive array targeting the dorsal hippocampus and mPFC. Recordings were taken from the hippocampus and mPFC while the rat performed the DA task both with and without muscimol infusions into RE/Rh. Results from this experiment show that RE/Rh inactivation cause severe performance deficits on the DA task, consistent with results from Experiment 1 of the dissertation. Performance deficits are accompanied by dramatic reductions in hippocampal-prefrontal synchrony while the rat is on the maze. RE/Rh inactivation decreases the entrainment of single units in the mPFC to hippocampal theta oscillations during the delay period. RE/Rh inactivation also decreases theta coherence, as

well as phase-amplitude coupling between theta and slow gamma oscillations while the rat moves through the T-intersection (choice points) of the maze prior to making a goal arm choice. The results of this study provide substantial support for the hypothesis that RE/Rh contribute to spatial working memory by gating the flow of information between the dorsal hippocampus and mPFC.

Chapter 4

DETAILED METHODS

4.1 Subjects

All subjects were adult (>90 days old), male, Long-Evans hooded rats. Subjects weighed between 250 and 650 grams at the time of surgery. Subjects were ordered from Harlan, shipped to the Office of Laboratory Animal Medicine (OLAM) at the University of Delaware, and pair housed for a period of one week in the Griffin laboratory's colony room within the OLAM facility. During this one week acclimation period, subjects were given ad libitum access to food and water. Following the one week acclimation period, subjects were separated and individually housed. Directly following separation, each subject was placed on mild food restriction (4-5 food pellets per day) in order to keep each subject at ~90% of his ad libitum body weight. The colony room was temperature and humidity-controlled, and each subject was maintained on a 12 hour light/dark cycle. All experiments were performed during the light cycle.

4.2 Handling

Following separation and introduction of the food restriction schedule each subject was handled by the experimenter for at least five days. Handling was done in order to familiarize the subject with the experimenter. During handling, the

experimenter sat with the subject on his/her lap for a period of 15-20 minutes. The experimenter picked up the subject prior to handling, and placed the subject back into his home-cage following handling. After the subject had been placed back into his home-cage, a plastic bottle cap (identical to those used during training and testing sessions on the T-maze) was filled with 5-10 chocolate sprinkles and placed into the subject's home-cage. After either the subject had eaten all of the sprinkles or a period of one hour had passed (whichever came first), the plastic bottle cap was removed from the home-cage.

4.3 Behavioral Apparatus and Testing Room

The behavioral apparatus was a modified T-maze that was made of wood and painted black (see Figure 4.1). The maze consisted of a central stem (116 x 10 cm), two goal arms (56.5 x 10 cm each), and two return arms (112 x 10 cm). Each section of the maze was surrounded by 6 cm high wooden walls. Between trials, rats waited on a pedestal (a barstool with a ceramic dish attached to the top) that was located at the base of the T-maze. During inter-trial intervals, the pedestal was occluded from the T-maze by a large wooden barricade that was placed between the pedestal and the maze stem. The T-maze was located in a room that was separated from the common space in the lab by a door, and was completely surrounded by black curtains. Several large visual cues were attached to the curtains (strips of red and green tape, patterned circles and triangles). The room was dimly illuminated by a compact fluorescent bulb. For *in vivo* recording experiments, rats were placed in a black plastic enclosure (8 inches tall, 14 inches

in diameter) that was attached to the top of another stool. The bowl was lined with a thin sheet of cotton and placed in the corner of the testing room. Rats were placed in this bowl during attachment and detachment of the recording headstage, and while while tetrodes were being advanced into the mPFC and dorsal hippocampus. For Experiment 2, rats also waited in the enclosure during pre and post-recording sleep sessions.

4.4 Pre-Training

4.4.1 Goal Box Training

During goal box training, the rat consumed a chocolate sprinkle reward from plastic bottle caps located at the end of either goal arm of the T-maze (goal zones). The bottle caps were attached to the floor of the T-maze by Velcro. Each goal zone was blocked off from the rest of the maze with two large wooden barricades (one blocking access to the return arm, and one blocking access to the rest of the goal arm). During a goal box trial, the rat was placed into either the right or left goal zone (determined randomly). The rat was then given a period of 3 minutes to consume the chocolate sprinkle reward from the bottle cap. After either the rat had consumed the chocolate sprinkle reward, or the 3 minute period had passed (whichever came first), the rat was picked up and placed into the opposite goal zone for the next goal box trial. One goal box session consisted of six such goal box trials. Rats were given one goal box session per day until they had successfully consumed the chocolate sprinkles on every goal box trial in less than

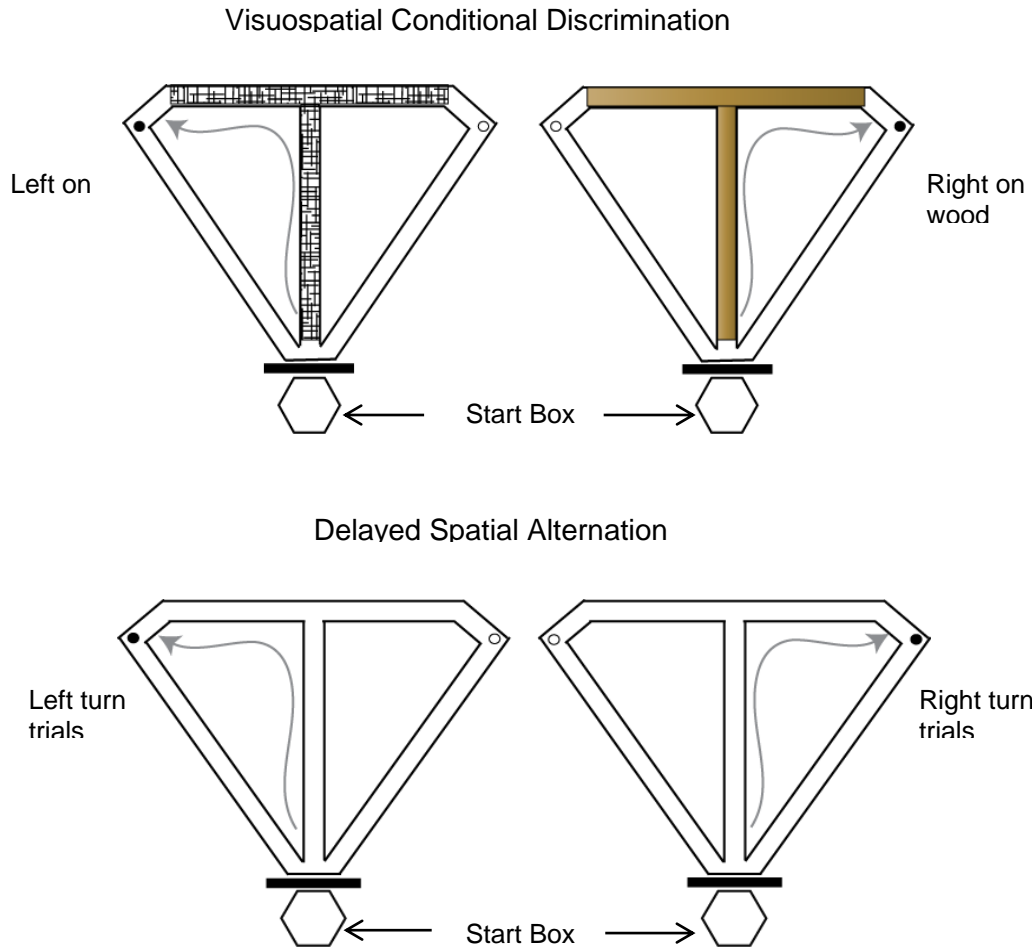


Figure 4.1. Schematic of the DA and CD T-Maze Tasks

The non-working memory-dependent CD task (top), and the spatial working memory-dependent DA task (bottom). During the CD task, the texture of the wood insert cue is pseudorandomly presented from trial to trial – the location of the food reward is based on the texture of the cue. During the DA task, the rat must alternate between the left and right goal arms on successive trials. Both tasks feature a 30-second inter-trial period, during which the rat waits on the “start box” which is occluded from the maze with a large wooden blocker. During both tasks, the rat runs up the central stem, chooses a goal arm, and returns to the start box via the modified return arms.

90 seconds for two consecutive goal box sessions. After reaching this set of performance criteria, rats were advanced to the next stage of pre-training.

4.4.2 Forced Run Training

During forced run training, the rat was shaped to run down the stem of the T-maze, enter a goal arm, consume the chocolate sprinkle reward from the bottlecap in the goal zone, and return to the inter-trial interval pedestal via the return arm. This sequence of events constituted one forced run trial. The experimenter prevented rats from traversing the maze in any other way (e.g., doubling back down the stem, entering a return arm from the start box) by blocking them with a wooden stick. During each forced run trial, one goal arm was rendered inaccessible to the rat by placing a removable wooden barrier at the entrance to that goal arm. The goal arm that was blocked was chosen according to a pseudorandom sequence (Fellows, 1967). Thus, rats only had access to one goal arm on each trial. One forced run session consisted of 12 trials, and successful completion of each trial required that the rat run down the stem and into the non-blocked goal arm, consume the chocolate sprinkle reward, and successfully return to the inter-trial interval pedestal via the return arm. Rats were given one forced run session per day. Once rats had successfully completed at least 10 out of 12 trials for two consecutive forced run sessions, they were advanced to behavioral training.

4.5 Behavioral Training

4.5.1 Experiments 1 & 3

For experiments 1 & 3, rats were trained on a spatial delayed alternation (DA) task with a 30-second delay between trials. During this task, rats were rewarded for alternating between the left and right goal arms from trial to trial. For the first trial of each session, both goal arms were rewarded. From the second trial through the last trial of the session, the goal arm that was not visited during the previous trial was rewarded. Between trials, rats waited on the inter-trial interval pedestal for 30 seconds. Rats performed one session of DA per day, with each session consisting of 25 trials (24 alternation trials, as both goal arms were rewarded during the first trial). Rats were not allowed to correct erroneous choices. Once rats reached a performance criterion of at least 80% correct choices (at least 20/24 correct) for two consecutive sessions, they underwent surgery for implantation of a guide cannula (for Experiment 1), or implantation of a recording microdrive and guide cannula (for Experiment 3).

4.5.2 Experiment 2

For Experiment 2, rats were first trained on a tactile-visual conditional discrimination (CD) task. During this task, rats learned to make a behavioral response based on the texture and color of floor inserts that spanned the length of the stem and both goal arms. One side of the maze inserts was covered with black mesh, and the other side of the maze inserts was smooth wood (light brown). During each trial, either mesh or wood was presented according to a pseudorandom sequence (Fellows, 1967). Half of the rats were rewarded for turning right when mesh was present, and left when wood was present; the other

half of the rats learned the opposite rule (left on mesh, right on wood). The cue inserts were flipped between each trial, even if the same cue was presented on consecutive trials. This was done in order to ensure that the rat could not solve the task by using auditory cues. Between each trial, rats waited on the inter-trial interval pedestal for 30 seconds, at which time the experimenter prepared the inserts for the next trial and baited the appropriate goal zone. Rats were given one session of CD per day, with each session consisting of 24 trials.

Once rats had reached a predetermined performance criterion of at least 80% correct choices (20/24 correct trials) for two consecutive sessions, the 30-second DA task was introduced into the training sessions. Rats were given 24 trials of CD, and then placed in their home-cages for a period of 20 minutes. After the 20-minute period had ended, rats were trained on the DA task with the same protocol that was used for behavioral training in experiments 1 & 3 (detailed in section 1.5a of this chapter). Once rats learned to perform both the CD and DA tasks at a level of 80% correct choices (20/24 correct trials for both tasks), they underwent surgery for implantation of the recording microdrive.

4.6 Surgical Procedures

Rats were given a subcutaneous injection of Atropine (AtroJect; 0.05 mg/kg), and anesthetized with isoflurane (1.0 – 3.0% in oxygen) in a transparent Plexiglas induction chamber. Once the rat was anesthetized, it was placed into a stereotaxic instrument (Kopf) that had a specialized nose cone for continuous flow of isoflurane throughout the duration of the surgery. The rat's breathing rate was

constantly monitored, and isoflurane levels were adjusted accordingly. The stereotaxic instrument sat on top of a heating pad that was turned to the “medium” setting. Puralube was applied to the rat’s eyes, and the incision site was subcutaneously injected with lidocaine and sterilized with Novalsan. An incision was made, the head was leveled, and bregma coordinates were identified. For Experiment 1, four small bone screws (Fine Science Tools) were fitted into four small burr holes that were made with a stereotaxically-mounted drill (Fine Science Tools). Dental acrylic (Lang Dental) was applied to anchor the screws to the skull. To target the reuniens/rhomboid nuclei (RE/Rh), a circular hole was drilled 1.8 mm posterior to bregma and 2.0 mm lateral to the midline. An 8.0 mm guide cannula (PlasticsOne) was lowered 6.5 mm ventral to the surface of the brain at a 15 degree angle. Since RE/Rh are midline structures, only one cannula was implanted. The cannula was cemented to the skull with dental acrylic, and a dummy cannula made to fit the guide cannula with a 1.0 mm projection was inserted. For Experiment 2, one circular hole was drilled above the mPFC (3.1 mm anterior to bregma, 0.5 – 2.0 mm from the midline, depending on angle of the microdrive bundle), and one hole was drilled above the dorsal hippocampus on the ipsilateral hemisphere (3.0 – 4.0 mm posterior to bregma, 1.5 – 3.0 mm from the midline, depending on angle of the microdrive bundle and distance from the mPFC bundle). A microdrive array with two tetrode-containing bundles (mPFC bundle: 7 tetrodes; hippocampal bundle: 12 tetrodes for rats 1-4, and 2 tetrodes for rats 5-6) was lowered onto the surface of the brain and cemented to the skull with dental

acrylic. For Experiment 3, a guide cannula targeting RE/Rh was implanted using the same procedures detailed above for Experiment 1. After the acrylic was dry, a dual-site microdrive targeting the mPFC and dorsal hippocampus was implanted using the same procedures detailed above for Experiment 2. The guide cannula and microdrive were implanted in opposite hemispheres. For all experiments, the hemisphere of implantation was counterbalanced across rats. For experiments 2 & 3, the microdrive was attached to a ground screw (a self-tapping bone screw with a piece of wire soldered to it), which was fitted into a small burr hole directly above lambda. Each tetrode was then advanced 1.13 mm into the brain. All rats received a subcutaneous shot of Flunixin (Banamine; 2.5 mg/kg), and children's Ibuprofen (30 mg/kg) in their drinking water for two days post-surgery. Rats were allowed to recover for a period of at least 5 days following surgery before behavioral testing began. All procedures were approved by the University of Delaware Institutional Animal Care and Use Committee.

4.7 Microdrive Arrays and Recording System

Microdrive arrays were custom made, with pieces of 30-gauge hypodermic tubing (Component Supply Co.) passing through a disc made from a polyurethane blend (SmoothOn) and into a custom-made jig (University of Delaware Machine Shop) that held the tubing together in specific geometrical configurations (see Figure 4.2a). Pieces of 30-gauge tubing that were grouped together by the jig are referred to as "bundles". The jig separated the pieces of 30-gauge into two bundles. One bundle was rectangular (2 pieces of 30-gauge tubing by 4 pieces), and was

designed to target the mPFC. The other bundle was circular, and was designed to target the dorsal hippocampus. A hollow piece of silicon tubing (PolyMicro) was then inserted into each piece of 30-gauge, and attached to an independently moveable brass screw that was inserted into the disc. A tetrode (12.7 μm wire made of a nichrome blend (Sandvik) and twisted together to produce a four-channel recording surface) was inserted and glued to each piece of silicon tubing. Thus, each tetrode could be lowered and raised independently by turning its associated brass screw clockwise or counter-clockwise respectively. The top of each tetrode was split into four independent channels and secured to an electronic interface board (EIB; Neuralynx) with gold-plated pins (Neuralynx). One end of a ground wire was also attached to the EIB, and the other end of the wire was attached to the ground screw during surgery. Each channel was electrophoretically plated with a gold solution (Neuralynx) until it reached a target impedance range of 200 – 300 kOhms. A plastic shield was attached to the microdrive's disc, and the distance between the bottoms of the hippocampal and mPFC bundles was measured in order to calculate surgical coordinates.

All recordings were made with a 64-channel digital recording system (Digital Lynx; Neuralynx). Neural signals were pre-amplified by unity gain operational amplifiers on the rat's headstage, which were attached to the EIB on top of the microdrive. Headstages were attached to the recording system by long tethers. The tethers were held in place during recording sessions by a piece of fishing wire that was attached to a counterweight via a pulley wheel located on the

ceiling of the recording room. A ceiling-mounted video camera captured position data (30 Hz) by recording luminance emitted by two LEDs attached to the rat's headstage. The LEDs were positioned on opposite sides of the headstage and were different colors (red and green) so that the rat's head direction angle could also be captured during recording sessions. Cheetah software (Neuralynx) was used to visualize spikes from single units, as well as the continuously sampled local field potential (LFP) from the mPFC and dorsal hippocampus. LFP data were sampled at a rate of 2034 Hz. Clusters of spikes were identified by comparing the peak wavelengths across recording channels within each tetrode. If a neuron is physically closer to one channel of a tetrode (for example, channel 1), then the peak spike wavelength emitted by that neuron will be larger on that channel as compared to the other three channels (channels 2, 3, & 4). Spikes belonging to that neuron could then be identified by plotting the peak wavelength values for each spike on channel 1 (x-axis), vs. another channel (y-axis). If the peak wavelength on channel 1 is larger than the peak wavelength on the other channels, spikes will segregate into a cluster with high values on the x-axis and low values on the y-axis (see Figure 4.2b). Individual clusters of spikes (putative individual neurons) were identified by first auto-cutting them with KlustaKwik, and then manually plotting them using SpikeSort (Neuralynx) software.

4.8 Infusion Protocol

For experiments 1 & 3, dummy cannulas were removed, and an internal cannula made to fit the guide cannula with a 1.0 mm projection was inserted.

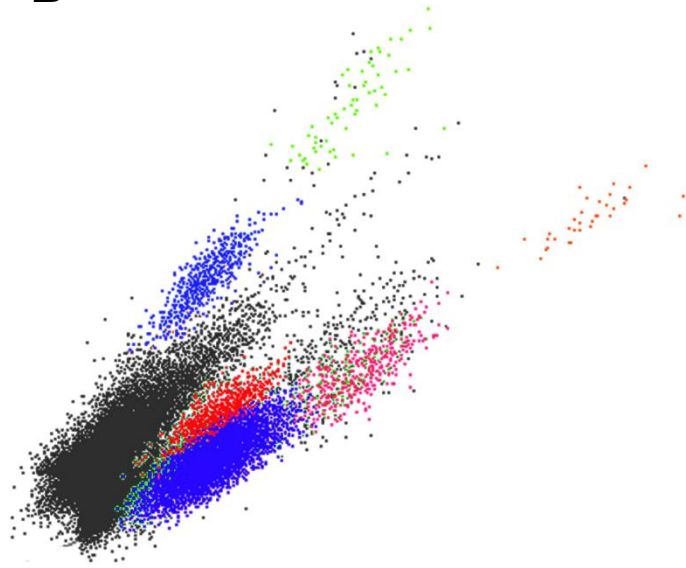
A**B**

Figure 4.2. Bundle Configuration and Cluster Cutting Schematic

(A) Picture of the two bundles that house tetrodes which target the mPFC and hippocampus simultaneously. (B) Depiction of the “cluster-cutting” software that is used for isolating individual units (putative neurons) from activity recorded from a single tetrode. Each color represents an individual unit (signal) that has been separated from other activity (noise) picked up by the tetrode. Each colored dot represents a spike (action potential) emitted by that particular neuron. Individual units are identified based on differences in waveform peak, valley, and energy between all four channels on the tetrode, and included for analysis based on published mathematical criteria (i.e., isolation distance and L-ratio) (Schmitzer-Torbert et al. 2005).

Internal cannulas were attached to a tube that contained either phosphate-buffered saline (PBS; Fisher Scientific), or muscimol (a GABA_A receptor agonist; Life Technologies) diluted in PBS. The tube was attached to a microinfusion syringe (Hamilton), and placed into an automated infusion pump (World Precision Instruments) that controlled infusion rate and volume (0.25 µl/min and 0.5 µl, respectively). Position of the infusate was monitored by marking an air bubble that separated the infusate from distilled H₂O within the tubing. Internal cannulas sat in the brain for two minutes post-infusion. Behavioral testing took place 30 minutes after infusions were given. Rats sat on the experimenter's lap for the duration of the infusion.

4.9 Perfusion and Histology

For experiments 2 & 3, rats were anesthetized with isoflurane and marking lesions were made by passing 10 µA of current through one wire of each tetrode and the reference electrodes. Rats were then returned to their home cages. After 24 hours, rats were perfused transcardially with 0.9% saline, followed by 10% buffered formalin (Experiment 2), or 4% paraformaldehyde (Experiment 3), and the head was soaked in formalin or paraformaldehyde for 2–3 days. After raising the tetrodes out of the brain, the brain was removed from the skull and placed in a 9% sucrose solution. After sinking, the brains were frozen and sectioned (40 µm).

For experiments 1 & 3, rats were given an infusion (0.5 µl volume) of a fluorophore-conjugated muscimol (BODIPY TMR-X; Life Technologies) 30

minutes prior to perfusion in order to visualize the spread of the muscimol in brain (Allen et al., 2008). The fluorescent muscimol was diluted to a concentration of 0.25 $\mu\text{g}/\mu\text{l}$ by placing the powder into a solution made of half PBS and half DMSO to aid in dissolution. Thirty minutes after infusion of the fluorescent muscimol, rats were transcardially perfused with 0.9% saline and 4% paraformaldehyde. Brains were sectioned with a cryostat (40 μm). In order to visualize the placement of the internal cannulas for experiments 1 & 3, half of the brain slices from RE/Rh were mounted on slides and stained using cresyl violet (Paxinos and Watson, 2005). The other half of the brain slices were mounted on slides and stained with ProLong Gold with DAPI (Life Technologies) in order to visualize the spread of the fluorophore-conjugated muscimol. Brain slices containing tetrode tracks in the mPFC and dorsal hippocampus from experiments 2 & 3 were mounted and stained with cresyl violet. DAPI-stained brain slices were visualized with a confocal microscope (LSM 710; Zeiss), and tiled fluorescent images were created using ZEN software (Zeiss). Cannula placement and tetrode tracks were visualized by placing digital plates from the Paxinos and Watson (2005) rat brain atlas over pictures of the cresyl-stained brain slices using Adobe Illustrator.

4.10 Analysis of Electrophysiological Data

4.10.1 Identification of Single Units in mPFC

Individual clusters of spikes were identified manually using SpikeSort (Neuralynx), as described in section 1.7 of this chapter. For each cluster, L-ratio

and isolation distance values were calculated automatically by SpikeSort. L-ratio and isolation distance are measures of a cluster's signal to noise ratio, as they provide a metric of a cluster's distance when plotted between channels from the rest of the recorded spikes within a session. Only clusters with an L-ratio less than 0.1 were included for subsequent analyses (Schmitzer-Torbert, 2005). Cluster stability was assessed by plotting the cluster's peak wavelength over time, and only clusters with a peak wavelength that remained stable across the recording session were used (see Figure 4.3). Pyramidal neurons were distinguished from interneurons based on mean firing rate across the session (> 2 Hz for interneurons), and spike duration (< 0.3 milliseconds for interneurons) (Ranck, 1973).

4.10.2 Analysis of Position Data

X-coordinates, Y-coordinates, and position timestamp data were imported to MATLAB with the function "**N1x2MatVt.m**" (see Appendix for code). The maze was then segmented into stem, choice point (T-intersection), goal arm, return arm, and inter-trial interval pedestal sections using the custom MATLAB function "**Int_DA.m**". Session data were cross-checked with online analysis of position data using Video Tracker File Playback software (Neuralynx), and any errant timestamp values were corrected.

4.10.3 Quality Control of Continuously Sampled Data

For all LFP analyses, continuously sampled data were first scrubbed for 60 Hz noise using the "**cleaningscript.m**" function in the Chronux toolbox for

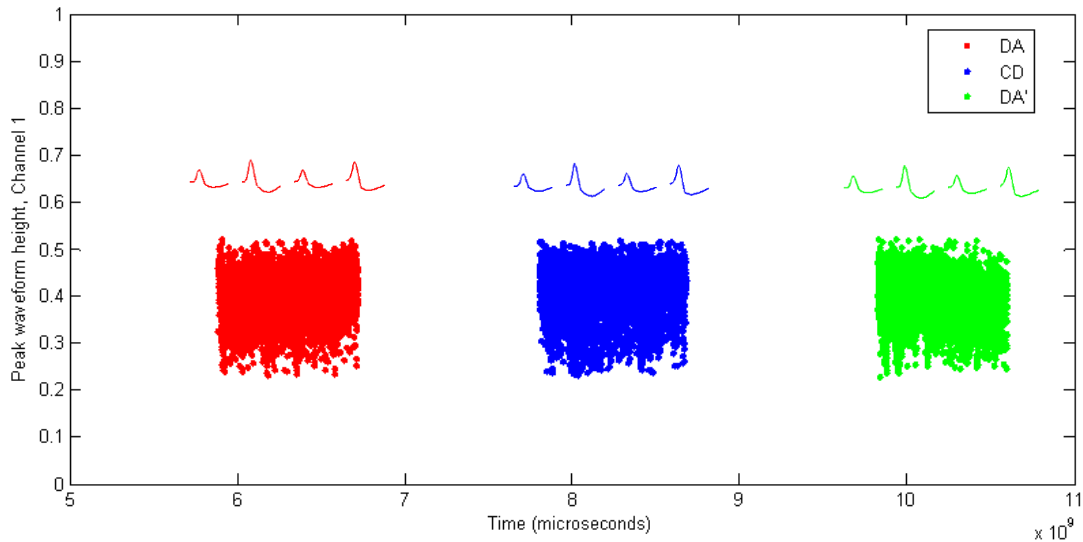


Figure 4.3. Quantification of Cluster Stability

Identification of cluster stability between task epochs from an example single unit in the mPFC from Experiment 2. Peak wavelength is plotted across time, and each color represents a separate task epoch (red = DA, blue = CD, and green = second DA). Peak wavelength did not change during the recording session, indicating that the single unit remained stable across the recording session.

MATLAB. Continuously sampled data were then de-trended (low-frequency “drifting” artifacts were removed) using a custom MATLAB function (“**Detrend_LFP.m**”) that fits a third degree polynomial to the data and then subtracts the polynomial’s coefficients from the data in order to remove low-frequency noise:

$$p(x) = p_1x^n + p_2x^{n-1} + \dots + p_nx + p_{n+1}$$

Where $p(x)$ is equal to a polynomial of degree n that is a best fit for the data in a given vector.

4.10.4 Firing Rate Analyses

Spike timestamps for each cluster were saved as .txt files and loaded directly into the MATLAB workspace. For the purpose of the thesis experiments, a neuron’s firing rate (in Hz) is defined as the number of spikes emitted divided by the time the rat spent in a specific segment of the maze. Firing rate during delay pedestal occupancy was calculated using the custom MATLAB function “**PETH_Delay.m**”. Briefly, this function finds spikes that occurred while the rat occupied the delay pedestal during each trial, and then assigns each spike to a 1-second time bin between -30 seconds (beginning of inter-trial interval) and 0 seconds (end of inter-trial interval). Firing rate is calculated for each time bin by summing the number of spikes occurring within that time bin over all trials, and dividing the total amount of spikes by the number of trials. In order to assess

whether firing rate changed as a function of time during the inter-trial interval (“ramping” behavior; see Fuster et al., 1982; Lewis & Miall, 2006), the built in MATLAB function “**glmfit.m**” was used to regress firing rate onto time while adjusting for non-normal distributions of firing rate by using a Poisson model:

$$E(Y|x) = e^{\theta'x}$$

Where Y_i and x_i are firing rate and time, respectively, and θ is a given set of parameters that is estimated by maximum likelihood. A p value less than 0.05 identified neurons that significantly altered their firing rate over time during inter-trial intervals, and the sign of the correlation coefficient showed whether a neuron increased or decreased its firing rate throughout the inter-trial interval (positive values indicated “ramping” activity, while negative values indicated “decay” activity). **PETH_Delay.m** was also used to construct peri-event time histograms and smoothed firing rate plots (using a Savitzky-Golay filter) for visual inspection of the data.

4.10.5 Entrainment of mPFC Single Units to the Hippocampal Theta

Oscillation

Spikes from individual neurons in the mPFC co-occur with theta oscillations in the hippocampus, and previous research has shown that many neurons in mPFC emit a higher number of spikes during a preferred phase of the hippocampal theta oscillation as compared to all other phases (Siapas et al., 2005; Hyman et al., 2005; Jones & Wilson, 2005; Hyman et al., 2010; Sigurdsson et al., 2010; O’Neill et al.,

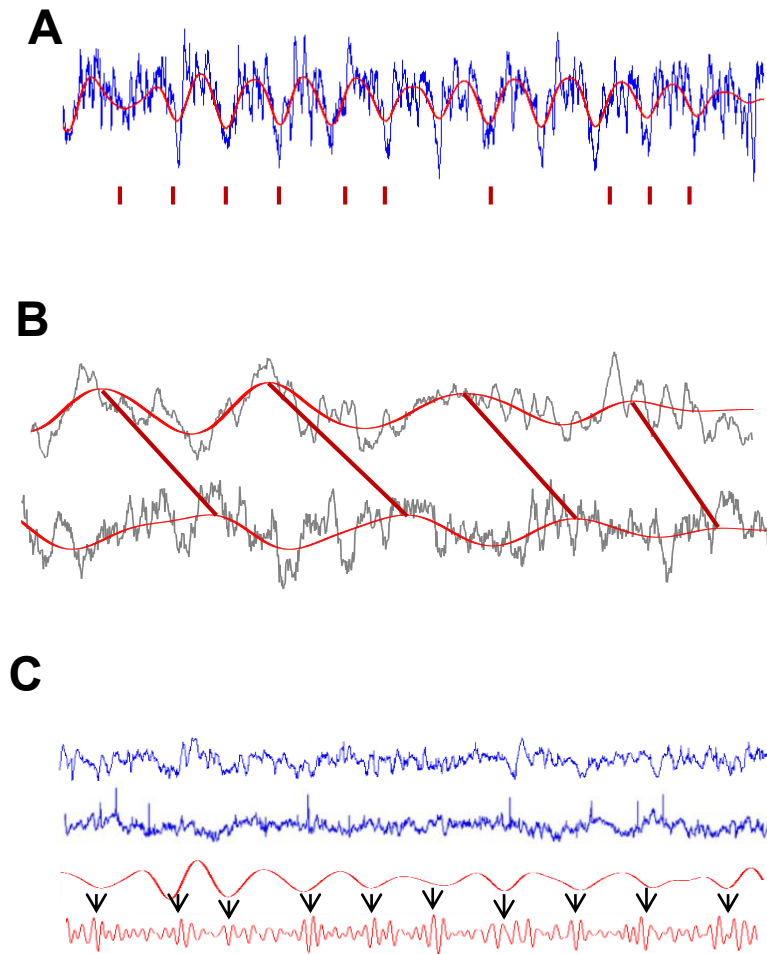


Figure 4.4. Representations of Entrainment, Coherence, and Phase-Amplitude Coupling

(A) Representative schematic of single unit entrainment to the hippocampal theta oscillation. Individual spikes from one neuron are represented as red tick marks on the bottom, and theta (red) is superimposed over the raw LFP from the hippocampus. (B) Schematic of phase coherence between simultaneously recorded theta oscillations (red traces) recorded from the hippocampus (top) and mPFC (bottom). Notice that lines drawn between peaks are roughly parallel across cycles. (C) Schematic of phase-amplitude coupling between hippocampal theta (top-most red trace) and mPFC slow gamma (bottom-most red trace).

2013). A neuron is therefore “entrained” to hippocampal theta if it tends to emit a spike on or around the same phase of the theta oscillation on successive cycles (see Figure 4.4a). Theta entrainment during inter-trial intervals was calculated for each recorded single unit from the mPFC with the custom MATLAB function **“Entrainment_Delay.m”**. The function first isolates hippocampal LFP samples and timestamps that occur during inter-trial interval periods. Theta (6-10 Hz) is then extracted from the hippocampal LFP with a third-degree Butterworth filter (custom MATLAB function **“Skaggs_filter.m”**). A butterworth filter was chosen because it minimizes ripple artifacts in the passband and rolls off toward zero in the stopband (there is virtually no chance that the filtered signal contains anything other than theta). The instantaneous phase of each sample from the filtered signal is then extracted using the custom MATLAB function **“PhaseFreqDetect.m”**, which identifies peaks, troughs, and zero crossings and then interpolates phase for all LFP samples. Theta phase values are then converted from degrees to radians ($radians = degrees * (\frac{\pi}{180})$). Samples where theta is not detected in the hippocampal LFP are not assigned a phase value. Spike timestamp values that occurred during inter-trial interval periods are then isolated from a given cluster, and each spike timestamp is assigned a phase value by cross-referencing the spike timestamp value with the LFP timestamp value. Spikes that occurred during non-theta periods are not assigned a phase value. Only clusters that contain at least 50 spikes that are able to be assigned a phase value are used

for analysis. Rayleigh's test of non-uniformity is then used to test the null hypothesis that spikes are uniformly distributed across all theta phases. The function "`circ_rtest.m`" from the Circular Statistics toolbox assigns a z-value (against the hypothetical uniform distribution) and corresponding p value for the spike-phase distribution. The distribution of z-values for all recorded neurons in a given condition can then be compared with the distribution of z values for all recorded neurons in another condition with a Kolmogorov-Smirnov test. The function "`circ_r.m`" from the Circular Statistics toolbox calculates the mean resultant vector length for the spike-phase distribution, which indicates the direction (preferred phase) and magnitude of directionality (length) for the given distribution by first averaging direction vectors:

$$\bar{r} = \frac{1}{N} \sum_r r_i$$

Then calculating the preferred phase angle:

$$\cos a + i \sin a = \exp(ia)$$

And finally calculating the length of the mean resultant vector:

$$R = ||\bar{r}||$$

This results in a value between 0 and 1, with 0 indicating no directionality, and 1 indicating maximum directionality. Mean resultant vector lengths can be averaged across neurons and compared using a student's t -test (in the case of comparison between two groups), or ANOVA (in the case of comparison between three or

more groups). One complication when using mean resultant vector length as a dependent variable is that vector length is affected by the number of spikes contained within the spike-phase distribution. A bootstrapped mean resultant vector length for each neuron is thus calculated by randomly sub-sampling 50 spike-phase pairs from the distribution 1000 times and taking the mean of the bootstrapped distribution to obtain a normalized mean resultant vector length (Sigurdsson et al., 2010). For visualization of the spike-phase distribution, **Entrainment_Delay.m** calls the function “**circ_plot.m**” (part of the Circular Statistics toolbox), which makes a rose plot (circular histogram) of the distribution with proportion of the total number of spikes contained within each phase bin. Linear histograms can also be created with theta phase on the x-axis and number of spikes on the y-axis.

4.10.6 Power Spectral Density

Power spectral density is a measure of the magnitude of a signal of a given frequency within the LFP. Power is equivalent to the squared amplitude of a signal, and is useful for quantifying the strength of an oscillation within a given frequency band. A discrete Fourier transform can be used for frequency decomposition (separating the LFP signal into discrete frequency components):

$$X_k = \sum_{n=0}^{N-1} X_n e^{-i2\pi k \frac{n}{N}}$$

Evaluation of a discrete Fourier transform requires $O(N^2)$ operations. A faster method of Fourier decomposition is the fast Fourier transform (FFT), which requires $O(N \log N)$ operations. Because of its computational efficiency, FFT algorithms are preferred over discrete Fourier transform methods of frequency decomposition. For averaged spectral density estimation during delay pedestal, maze stem, and choice point occupancy in experiments 2 & 3, a derivative of the FFT method of spectral density estimation called the Multi-taper method was used (Jarvis & Mitra, 2001). The Multi-taper method creates sliding windows within which multiple independent estimates of component frequencies are taken, which overcomes a limitation of basic FFT algorithms which often violate an underlying assumption that each Fourier component is representative of the amplitude and phase of the component frequency. In order to calculate a Multi-taper estimate of spectral power density, the custom MATLAB function “`spectral_power.m`” was used, which calls the Chronux function “`mtspectrumc.m`”. Samples from the hippocampal and mPFC LFP were extracted from periods of inter-trial interval pedestal occupancy, stem occupancy, and choice point occupancy. Power spectral density was first estimated across all frequency bands, and then mean power spectral density estimates were calculated separately for frequency bands of interest (delta, theta, beta, and gamma). Mean power spectral density estimates (in dB units) for each frequency band can be compared between conditions (within subjects) with a Wilcoxon signed-rank test,

which is a non-parametric test that can be used to replace a paired-samples t -test when data cannot be assumed have a normal distribution.

For time-frequency analysis of spectral power density during inter-trial interval and choice point periods, samples from the hippocampal and mPFC LFP were taken during temporally-equivalent time windows across trials (time locked to between -30 seconds and 0 seconds prior to stem entry for inter-trial interval periods, and time locked to between 1 second prior to and 1 second following choice point entry by using the custom MATLAB function “**Chronux_LFP.m**”). A Morlet wavelet approach was taken to extract frequency and power information across time because the kernel used in FFT analyses for dot product convolution (a sine wave) does not permit a detailed view of changes in power across frequencies within a temporally defined window (Cohen, 2014). The Morlet wavelet solves this problem by using a sine wave multiplied by a Gaussian window as a kernel, allowing for a trade-off between temporal precision and frequency precision. The Gaussian window for a Morlet wavelet is defined by:

$$GaussWin = ae^{-(t-m)^2/(2s^2)}$$

Where a equals amplitude, t equals time, and s is the standard deviation of the Gaussian, defined as:

$$s = \frac{n}{2\pi f}$$

Where f is frequency, and n is the number of wavelet cycles. Wavelet-transformed spectrograms were created using the custom MATLAB function

“`wavelet_spec.m`”, which was adapted from code introduced in chapter 12 of Cohen (2014). Spectrograms were created for visualization purposes only, and were not compared statistically.

4.10.7 Phase Coherence

Phase coherence is defined as the degree to which the phase of one oscillation within a defined frequency band predicts the phase of a second oscillation within a defined frequency band across multiple cycles (see Figure 4.4b). In humans, phase coherence in the theta frequency range between the prefrontal cortex and medial temporal lobe increases during the delay period of a working memory task (Sarnthein et al., 1998; Sauseng et al., 2004), and the magnitude of theta coherence between the mPFC and hippocampus in rodents is correlated with spatial working memory performance (Jones & Wilson, 2005; Sigurdsson et al., 2010). Theta phase coherence has been proposed to support memory processes by facilitating long-term potentiation (LTP) and long-term depression (LTD) in functionally connected brain areas (Fell & Axmacher, 2011), which is supported by evidence that LTP is maximally induced on the ascending phase of theta, and LTD is maximally induced on the descending phase of theta (Pavlidis et al., 1988; Huerta & Lisman, 1995). Phase coherence ranges between values of 0 and 1, with the coherence value representing the fraction (percentage) of common variance between two time series through a linear relation. Spectral coherence for experiments 2 & 3 was estimated with a Multi-taper method (similar

to that used for power spectral density estimation; Jarvis & Mitra, 2001), where magnitude squared coherence estimates are calculated as:

$$C_{XY}(f) = \frac{|\sum_{k=1}^K \mu_k X_k(f) * Y_k(f)|^2}{\sum_{k=1}^K \mu_k |X_k(f)|^2 \sum_{k=1}^K \mu_k |Y_k(f)|^2}$$

Where k denotes the number of tapers used, and X_k and Y_k represent the discrete Fourier transformed estimates of time-series X and Y . In order to calculate coherence between the hippocampal and mPFC LFPs during inter-trial interval pedestal, stem, and choice point occupancy periods, a custom MATLAB function (“**coherence.m**”) was used to first isolate LFP samples occurring at specific locations on the maze. A function in the Chronux toolbox (“**coherencyc.m**”) was then called to compute coherence across frequency bands for each maze location, as well as coherence within defined frequency bands (delta, theta, beta, and gamma). Mean coherence estimates were averaged across trials, and compared between conditions (within-subjects) for experiments 2 & 3 using a Wilcoxon signed-rank test (distributions of coherence values are not assumed to be normally distributed). For time-frequency estimations of spectral coherence, the Chronux function “**cohgramc.m**” was used to visualize changes in coherence across frequency bands as rats entered the choice point of the T-maze. Coherograms were used for visualization purposes only, and were not compared statistically. This function was also used to plot changes in theta coherence over time during choice point occupancy (between 1 second prior to and 1 second following choice point entry).

4.10.8 Phase-Amplitude Coupling

The phase of one oscillation may be synchronized with the phase of another oscillation within the same frequency band (phase coherence, as detailed in section 1.10g of this chapter). The phase of one oscillation may also be synchronized with the amplitude of another oscillation in a different frequency band (see Figure 4.4c). One influential model of working memory is that items are maintained within gamma cycles that are associated with specific theta ranges (Lisman & Idiart, 1995; Jensen & Lisman, 2005). In support of this theory, this “phase-amplitude coupling” between theta and gamma oscillations has been observed in the rat hippocampus and dorsal striatum (Tort et al., 2008; Belluscio et al., 2012), as well as in human scalp EEG (Demiralp et al., 2007; Sauseng et al., 2009) and intracranial recordings (Mormann et al., 2005; Canolty et al., 2006) during working memory tasks. Theta-gamma coupling may be a mechanism by which synchrony within populations of interneurons in one brain region (the synchronous firing of interneurons is thought to directly influence gamma amplitude; Traub et al., 2001; Bartos et al., 2007) is modulated by synchronous network activity in another brain region (Fell & Axmacher, 2011).

In order to quantify phase-amplitude coupling, a modulation index value was calculated according to the methods of Tort et al., (2010). The modulation index value is attained by first applying the Hilbert transform to extract instantaneous phase and frequency envelopes from filtered theta and gamma signals, respectively. Each amplitude value of the gamma oscillation is then

assigned a theta phase bin, and amplitude is normalized by averaging across the number of observations for each phase bin, such that:

$$P(j) = \frac{\langle A_{f_A} \rangle_{\varphi_{f_p}}(j)}{\sum_{k=1}^N \langle A_{f_A} \rangle_{\varphi_{f_p}}(k)}$$

Where φ_{f_p} is equal to the time series for phases, A_{f_A} is equal to the time series for amplitude envelope, and N is equal to the number of bin observations. If gamma amplitude is modulated by theta phase, the expectation would be that the binned phase-amplitude distribution would be non-uniform. In order to quantify deviation of the observed phase-amplitude distribution from a uniform phase-amplitude distribution, the Kullback-Leibler distance is then calculated, which infers the amount of distance between two distributions:

$$D_{KL}(P, Q) = \sum_{j=1}^N P(j) \log\left[\frac{P(j)}{Q(j)}\right]$$

The modulation index value represents the difference between the observed phase-amplitude distribution and a uniform phase-amplitude distribution, with higher values indicating a larger deviation.

In order to create co-modulogram heat maps of modulation index values between frequency for phase and frequency for amplitude pairs, a modulation index value was calculated for all possible phase and amplitude frequency pairs

with a custom MATLAB function (“**PAC_heatmap.m**”). Co-modulograms were used to verify that phase-amplitude coupling between theta and slow gamma oscillations in the hippocampus and mPFC was present. This function was also used to plot phase-amplitude coupling between theta and gamma oscillations as a function of gamma frequency for choice point occupancy. In order to determine the theta phase at which gamma amplitude was the highest, instantaneous theta phase was extracted by using Morlet wavelets, and a phase-amplitude distributions were calculated for a range of frequencies (30 – 120 Hz) within the gamma band. Normalized gamma amplitude was then plotted as a function of theta phase for each gamma frequency. In order to calculate a modulation index value between hippocampal theta and mPFC gamma for different points on the T-maze, the custom MATLAB function “**theta_mod_gamma.m**” was used to isolate LFP timestamps occurring during inter-trial interval pedestal, stem, and choice point occupancy. A modulation index value was then calculated for each maze location for each trial, and modulation index values were averaged across trials. Modulation index values were compared across conditions (within-rats) using Wilcoxon signed-rank tests (modulation index values cannot be assumed to be normally-distributed).

4.10.9 Analysis of Dependent Variables at Different Points Along the Maze Stem

In order to visualize changes in power, phase coherence, and modulation index as a function of position along the maze stem, the stem was segmented into 30 cm bins by the custom MATLAB function “**stem_binner.m**”, which uses x-y coordinates for the beginning and end of the maze stem to calculate bin boundaries, and then finds position timestamps that correspond to bin entry and exit for each trial. LFP samples were then isolated for occupancy periods for each bin, and the above analyses were applied to data from each spatial bin with the custom MATLAB function “**bin_my_data.m**”.

4.11 Summary Analysis of Data

For experiments 2 & 3, all dependent variables (choice accuracy, stem velocity, time spent at choice point, power, coherence, and modulation index) were normalized by subtracting baseline scores from testing scores in Experiment 3, and by subtracting DA scores from CD scores in Experiment 2. If no difference is expected between baseline and testing epochs in Experiment 3, and DA and CD epochs in Experiment 2, then the null hypothesis would be that normalized scores should not be significantly different from zero. This null hypothesis was tested with one-sample t-tests. Dependent variables in Experiment 3 were further analyzed with mixed-factorial ANOVAs (described in greater detail in the Methods section of chapter 7). Pairwise comparisons were made for all ANOVAs with Bonferroni tests. An alpha level of .05 was used for all statistical tests.

Chapter 5

EXPERIMENT 1: EFFECTS OF RE/RH INACTIVATION ON DELAYED SPATIAL ALTERNATION PERFORMANCE

5.1 Introduction

The current experiment was designed to test the hypothesis that RE/Rh are a component of a brain circuit that is necessary for spatial working memory in rodents. Rats were first trained on a spatial delayed alternation (DA) task with a 30-second delay interposed between trials. Once rats attained a predetermined performance criterion (see chapter 4: section 4.5a), a guide cannula was surgically implanted and muscimol was infused into RE/Rh in order to cause transient activation of GABA_A receptors in the two thalamic nuclei. We predicted that muscimol infusions would cause a decrease in performance of the DA task, supporting the hypothesis that RE/Rh function is critical for spatial working memory.

5.2 Materials and Methods

Out of 10 rats (see chapter 4: section 4.1), nine were included in analyses for this experiment based on histological confirmation of cannula placements in RE/Rh. Behavioral training and surgical procedures were performed as outlined in chapter 4.

5.2.1 Experimental Design

Following recovery from surgery, rats were re-trained on the DA task until they reached pre-surgical levels of performance (at least 80% correct for two consecutive sessions). Rats were then given four infusions (see chapter 4: section 4.8) across multiple days. PBS, a 0.125 $\mu\text{g}/\mu\text{l}$ dose of muscimol in PBS, a 0.25 $\mu\text{g}/\mu\text{l}$ dose of muscimol, and a 0.5 $\mu\text{g}/\mu\text{l}$ dose of muscimol were infused in counterbalanced order. 30 minutes after the infusion was given, rats were tested on a 24-trial session of the DA task. Between muscimol infusion sessions, rats were given as many infusion-free DA sessions as needed to return to a performance criterion of 80% correct for one session. This was done in order to rule out the possibility that carry-over effects from muscimol infusions affected the results.

5.2.2 Data Analysis

A repeated-measures ANOVA with % correct choices as the dependent variable was used to determine whether a main effect of infusion session was present. Pairwise comparisons were used to analyze whether a significant difference in performance was present between the saline infusion session and any of the three muscimol infusion sessions (see chapter 4: section 4.11). Histological analysis was performed according to chapter 4, section 1.9.

5.3 Results

5.3.1 Behavior

Rats took an average of 14.2 sessions (± 5.7 sessions) to reach pre-surgical performance criterion on the DA task. A repeated-measures ANOVA revealed a main effect of infusion session [$F(1.543,13.885) = 11.824, p = .002$], as mean performance during the three muscimol infusion sessions ($M = 50.4\% \pm 8.5\%$ for the 0.125 $\mu\text{g}/\mu\text{l}$ dose, $M = 41\% \pm 15.6\%$ for the 0.25 $\mu\text{g}/\mu\text{l}$ dose, and $M = 52.9\% \pm 16.3\%$ for the 0.5 $\mu\text{g}/\mu\text{l}$ dose) was lower than mean choice accuracy during the saline infusion session ($M = 74.2\% \pm 9\%$) (see Figure 5.1). Post-hoc analyses further revealed that mean choice accuracy did not significantly differ between any of the three muscimol infusion sessions ($p > .257$ in all cases), but that mean choice accuracy during the saline session was significantly higher than mean choice accuracy during each of the three muscimol infusion sessions ($p < .004$ in all cases).

5.3.2 Histology

Of the 12 implanted rats, 9 rats had internal cannula tracks that terminated in RE/Rh (see Figure 5.2). In agreement with a previous study (Hallock et al., 2013b), confocal microscopy revealed that fluorophore-conjugated muscimol spread to within 1 mm of the tip of the internal cannula in all directions.

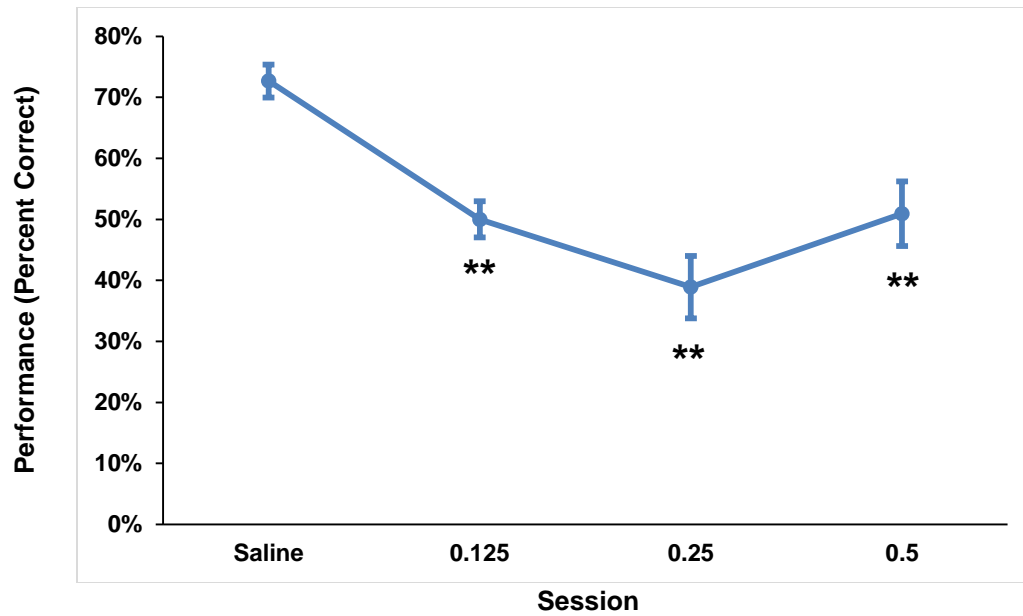


Figure 5.1. RE/Rh Inactivation Disrupts DA Task Performance

Muscimol infusions into RE/Rh significantly impaired DA task performance at all three doses as compared to saline infusion sessions. ** $p < .01$. Error bars = SEM.

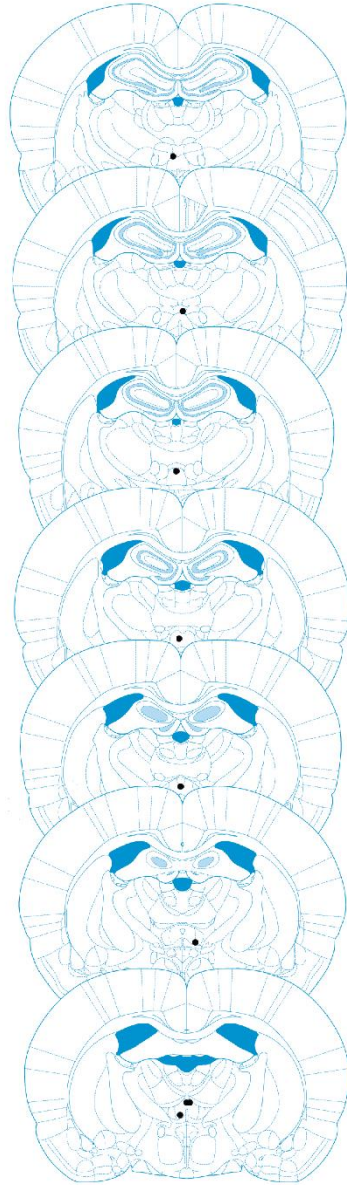


Figure 5.2. Placement of Internal Cannulas in RE/Rh Compiled histology showing placements of internal cannula tips in the ventral midline thalamus for all rats included in the experiment.

Fluorescence was observed in RE/Rh in all animals, with minimal fluorescence also observed in the paraxiphoid and submedius thalamic nuclei in some animals.

5.4 Discussion

The findings from this experiment demonstrate that functional inactivation of RE/Rh significantly disrupts performance on a spatial working memory-dependent DA task. This result is in agreement with several other studies (Hembrook & Mair, 2011; Hembrook et al., 2012; Hallock et al., 2013b) that have demonstrated spatial working memory deficits following RE/Rh inactivation, and extends these findings by showing that the functional integrity of RE/Rh is necessary for a spatial working memory task for which the hippocampus is also necessary (Ainge et al., 2007; Hallock et al., 2013a). A previous study from our laboratory has shown that RE/Rh inactivation does not cause significant performance impairments in the non-working memory-dependent tactile-visual conditional discrimination (CD) task (Hallock et al., 2013b), suggesting that RE/Rh have a spatial working memory-specific function, independently of the contributions of these nuclei to sensorimotor (Dolleman-van der Weel et al., 2009), attentional (Prasad et al., 2013), strategy-switching (Cholvin et al., 2013) and long-term memory consolidation aspects (Loureiro et al., 2012) of other tasks. Although it is known that RE/Rh are necessary for spatial working memory, the

mechanisms by which RE/Rh facilitate memory-guided decision making remain unknown. One hypothesis is that RE/Rh contribute to spatial working memory by gating the flow of information between the medial prefrontal cortex (mPFC) and hippocampus, which are thought to form a circuit that is critical for spatial working memory-guided behavior (Gordon, 2011; Colgin, 2011). This hypothesis is tested in Experiment 3 (chapter 7) of the dissertation.

Chapter 6

EXPERIMENT 2: HIPPOCAMPAL-PREFRONTAL SYNCHRONY AND SPATIAL WORKING MEMORY

6.1: Introduction

Spatial working memory, operationally defined as “a type of short term memory for stimuli or spatial locations that is typically used within a testing session, but not between testing sessions” (Dudchenko, 2004; pg. 708), is thought to depend on interactions between the hippocampus and medial prefrontal cortex (mPFC) (Colgin, 2011; Gordon, 2011). Previous findings that putative individual pyramidal neurons in the mPFC entrain (fire action potentials on the same phase of successive oscillatory cycles) to the hippocampal theta oscillation (Siapas et al. 2005, Hyman et al. 2005) provided one potential signature of *in vivo* communication within the anatomically-connected hippocampal-prefrontal pathway (Swanson 1984, Ferino et al. 1987, Jay and Witter 1991). Further research showed that the strength of hippocampal theta entrainment in mPFC neurons is positively correlated with performance in spatial alternation tasks (Jones and Wilson 2005, Hyman et al. 2010, Sigurdsson et al. 2010). The same studies showed that phase coherence (the degree to which the phase of one oscillation consistently cycles during the same phase of a second oscillation within

the same frequency band) between theta oscillations in the mPFC and hippocampus is also observed and is positively correlated with spatial alternation task performance (Jones and Wilson 2005, Sigurdsson et al. 2010), suggesting that synchronous activity in the hippocampal-prefrontal network is important for memory-guided behavior, a finding that is supported by studies that have used fMRI to examine co-activation in the prefrontal cortex and hippocampus during memory tasks in humans (e.g., Kirchoff et al. 2000). Individual putative pyramidal neurons in both the mPFC (Jung et al. 1998) and hippocampus (Wood et al. 2000, Lee et al. 2006, Griffin et al. 2007, Ainge et al. 2007, Pastalkova et al. 2008, Hallock and Griffin 2013) also demonstrate firing rate differences that can be linked to behavior during spatial alternation and win-shift radial arm maze task performance, indicating that both rate coding in individual neurons and oscillatory activity in neuronal networks both within and between the hippocampus and mPFC might support memory-guided behavior in these tasks.

Despite these findings, a systematic examination of the relationship between neuronal activity in the hippocampal-prefrontal circuit and spatial delayed alternation performance has been lacking. Firing rate differences that appear to predict the future behavior of an animal in both hippocampal (Bower et al. 2005) and medial prefrontal (Cowen and McNaughton 2007) neurons during spatial

memory tasks can be accounted for by variations in behavior (such as the trajectory taken by the animal through the environment and slight changes in head direction) rather than the mnemonic demands of the task per se. Furthermore, rate coding in hippocampal neurons is observed during tasks that are not dependent on hippocampal function (Wood et al. 2000, Ferbinteanu et al. 2011), casting doubt on the notion that firing rate differences in individual neurons are a necessary component of memory-guided task performance (Griffin and Hallock 2013). Theta phase entrainment and theta phase coherence in the hippocampal-prefrontal network may be possible mechanisms by which the brain assembles large networks of neurons in discrete brain regions that interact to support memory-guided behavior; however, it is not known whether either the hippocampus or mPFC is necessary for the performance of the tasks in which hippocampal-prefrontal theta entrainment and coherence have been measured (Jones and Wilson 2005, Hyman et al. 2010, Sigurdsson et al. 2010, O'Neill et al. 2013). Dynamic coupling between oscillations of different frequencies has also been linked to memory performance in the human (Cohen et al. 2009), monkey (Siegel et al. 2009), and rodent (O'Neill et al. 2013) prefrontal cortices. Phase-amplitude coupling (the extent to which the phase of a low-frequency oscillation, such as theta, predicts the amplitude of a high-frequency oscillation, such as gamma) is also observed both within the hippocampus (Bragin et al. 1995, Belluscio et al. 2012) and between the hippocampus and striatum (Tort et al. 2008), suggesting that oscillations of different frequencies might dynamically interact during

memory-guided tasks to support the temporal segregation and synchronization of specific cell assemblies in neural networks that are important for the coding of memory-specific information (Jensen and Lisman 1996, Lisman 2005).

In order to examine the relationship between hippocampal-prefrontal synchrony and spatial working memory, we trained rats to switch between two tasks within one testing session. The first task was a spatial working memory-dependent delayed spatial alternation (DA) task. The second task was a non-spatial working memory-dependent conditional discrimination (CD) task. Once rats learned to perform both tasks, they were implanted with a recording microdrive that contained tetrodes that targeted both the dorsal hippocampus and mPFC simultaneously. This experimental design allowed us to observe whether hippocampal-prefrontal synchrony is a function of task by holding the behavioral apparatus and testing room constant during recording sessions. We predicted that measures of synchrony between the two brain regions (entrainment, phase coherence, phase-amplitude coupling) would be higher during the DA task than during the CD task.

6.2: Materials and Methods

6.2.1: Subjects

Five male, adult, Long-Evans hooded rats (weighing 400 – 500 g) were individually housed in a temperature and humidity-controlled colony room on a 12 hour light/dark cycle. All behavioral training and recording was done during the light portion of the cycle. During handling, pre-training, behavioral training and

recording sessions, rats were food restricted in order to maintain them at 80-90% of their free-feeding body weight.

6.2.2.: Pre-Training and Behavioral Training

All pre-training and behavioral training procedures are described in detail in sections 4.5 and 4.4 of chapter 4. Briefly, rats were given goal box and forced run training. Rats were then trained on the non-spatial working memory-dependent CD task. Once rats had reached a performance criterion of at least 80% correct choices for two consecutive sessions on the CD task, a working memory-dependent delayed spatial alternation (DA) task was introduced into the training sessions. Rats were trained to run 24 trials of the DA task, followed by 24 trials of the CD task, and vice versa. Rats were introduced to the DA task only after they could perform the CD task at asymptotic performance levels in order to avoid the possibility that the rats would confuse the two tasks, and therefore not learn to perform either task well.

6.2.3: Experimental Design

After reaching performance criterion for both tasks, dual-site microdrives containing tetrodes that targeted the dorsal hippocampus and mPFC simultaneously were implanted (see section 4.6 of chapter 4). Following surgery, rats were re-trained on the DA and CD tasks until they re-attained pre-surgical performance levels. Following re-training sessions, tetrodes were gradually advanced into the mPFC (until well-isolated single units appeared with at least a 3:1 signal to noise ratio), and dorsal hippocampus (until large-amplitude theta

oscillations were observed in the local field potential). Recording sessions consisted 12-18 trials of DA and 12-18 trials of CD. Task epochs were separated by a 20 minutes, during which the rat remained plugged in and sat in a bowl beside the maze in the recording room. “Pre-sleep” and “post-sleep” epochs, during which the rat sat in the bowl for one hour prior to and following task performance, were also recorded for rats 1-3. Rats 1 & 2 performed a 12-trial epoch of DA, followed by an epoch of CD, and ending with another epoch of DA. Rats 3-5 performed 18-trial epochs of DA and CD during recording sessions. Task order was switched from day to day (rats performed DA first on every other recording day). The number of sessions recorded from each rat varied between rats, as recordings were stopped once reductions in signal to noise ratio prevented well-isolated clusters from the mPFC from being identified, indicating that tetrode impedance was rising and the tetrodes were no longer capable of producing high-fidelity recordings.

6.2.4: Data Analysis

Detailed analysis procedures are given in chapter 4 of the dissertation. Briefly, prefrontal clusters were isolated offline. The rat’s position along the maze for each trial was calculated with custom MATLAB functions (see Appendix for a complete list of code), and behavioral performance, time spent at the choice point, and stem velocity were calculated for each trial and averaged across trials for each rat using custom MATLAB functions. Spikes for each single unit (putative pyramidal neuron) were isolated for start box occupancy, and a Poisson linear

regression model was fitted to each neuron in order to detect “ramping” or “decay” activity (see chapter 4 for detailed methods). For firing rate and entrainment analyses, sessions were separated into “Good Performance” (sessions in which rats attained > 75% correct choices for both tasks), “DA Bad” (sessions in which rats attained < 75% correct choices on the DA task), and “CD Bad” (sessions in which rats attained < 75% correct choices on the CD task) sessions. No sessions were recorded in which performance was <75% correct choices for both tasks. For rats 1 & 2, the two DA epochs in each session were counted separately. For example, if a rat performed well during the first DA epoch, performed well during the CD epoch, and performed poorly during the second DA epoch, the first DA and CD epochs were counted as a “Good Performance” session, and the CD epoch and last DA epoch were counted as a “DA Bad” session. A firing rate, Rayleigh’s z-statistic, and subsampled mean resultant vector length (MRL; see chapter 4) were assigned to each putative pyramidal neuron for each epoch while the rat waited on the start box between trials. Normalized firing rate, z-statistic, and MRL values were calculated by subtracting each value during DA from each value during CD for each pyramidal neuron. Normalized values were then separated into “Good Performance”, “DA Bad”, and “CD Bad” categories. If hippocampal-prefrontal synchrony is higher during spatial working memory, then normalized scores should be significantly lower than zero during good task performance, signifying that values decreased from DA to CD. This prediction was tested with one-sample t-tests for values in each category. For phase coherence analyses, a coherence

score between the dorsal hippocampal and prefrontal LFPs was calculated for four distinct frequency bands (delta; 1-4 Hz, theta; 4-12 Hz, beta; 15-30 Hz, and gamma; 30-80 Hz) while the rat occupied the start box, maze stem, and maze choice point for each epoch. Epochs were separated into good performance (> 75% correct choices) and bad performance (< 75% correct choices) epochs. Coherence was compared between epochs, and within frequency bands and maze locations, using Wilcoxon rank-sum tests. For phase-amplitude coupling, a modulation index (MI) value was calculated between theta and gamma oscillations within the hippocampus, within the mPFC, and between the hippocampus and mPFC for each maze location for each epoch. Epochs were again separated into good performance and bad performance epochs, and MI value was compared between epochs, but within brain region, using Wilcoxon rank-sum tests. **6.3:**

6.3 Results

6.3.1: Behavior

In order to compare overt behavior between the two tasks, time spent at the choice point and stem velocity were calculated and averaged across trials for each epoch. Wilcoxon sign-rank tests revealed no significant difference in time spent at the choice point between good DA epochs and good CD epochs ($p = .83$), nor between bad DA epochs and bad CD epochs ($p = .66$). Wilcoxon sign-rank tests also revealed no significant difference in velocity on the maze stem between good DA epochs and good CD epochs ($p = .78$), nor between bad DA epochs and bad CD epochs ($p = 1$) (see Figure 6.1).

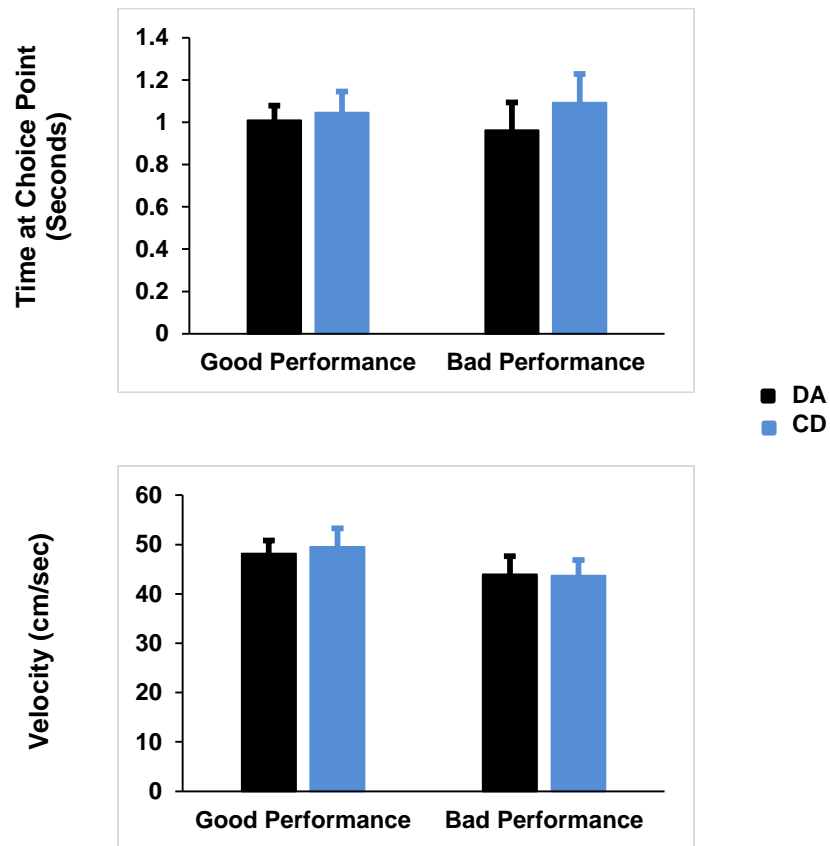


Figure 6.1. Maze Behavior Across Task Epochs

Top: Time spent at the choice point is not significantly different between good performance (> 75% correct choices) or bad performance (< 75% correct choices) epochs. Bottom: Stem velocity is not significantly different between task epochs.

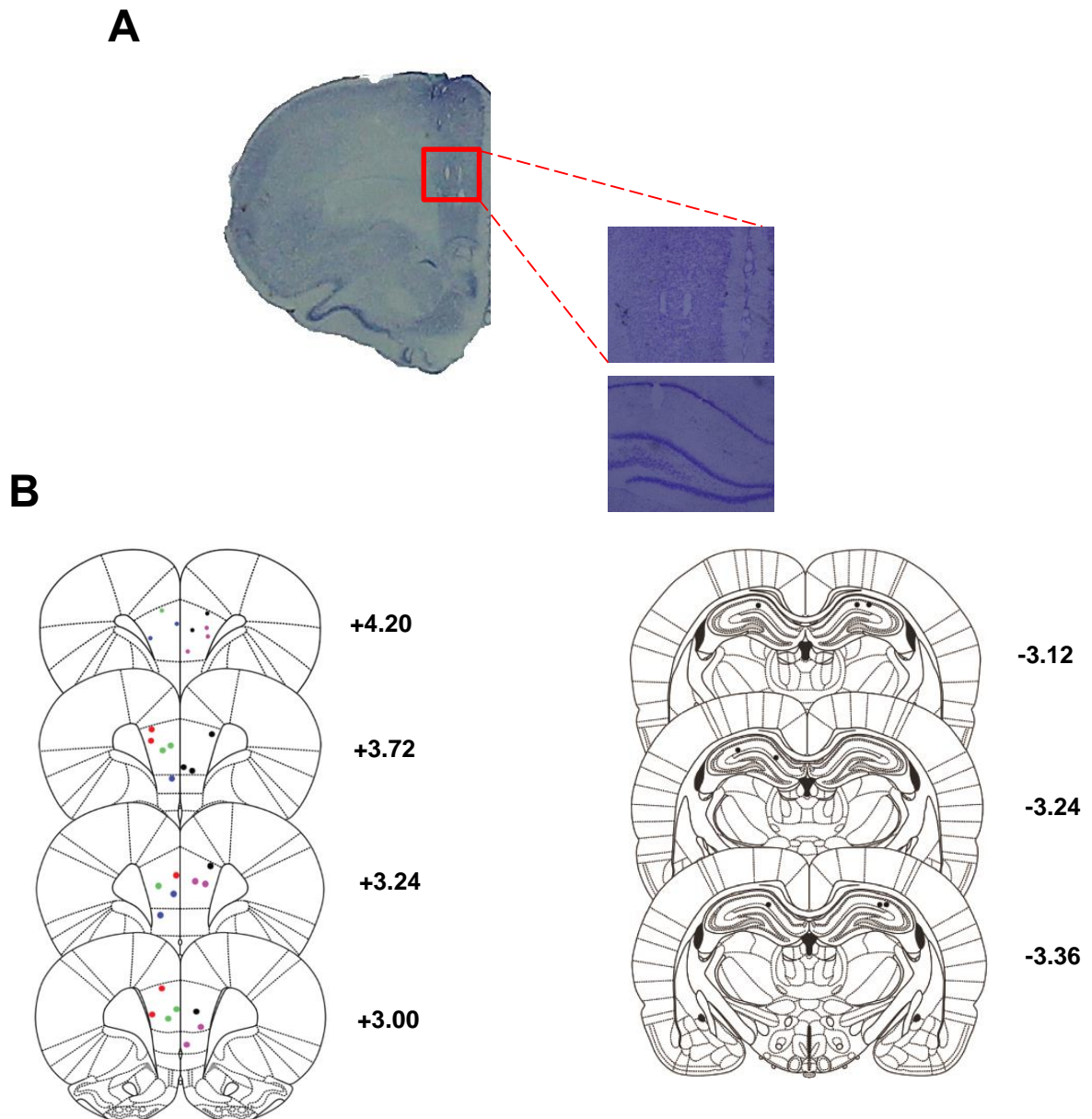


Figure 6.2. Tetrode Placements in mPFC and Hippocampus

(A) Representative nissl-stained coronal sections from one rat showing placement of tetrode tips in the mPFC (top) and dorsal hippocampus (bottom). **(B)** Coronal sections showing placement of tetrode tips in mPFC (left panel; different colors are equal to individual rats), and dorsal hippocampus (right panel) for all animals.

6.3.2: Firing Rate

A total of 210 putative pyramidal neurons in the mPFC were isolated and included in analyses (for a detailed description of inclusion procedures for single units, see chapter 4). These single units were spread out across three rats (rats 4 & 5 did not have any well-isolated single units, and were solely used for LFP analyses). Single units were spread out over 24 “Good Performance” sessions, 14 “DA Bad” sessions, and 10 “CD Bad” sessions (for a summary of number of sessions and single units per rat, see Table 6.1). “Ramping” and “decay” activity was relatively rare among the recorded population of pyramidal neurons (15 total neurons displayed significant ramping or decay activity during one or more task epochs), and this activity did not seem to be tied to task; rather, ramping or decay activity was usually consistent between task epochs. Even though ramping and decay activity did not seem to be tied to task, the overall firing rates of mPFC single units during the inter-trial interval period decreased significantly with corresponding decreases in working memory demand. One-sample t-tests revealed that normalized firing rates during “Good Performance” sessions were significantly lower than zero ($M = -.2356$, $SD = .854$, $t(83) = -2.527$, $p = .013$), while normalized firing rates during “DA Bad” ($M = -.019$, $SD = .656$, $t(88) = -.281$, $p = .779$) and “CD Bad” ($M = -.08$, $SD = .61$, $t(66) = -1.097$, $p = .276$) were not significantly different from zero (see Figure 6.4c). This drop in firing rate between successful DA and CD task epochs was not seen during stem ($M = -.03$, $SD = .777$, $t(83) = -.293$, $p = .771$) or choice point ($M = -.14$, $SD = 1.03$, $t(83) = -$

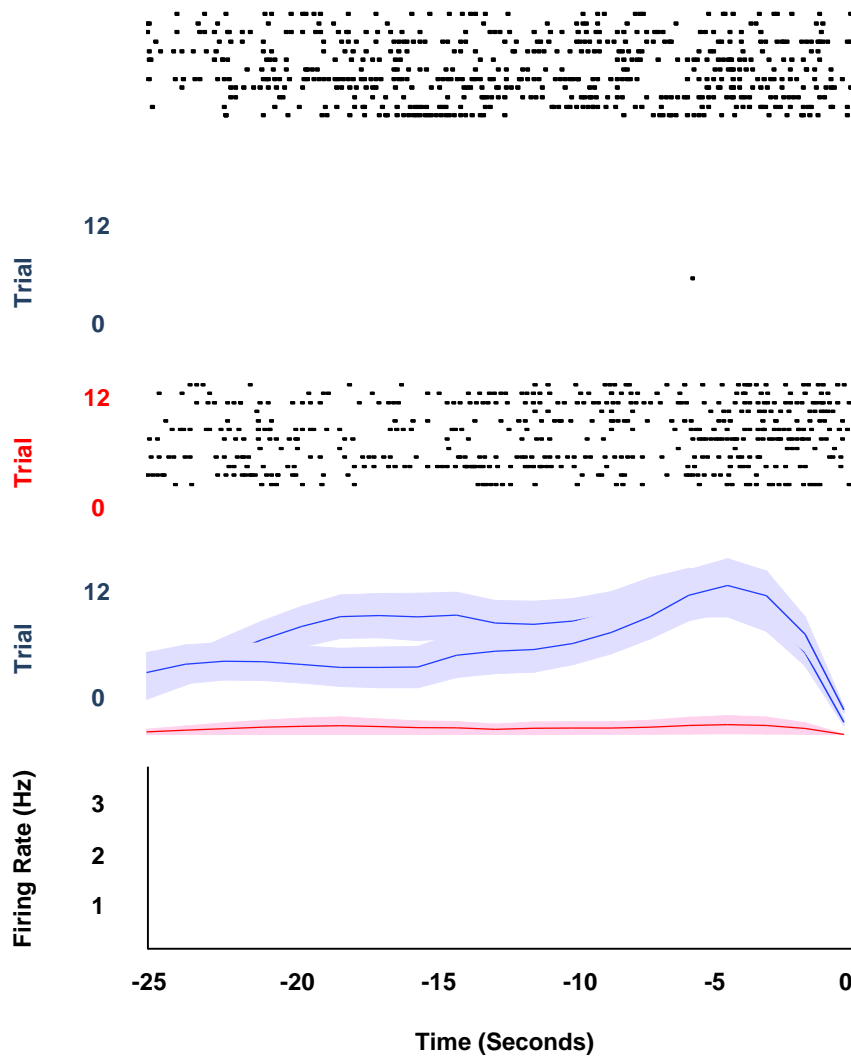


Figure 6.3. Delay Period Firing Rates of mPFC Neurons are Task-Sensitive

Representative example of an mPFC single unit that is sensitive to task. Raster plots represent individual spikes emitted over time during start box occupancy for a DA epoch (top panel), a CD epoch (middle panel), and a second DA epoch (bottom panel) within a single recording session. The bottom firing rate plot shows trial-averaged firing rate as a function of time for DA epochs (blue) and the CD epoch (red). This single unit dramatically decreased its firing rate during the CD epoch. The 0 on the far right of the x-axis represents termination of the delay period.

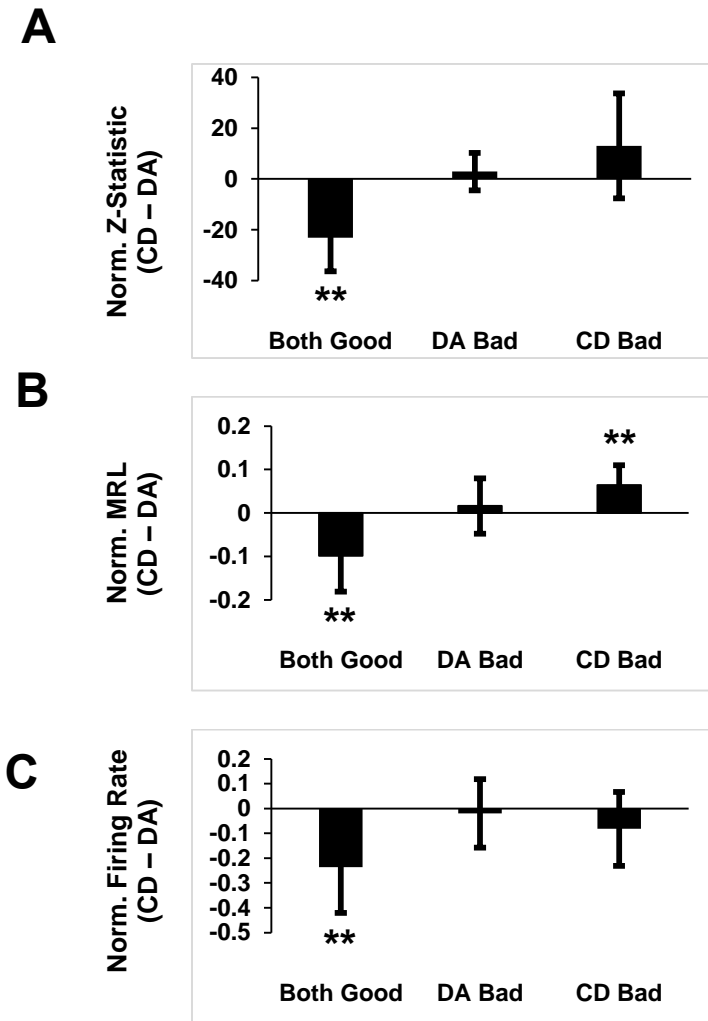


Figure 6.4. Single Unit Entrainment and Firing Rate Across Epochs

(A) Rayleigh's z-statistic was normalized within neurons and compared across sessions in which the rat performed poorly and sessions in which the rat performed well. Rayleigh's z-statistic dropped significantly from DA to CD epochs in which the rat performed well, but not epochs in which the rat performed poorly. **** $p < .01$.** Error bars = 95% confidence intervals. (B) Mean resultant vector length (MRL) dropped significantly from good DA epochs to good CD epochs. MRL also increased significantly from good DA epochs to bad CD epochs. **** $p < .01$.** Error bars = 95% confidence intervals. (C) Firing rate on the start box dropped significantly from good DA epochs to good CD epochs. **** $p < .01$.** Error bars = 95% confidence intervals.

1.179, $p = .242$) traversals. Thus, prefrontal firing rates during the inter-trial interval period were higher overall when a working memory strategy was used to successfully perform the DA task (see Figure 6.3).

6.3.3: Entrainment

A total of 90 pyramidal neurons emitted enough spikes (> 50) during the inter-trial interval period of each task epoch to be included in entrainment analyses. One-sample t-tests revealed that normalized Rayleigh's z-statistic values (the higher the z-statistic, the higher the entrainment) were significantly lower than zero for "Good Performance" sessions ($M = -23.14$, $SD = 43.68$, $t(44) = -3.554$, $p = .001$), but not for "DA Bad" ($M = 1.90$, $SD = 27.06$, $t(42) = .647$) or "CD Bad" ($M = 13.06$, $SD = 58.3$, $t(32) = .207$) sessions (see Figure 6.4a). The same analyses for normalized mean resultant vector length revealed a significant decrease for "Good Performance" sessions ($M = -.0984$, $SD = .275$, $t(44) = -2.401$, $p = .02$), no significance for "DA Bad" sessions ($M = .016$, $SD = .206$, $t(42) = .508$, $p = .614$), and a significant increase for "CD Bad" sessions ($M = 13.06$, $SD = 58.3$, $t(32) = .207$) (see Figure 6.4b). The increased normalized score for "CD Bad" sessions may reflect the incorrect usage of a working memory strategy during poor CD performance.

6.3.4: Coherence

A total of 33 good DA epochs, 22 good CD epochs, 15 bad DA epochs, and 8 bad CD epochs were used for coherence analyses. Analyses revealed that phase coherence between theta oscillations in the hippocampus and mPFC were

higher during good performance of the DA task as compared to good performance of the CD task while rats passed through the choice point of the T-maze. This coherence difference was not present during poor performance of either task. Wilcoxon rank-sum tests revealed that choice point theta coherence during good DA epochs was significantly higher than theta coherence during good CD epochs ($p = .007$), and was also significantly higher than theta coherence during bad DA epochs ($p < .001$) (see Figure 6.5). Theta coherence during bad DA epochs was not significantly different than theta coherence during bad CD epochs ($p = .07$). Theta coherence during good CD epochs was also not significantly different than theta coherence during bad CD epochs ($p = .8$). Wilcoxon rank-sum tests also revealed that delta coherence was not significantly different between good DA and good CD epochs ($p = .06$), nor between bad DA and bad CD epochs ($p = .61$). Beta coherence was also not significantly different between good DA and good CD epochs ($p = .51$), nor between bad DA and bad CD epochs ($p = .12$). Finally, gamma coherence was not significantly different between good DA and good CD epochs ($p = .79$), nor between bad DA and bad CD epochs ($p = .76$) (see Figure 6.6). The theta effect was also specific to the choice point, as theta coherence on the maze stem did not differ between good DA and good CD epochs ($p = .79$), nor between bad DA and bad CD epochs ($p = .81$), nor between good DA and bad DA epochs ($p = .44$). Similarly, theta coherence on the start box did not differ between good DA and good CD epochs ($p = .65$), nor between bad DA and bad CD epochs ($p = .43$), nor between good DA and bad DA epochs ($p = .06$) (see Figure 6.7).

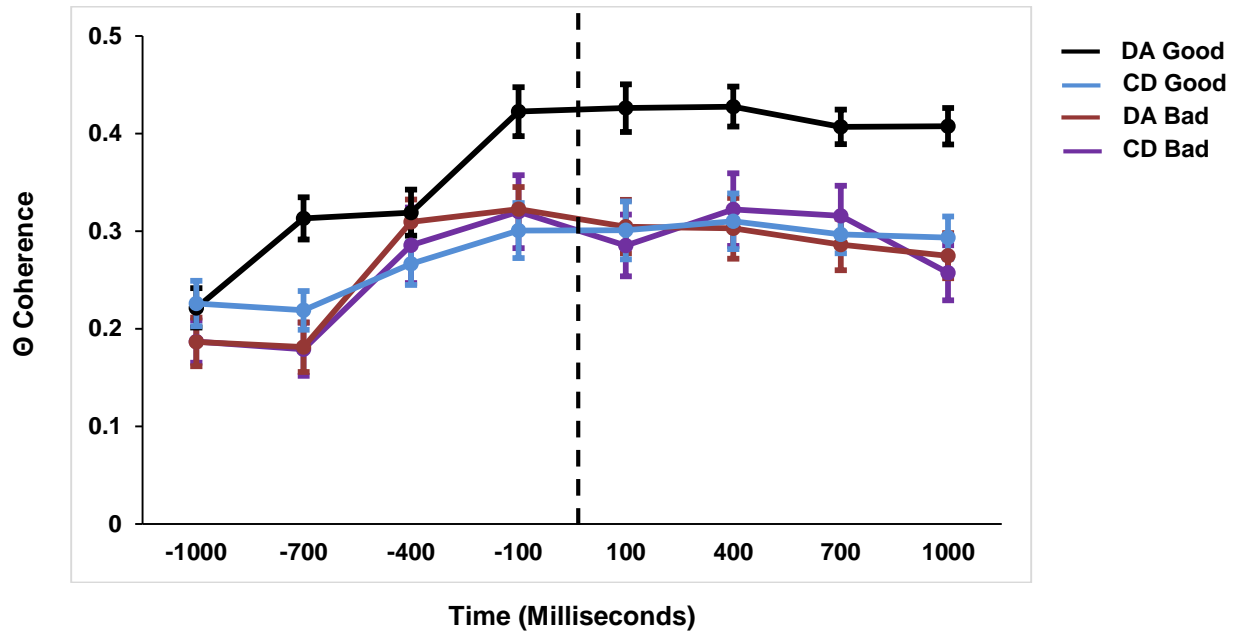


Figure 6.5. Theta Coherence During Choice Point Traversals

Theta coherence as the rat moves through the choice point is higher during good DA epochs (black line), as compared to good CD epochs (blue-grey), bad DA epochs (orange), and bad CD epochs (purple). Dashed line indicates choice point entry (time 0).

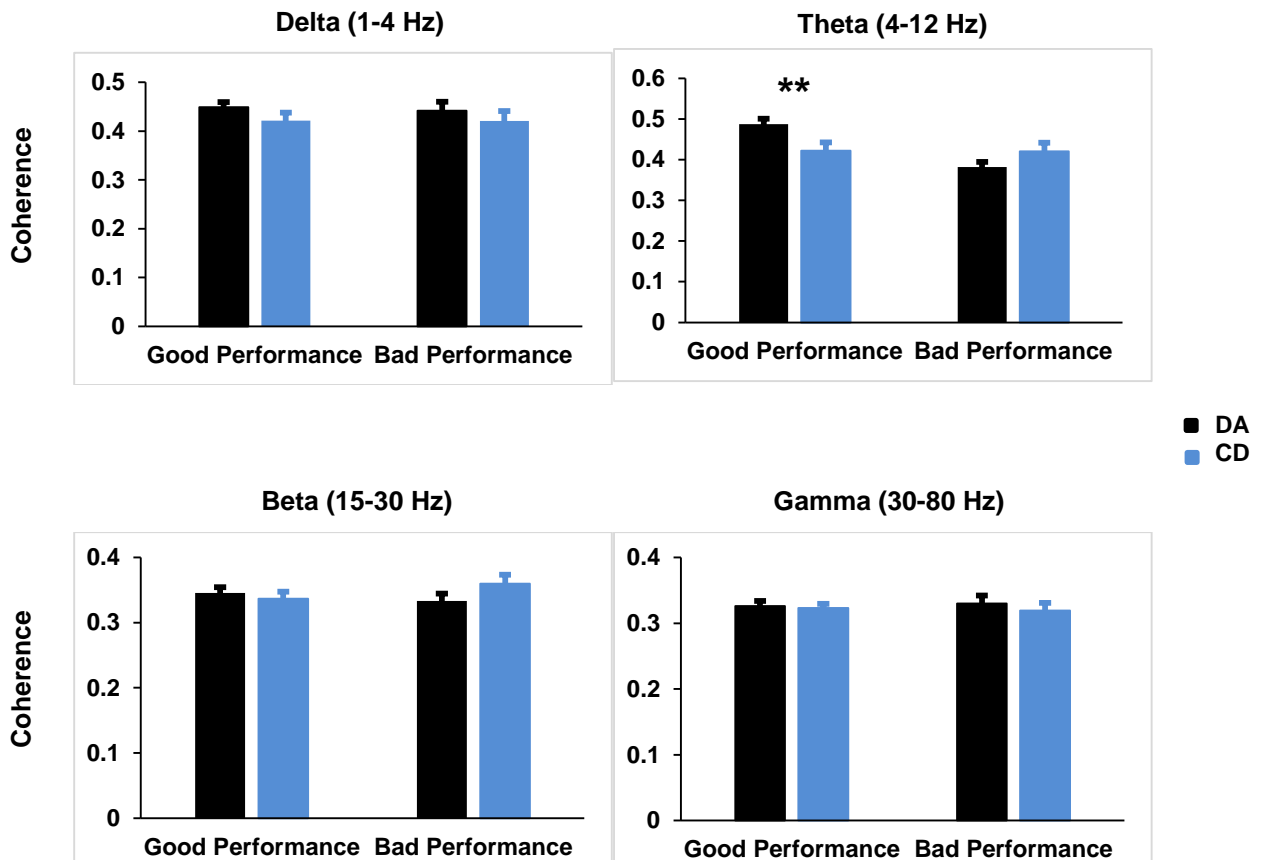


Figure 6.6. Choice Point Coherence Across Frequency Bands

Theta coherence at the maze choice point is significantly higher during good DA epochs than during good CD epochs. Coherence differences between epochs are specific to the theta frequency band. ** $p < .01$. Error bars = SEM.

These results suggest that theta coherence at the maze choice point is strongly tied to a spatial working memory performance.

6.3.5: Phase-Amplitude Coupling

Phase-amplitude coupling between theta and gamma oscillations at the maze choice point was also tied to spatial working memory. Wilcoxon rank-sum tests revealed that MI values within the mPFC at the maze choice point were significantly higher during DA good than CD good sessions ($p < .001$). This was also true for theta-gamma coupling between the hippocampus and mPFC ($p < .001$). Theta-gamma coupling within the hippocampus was not significantly different between good DA and good CD epochs ($p = .44$) (see Figure 6.8). The same Wilcoxon rank-sum tests revealed no significant differences between good DA and good CD epochs, nor between bad DA and bad DA epochs, for any other point on the maze for any brain region ($p > .05$ in all cases).

6.4: Discussion

We predicted that signatures of hippocampal-prefrontal synchrony would be higher during the working memory-dependent DA task as compared to the non-working memory-dependent CD task. In support of this prediction, the entrainment of single units in the mPFC to hippocampal theta oscillations was significantly lower during the CD task as compared to the DA task. Furthermore, theta coherence and theta-gamma coupling between the hippocampus and mPFC while the rat moved through the maze choice point were lower during CD than during DA. Strikingly, differences in entrainment, phase coherence, and theta-gamma

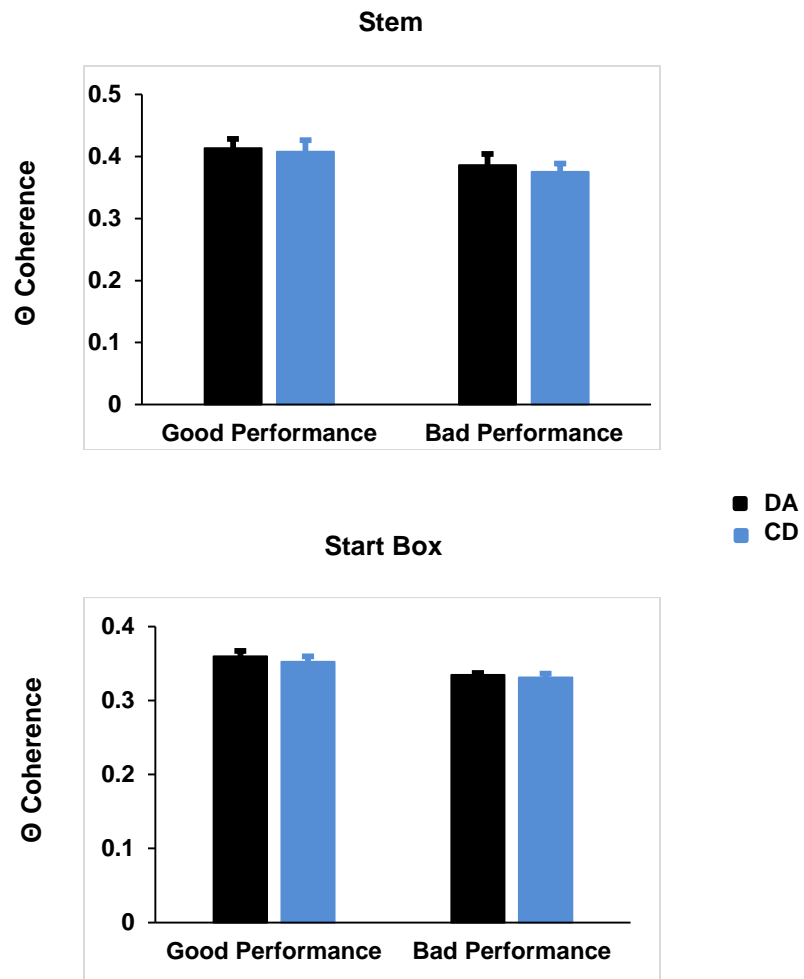


Figure 6.7. Theta Coherence Across Maze Locations

Theta coherence differences are not seen on the maze stem (top) or start box (bottom).

coupling were only observed when the rat performed both tasks well. This result strongly implicates hippocampal-prefrontal synchrony in spatial working memory by showing that levels of hippocampal-prefrontal synchrony are tied to performance during a working memory-dependent task. One possible explanation for decreases in single unit entrainment during CD performance is that decreases in overall firing rate during the inter-trial interval period biased spike-phasedistributions toward uniform distributions. However, firing rate differences between epochs were accounted for during MRL analyses by randomly subsampling spike-phase distributions to create MRL values that were based on bootstrapped distributions. Further evidence against the possibility that firing rate differences influenced entrainment results are presented in chapter 7. Past research has shown that hippocampal-prefrontal synchrony correlates with spatial working memory-specific task performance (Jones & Wilson, 2005; Hyman et al., 2010; Sigurdsson et al., 2010; O'Neill et al., 2013). These results provide an important contribution to the literature by showing that hippocampal-prefrontal synchrony increases during the successful performance of a working memory task that has been shown to be dependent upon dorsal hippocampal (Hallock et al., 2013a) and ventral midline thalamic (chapter 5 of this dissertation) function, while simultaneously showing that hippocampal-prefrontal synchrony is lower during the successful performance of a task that is not dependent on hippocampal (Hallock et al., 2013a), ventral midline thalamic (Hallock et al., 2013b), or mPFC (Shaw et al. 2013) function. Therefore, these results demonstrate a complimentary

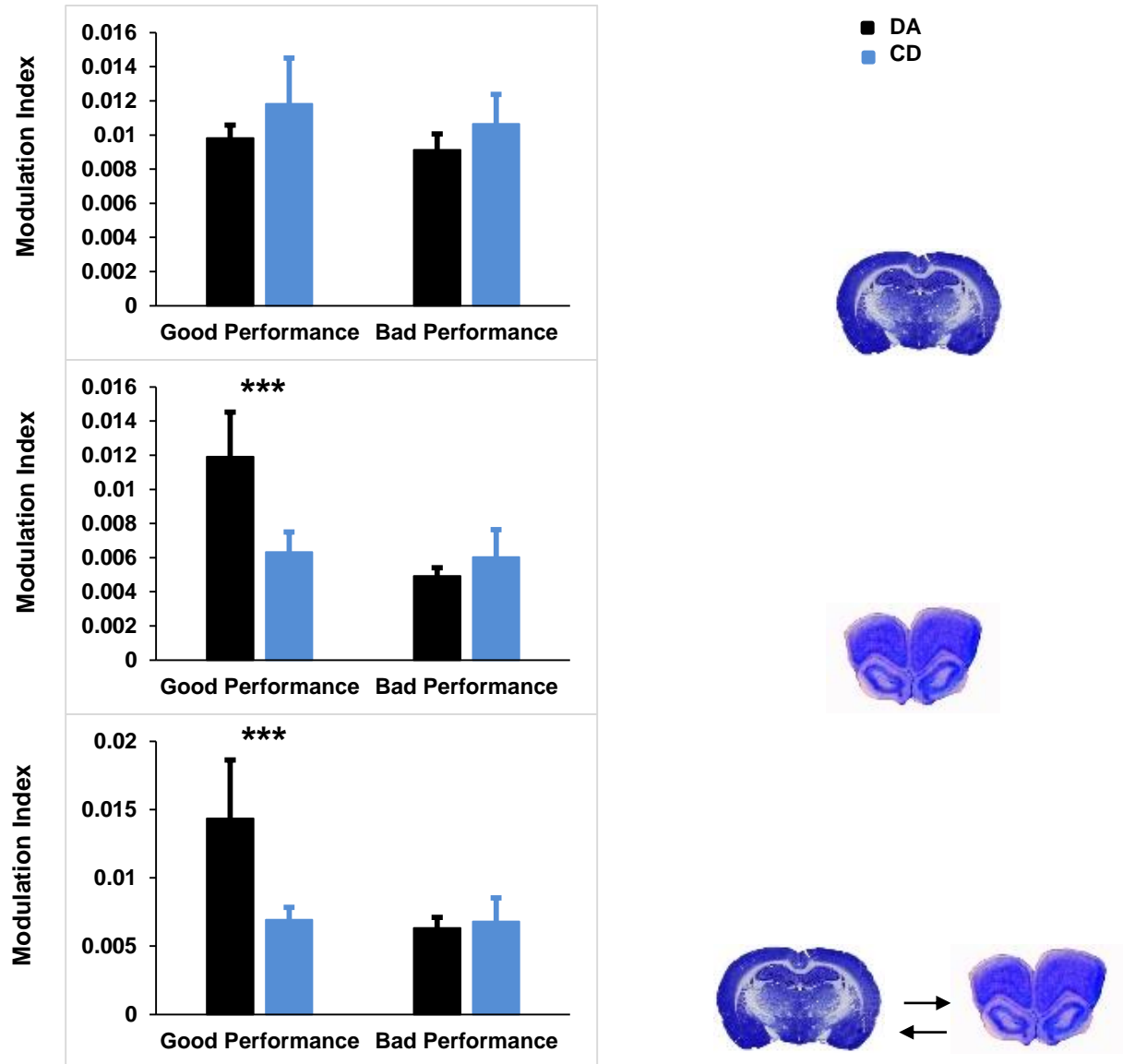


Figure 6.8. Phase-Amplitude Coupling at the Choice Point

Theta-gamma coupling at the choice point within the mPFC (middle panel) and between the hippocampus and mPFC (bottom panel) is significantly higher during good DA epochs as compared to good CD epochs. Theta-gamma coupling within the hippocampus (top panel) does not significantly differ between epochs. ** $p < .01$. Error bars = SEM.

relationship between neuropsychological and electrophysiological data for this task. Furthermore, these results demonstrate that different forms of hippocampal-prefrontal synchrony are tied to different locations on the maze, suggesting that different types of hippocampal-prefrontal synchrony are representative of distinct cognitive operations throughout the memory-guided decision making process. Previous research in primates has demonstrated that single units in the lateral PFC increase their firing rates during the delay period of spatial working memory tasks (“delay cells”; Fuster et al., 1982). Similarly, we found that firing rates of prefrontal pyramidal neurons were higher during the delay period of the working memory-dependent DA task than during the inter-trial interval period of the non-working memory-dependent CD task. This result provides a possible correlate of the primate “delay cell” in rodents. Previous research in rodents has failed to find such a correlate, possibly because delay period activity was not systematically examined (Jung et al., 1998), or because a true delay period was not given (For example, Baeg et al., (2003) only examined activity while rats consumed a reward on the stem of a figure-8 maze in between trials).

Alternatively, differences in mPFC population firing rates observed between DA and CD inter-trial interval periods could be a reflection of the need to reduce interference between tasks that take place in identical contexts, an operation for which the prefrontal cortex is necessary in both humans (Incisa della Rocchetta and Milner, 1993; Smith et al., 1995) and rodents (Granon et al., 1994; Peters et al., 2013). One argument against this interpretation, however, is that firing rate

differences between tasks were only seen during the inter-trial interval period, indicating that neuronal populations in the mPFC are particularly tied to the time period during which working-like memory is presumably taking place during the DA task.

“Ramping” and “decay” activity were uncommon among the recorded population of neurons, and this type of activity was not task-dependent. This result contradicts the theory that increases or decreases in prefrontal firing rates signal the passage of time between stimulus offset and decision making in working memory tasks (Lewis & Miall, 2006). Rather, the results support the hypothesis that population firing rates in the mPFC, and interactions between the PFC and other brain regions, are both necessary for spatial working memory.

In conclusion, the results of this study implicate hippocampal-prefrontal synchrony in spatial working memory, and further characterize delay-specific (entrainment) and decision-specific (phase coherence, phase-amplitude coupling) correlates of working memory-guided decision making. Since the dorsal hippocampus and mPFC are not directly connected with one another (Swanson, 1981; Ferino et al., 1987), one large question that looms is how functional connectivity can be observed between the two brain areas. One candidate brain area that has received increased attention is the ventral midline thalamic reuniens and rhomboid (RE/Rh) nuclei, which are reciprocally connected with both the dorsal hippocampus and mPFC. The relationships between RE/Rh function,

hippocampal-prefrontal synchrony, and spatial working memory are further investigated in chapter 7 of the thesis.

Table 6.1: Distribution of Pyramidal Neurons Across Rats and Session Types

Rat	# Sessions Total	# Good Performance Sessions	# DA Bad Sessions	# CD Bad Sessions
1202	19 Neurons: 158	12 Neurons: 107	5 Neurons: 24	2 Neurons: 27
1203	21 Neurons: 158	11 Neurons: 98	6 Neurons: 26	4 Neurons: 34
1206	8 Neurons: 86	1 Neurons: 11	3 Neurons: 25	4 Neurons: 50
1302	2 Neurons: 0	1 Neurons: 0	1 Neurons: 0	0 Neurons: 0
1305	4 Neurons: 0	3 Neurons: 0	0 Neurons: 0	1 Neurons: 0

Chapter 7

EXPERIMENT 3: ROLE OF RE/RH IN HIPPOCAMPAL-PREFRONTAL SYNCHRONY AND SPATIAL WORKING MEMORY

7.1: Introduction

Rhythmic activity in populations of neurons gives rise to oscillatory activity in the brain's local field potential (LFP) (Buzsaki, 2006). Oscillatory synchrony between LFPs in disparate brain areas is thought to underlie memory processing in mammals by facilitating communication between regions that are important for information encoding, consolidation, and retrieval (Fell & Axmacher, 2011). In particular, the hippocampal theta oscillation synchronizes with oscillatory activity in many brain regions during memory-guided behavior, including the entorhinal cortex (Yamamoto et al., 2014), orbitofrontal cortex (Young & Shapiro, 2011), ventral striatum (van der Meer & Redish, 2011; Lansink et al., 2012), amygdala (Seidenbecher et al., 2003), and medial prefrontal cortex (mPFC) (Siapas et al., 2005; Hyman et al., 2005; Jones & Wilson, 2005; Hyman et al., 2010; Benchenane et al., 2010; Kim et al., 2011; O'Neill et al., 2013). Phase synchrony between the hippocampus and mPFC in rodents has been hypothesized to underlie spatial working memory (Colgin, 2011; Gordon, 2011), and complimentary lines of research have supported this hypothesis by showing that

pharmacological disconnection of the mPFC from the hippocampus results in spatial working memory impairments (Lee & Kesner, 2003; Churchwell et al., 2011). Phase synchronization between the PFC and medial temporal lobe is also correlated with working memory performance in humans (Sarnthein et al., 1998; Serrien et al., 2004; Kopp et al., 2006; Payne & Kounious, 2009), suggesting that hippocampal-prefrontal synchrony may be important for promoting spatial working memory across mammalian species. Furthermore, decreases in hippocampal-prefrontal synchrony parallel spatial working memory deficits in both human schizophrenic patients (Lawrie et al., 2002; Meyer-Lindenberg et al., 2006) and a genetic mouse model of schizophrenia (Sigurdsson et al., 2010). These results highlight the potential therapeutic importance of understanding how the hippocampus and prefrontal cortex communicate with one another during working memory-guided behavior, which may provide crucial insight into the cognitive symptoms that accompany neuropsychiatric diseases and disorders.

Although hippocampal-prefrontal synchrony has been observed during spatial working memory tasks in rodents (Jones & Wilson, 2005; Hyman et al., 2010; O'Neill et al., 2013), the mechanisms that underlie this synchrony are not well understood. The mPFC receives direct inputs from the ventral hippocampus, but none from the dorsal hippocampus (Swanson, 1981; Ferino et al., 1987; Jay et

al., 1992). The reuniens and rhomboid nuclei (RE/Rh) of the ventral midline thalamus have been hypothesized to be mediators of hippocampal-prefrontal synchrony, based on efferent and afferent projections with both the mPFC and dorsal hippocampus (Vertes, 2006; Vertes et al., 2007). In support of this hypothesis, pharmacological inactivation of RE/Rh produces performance deficits in spatial working memory tasks (Hembrook & Mair, 2011; Hembrook et al., 2012; Hallock et al., 2013a). RE/Rh may therefore contribute to spatial working memory by orchestrating hippocampal-prefrontal interactions; however, this notion has not been directly tested. In the current study, we trained rats on a spatial working memory-dependent delayed alternation (DA) task that is dependent on the functional integrity of the dorsal hippocampus (Hallock et al., 2013b). We then recorded directly from populations of neurons in the mPFC and dorsal hippocampus both before and after pharmacological inactivation of RE/Rh while rats performed the DA task. We predicted that inactivation of RE/Rh would produce performance impairments in the DA task, and that these performance impairments would be accompanied by decreases in hippocampal-prefrontal synchrony.

7.2: Materials and Methods

Seven rats were included in analyses for this experiment based on histological confirmation of tetrode tracks in mPFC and dorsal hippocampus, as well as internal cannula tracks in RE/Rh. Behavioral training and surgical procedures were performed as outlined in chapter 4.

7.2.1: Experimental Design

Following recovery from surgery, rats were re-trained on the DA task until they reached pre-surgical levels of performance (at least 80% correct for two consecutive sessions). Hippocampal tetrodes were advanced into the dorsal hippocampal fissure, as evidenced by large-amplitude theta oscillations in the LFP. Prefrontal tetrodes were advanced into the mPFC until well-isolated clusters (at least a 3:1 signal to noise ratio) were able to be recorded. Once the rat was performing the DA task at pre-surgical levels, single units were observed on at least three out of seven prefrontal tetrodes, and high-amplitude theta was observed in the hippocampal LFP, recording sessions began. Each recording session consisted of a baseline epoch, consisting of 18 trials of the DA task. Directly following the baseline epoch, each rat received one of three treatments. For *no-infusion* sessions, rats were simply placed into their home-cages for 40 minutes. For *saline* sessions, rats were given an infusion of PBS into RE/Rh and placed into

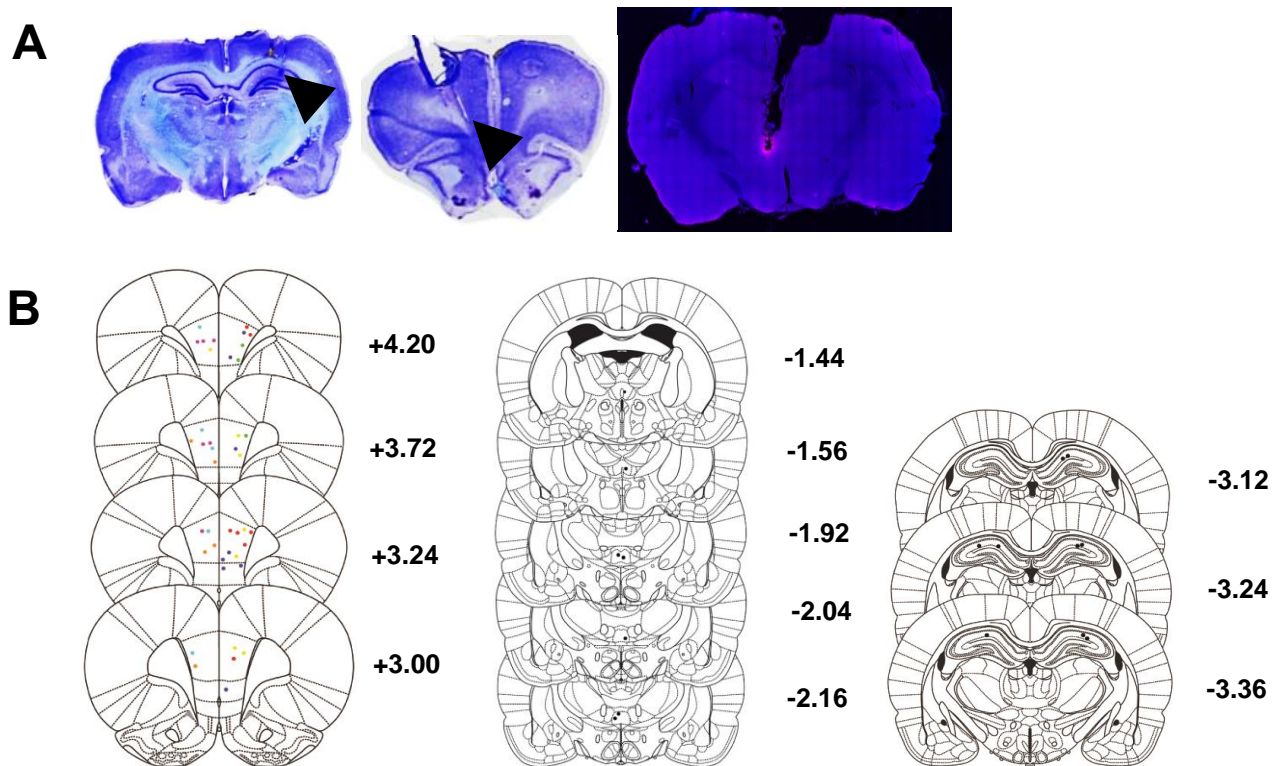


Figure 7.1. Histology

(A) Example histology from one rat. Coronal sections stained with cresyl-violet show the locations of tetrode tips in the mPFC (middle) and dorsal hippocampal fissure (left; black arrows). A coronal section that was counter-stained with DAPI shows the spread of fluorescent muscimol from the tip of the internal cannula in the ventral midline thalamus (right). **(B)** Coronal sections showing placements of tetrode tips in the mPFC (left panel; each color represents an individual rat), placements of internal cannula tips in the ventral midline thalamus (middle panel), and placements of tetrode tips in the dorsal hippocampus (right panel) for all rats.

their home-cages for 30 minutes (see chapter 4 for detailed infusion procedures). For *muscimol* sessions, rats were given an infusion of 0.25 $\mu\text{l}/\mu\text{g}$ of muscimol and placed into their home-cages for 30 minutes. Following treatment, a testing epoch took place which consisted of an additional 18 trials of the DA task. Session order was counterbalanced across rats. Each rat had one session (consisting of baseline and testing epochs) per day on consecutive days. After all three recording sessions had been given, rats were perfused for histological confirmation of cannula and tetrode placements (detailed procedures in chapter 4).

7.2.2: Data Analysis

Detailed analysis procedures are given in chapter 4 of the dissertation. Briefly, prefrontal clusters were isolated offline using SpikeSort 3D (Neuralynx). The events of interest for each trial were calculated with custom MATLAB functions (see Appendix for a complete list of code), and choice accuracy, time spent at the choice point, and the velocity of stem traversals were calculated for each trial and averaged across trials for each rat using custom MATLAB functions. Choice accuracy, time spent at the choice point, and stem velocity were compared between sessions with 2 (epoch) x 3 (session) repeated-measures ANOVAs. Choice accuracy, time spent at choice point, and stem velocity were further normalized across epochs by subtracting the baseline value from the testing value

for each session. One-sample t-tests were used to test the null hypothesis that normalized values were not significantly different from zero. Session-averaged firing rates were calculated for each prefrontal single unit, and putative pyramidal neurons were distinguished from putative interneurons based on firing rate profiles and waveform parameters (described in chapter 4). For each putative pyramidal neuron, firing rates were calculated for different positions along the maze (start box, stem, choice point) and compared between epochs using 2 (epoch) x 3 (maze location) repeated-measures ANOVAs. Firing rates during delay periods were further compared between epochs with Wilcoxon rank-sum tests. Based on results from chapter 6, as well as research in primates showing that increased firing rates in prefrontal neurons are linked with delay period activity in working memory tasks (Fuster et al., 1982), we predicted that RE/Rh inactivation would cause global decreases in firing rate in populations of mPFC neurons. For each prefrontal unit, delay period spikes were isolated and changes in firing rate across time during start box occupancy were analyzed with a Poisson-corrected general linear model (see chapter 4). This was done in order to test the hypothesis that linear increases or decreases in firing rate over time signal information maintenance during working memory tasks (Lewis & Miall, 2006). Single-unit entrainment to the hippocampal theta oscillation was analyzed for each prefrontal unit during start box occupancy, and each unit was assigned a mean resultant vector length and Rayleigh's z-statistic. Entrainment was only analyzed for delay period spikes, as most prefrontal units produced an insufficient number of spikes for reliable

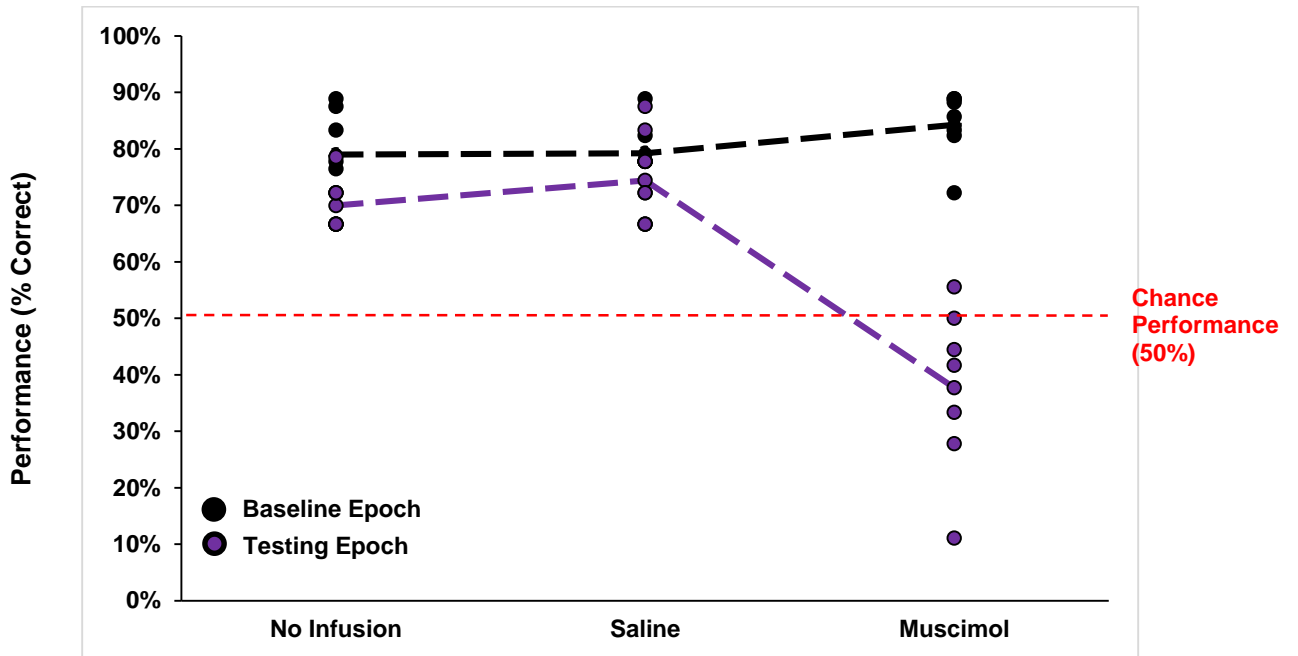


Figure 7.2. Choice Accuracy During the DA Task

Muscimol infusions into RE/Rh significantly impaired choice accuracy on the DA task, as compared to no infusion and saline sessions (individual dots are equal to individual rats).

statistical analysis during stem traversal and choice point occupancy. Mean resultant vector length was collapsed across neurons for each epoch, and epochs were compared within each session with Wilcoxon rank-sum tests. Distributions of Rayleigh's z-statistic values were created for each epoch, and z-statistic distributions were compared between epochs with Kolmogorov-Smirnov tests. For power analyses, Chronux toolbox routines were used to extract power from the hippocampal and prefrontal LFPs for four frequency bands: Delta (0-4 Hz), theta (4-12 Hz), beta (15-30 Hz), and slow gamma (30-80 Hz). Power within each frequency band for each LFP was extracted for each trial and averaged across trials for start box, maze stem, and choice point occupancy. Power in each frequency band for the muscimol session was further calculated for three distinct segments of the maze stem (early, mid, and late), as well as the reward arm, yielding power values for five different maze segments (early stem, mid-stem, late stem, choice point, and reward arm). Theta power was compared between muscimol baseline and testing epochs with a repeated-measures ANOVA for both the hippocampus and mPFC. Phase coherence was analyzed in a similar manner to power, with coherence extracted within each frequency band using Chronux routines. A repeated-measures ANOVA was used to compare theta coherence between muscimol epochs. A repeated measures ANOVA was used to compare coherence across frequency bands at the maze choice point during muscimol sessions. Finally, a repeated measures ANOVA was used to compare theta coherence at the

maze choice point across sessions. Theta coherence scores at the maze choice point were also normalized by subtracting the baseline coherence score from the testing coherence score for each session, and using one-sample t-tests on each normalized coherence score. For phase-amplitude coupling, a modulation index value was calculated for theta and slow gamma oscillations for hippocampal theta-prefrontal gamma coupling, hippocampal theta-gamma coupling, and prefrontal theta-gamma coupling. Modulation index (MI) scores were calculated for each maze position for each epoch for each brain region. MI scores were compared across sessions within each maze location and each brain region using repeated-measures ANOVAs. For the muscimol session, a repeated-measures ANOVA was used to compare MI values between epochs and across maze locations. MI scores were further normalized between baseline and testing epochs, and analyzed with one-sample t-tests. The optimal gamma frequency for theta phase was calculated by creating an MI value for each theta-gamma frequency pair, normalizing MI values for each gamma frequency between baseline and testing sessions, and comparing normalized values across sessions. Optimal theta phase for gamma amplitude was assessed by using Morlet wavelet analysis to extract phase and power information from each LFP and comparing normalized amplitude values across theta phase bins for each gamma frequency. All analysis methods are described in greater detail in chapter 4, and all code is provided in the Appendix.

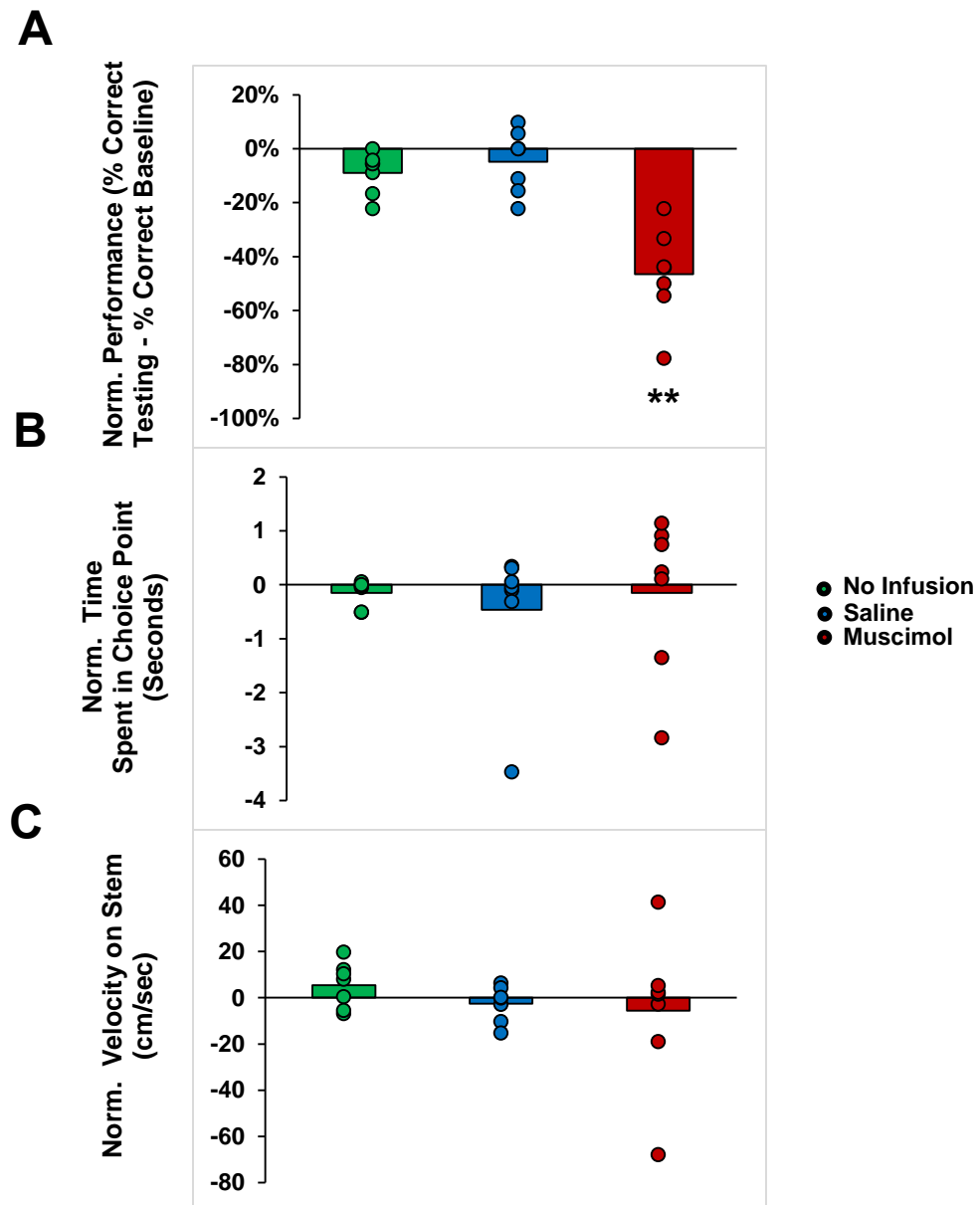


Figure 7.3. Behavior Across Sessions

(A) Normalized choice accuracy (testing epoch score – baseline epoch score) was significantly lower than zero for muscimol sessions only (** $p < .01$). (B) Normalized time spent in choice point (seconds) was not significantly different from zero for any of the three sessions. (C) Normalized stem velocity (cm/sec) was not significantly different from zero for any of the three sessions.

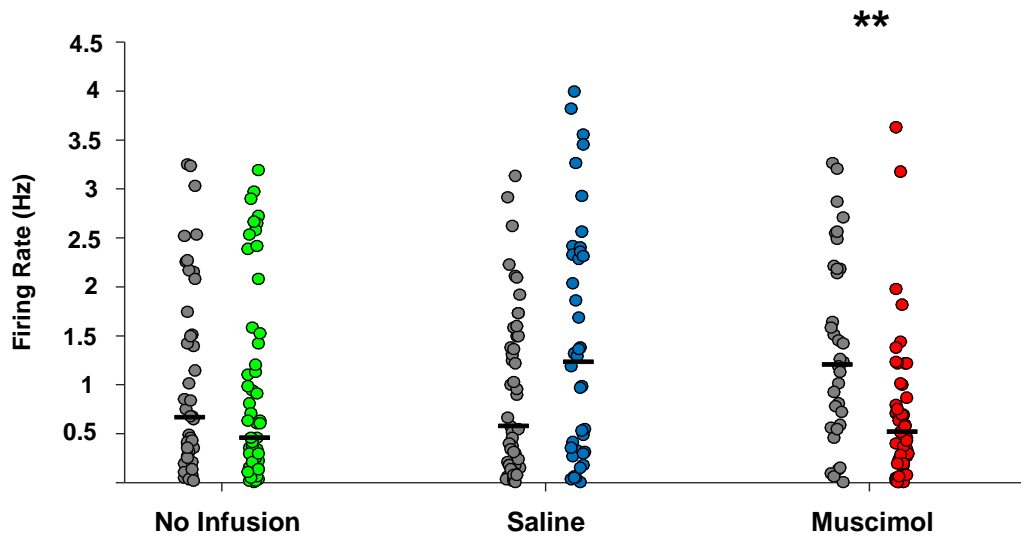


Figure 7.4. Delay Period Firing Rates Across Sessions

RE/Rh inactivation significantly decreased the firing rates of putative pyramidal neurons in the mPFC during the delay period. Each dot represents an individual pyramidal neuron. Black bars represent median firing rate (Hz). Grey dots represent baseline epochs, colored dots (green, blue, and red) represent testing epochs for the three sessions. ** $p < .01$, Wilcoxon's rank-sum test.

7.3: Results

7.3.1: Behavior

A 2 (epoch) x 3 (session) mixed-factorial ANOVA on choice accuracy (percent correct choices) revealed a significant main effect of session ($F(1,12) = 23.129, p < .001$), a significant epoch x session interaction ($F(2,24) = 41.68, p < .001$), and a significant main effect of epoch ($F(1,12) = 31.254, p < .001$) (see Figure 7.2).

Post-hoc analyses revealed that performance did not significantly differ between *no- infusion* and *saline* sessions ($p = .608$), but did differ significantly between *no- infusion* and *muscimol* sessions ($p = .002$), as well as *saline* and *muscimol* sessions ($p < .001$). This result confirms that RE/Rh are necessary for the successful performance of the spatial working memory-dependent DA task, and parallels previous studies that have demonstrated spatial working memory deficits following RE/Rh inactivation (Hembrook & Mair, 2011; Hembrook et al., 2012; Hallock et al., 2013a). Reductions in choice accuracy following muscimol infusions may be accompanied by differences in overt motor behavior on the part of the rat, such as differences in time spent on the maze stem or choice point. In order to test this possibility, time spent at the choice point and stem velocity were analyzed between sessions. A 2 (epoch) x 3 (session) ANOVA for time spent at the choice point revealed no significant main effect of session ($F(2,24) = 3.2, p = .059$), no epoch x session interaction ($F(2,24) = .114, p = .754$),

and no main effect of epoch ($F(1,12) = .648, p = .436$). Similarly, a 2 (epoch) x 3 (session) ANOVA for stem velocity revealed no main effect of session ($F(2,24) = 1.286, p = .295$), no epoch x session interaction ($F(2,24) = .419, p = .662$), and no main effect of epoch ($F(1,12) = .027, p = .872$) (see Figure 7.3b and Figure 7.3c). Taken together, these results indicate that muscimol infusions did not affect overt behavior on the maze, even though choice accuracy was severely disrupted.

7.3.2: Prefrontal Firing Rates

For *no-infusion* sessions, a total of 99 well-isolated putative pyramidal neurons from the mPFC were included in analyses (44 neurons for baseline epoch; 55 neurons for testing epoch; see Table 7.1 for distribution of neurons across rats). For saline sessions, a total 90 putative pyramidal neurons were included (50 for baseline epoch; 40 for testing epoch), and for muscimol sessions, a total of 81 putative pyramidal neurons were included (36 for baseline; 45 for testing). For delay period firing rates, Wilcoxon rank-sum tests revealed no difference between no infusion baseline and testing epochs ($p = .43$), no significant difference between saline baseline and testing epochs ($p = .07$), and a significant drop in firing rate between muscimol baseline and testing epochs ($p = .003$) (see Figure 7.4). The same analyses were performed on only prefrontal single units that were included in entrainment analyses (emitted > 50 total spikes during epoch delay periods), and again revealed no significant difference in firing rate between no infusion baseline and testing epochs ($p = .64$), but did reveal a significant increase in median firing rate from saline baseline to saline testing epochs ($p = .04$), as well as a significant

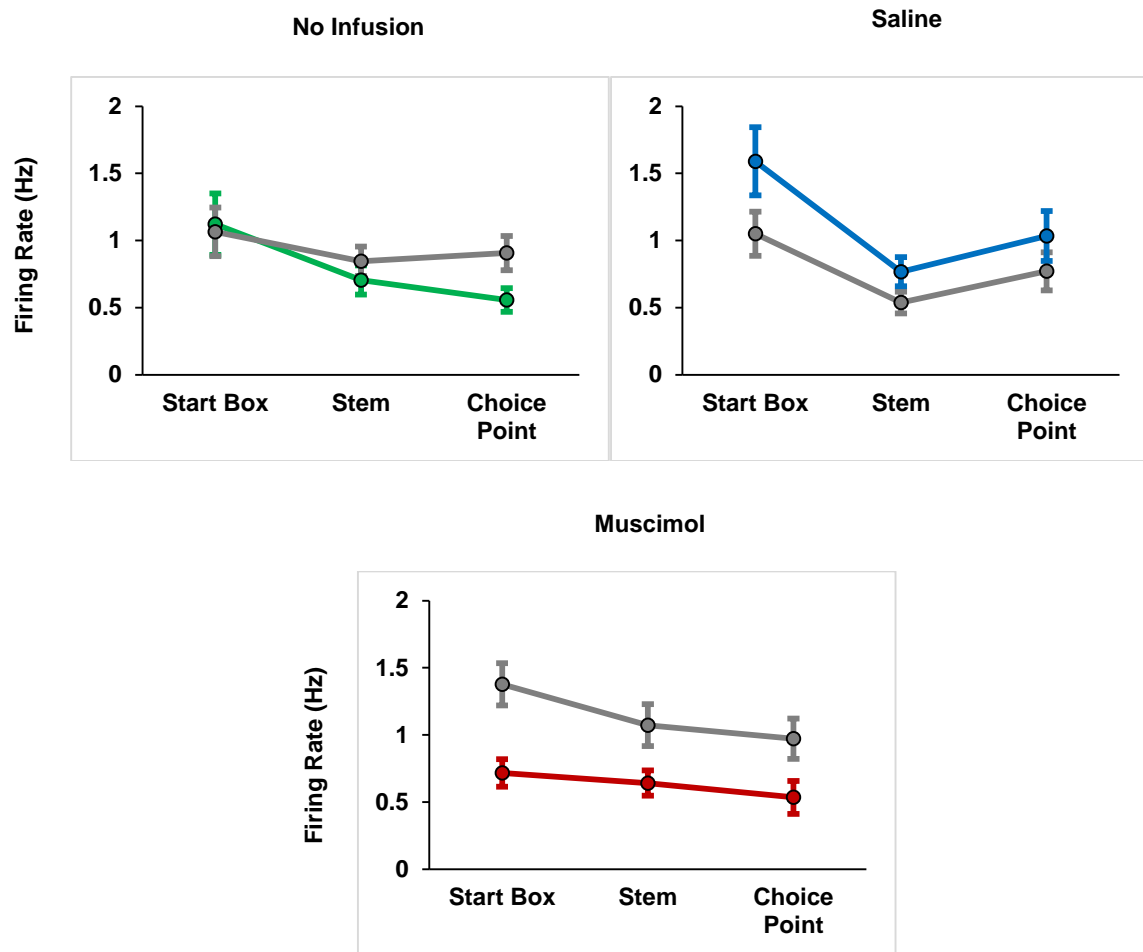


Figure 7.5. mPFC Firing Rates Across Maze Locations

Mean firing rates of mPFC pyramidal neurons as a function of epoch and maze location. Muscimol infusions significantly reduced mean firing rate across all maze locations. Grey lines represent baseline epochs, colored lines represent testing epochs. Errors bars = SEM.

decrease in median firing rate from muscimol baseline to testing epochs ($p < .001$). Within each session, 2 (epoch) x 3 (maze location) ANOVAs were used to compare mean firing rates between the delay pedestal, maze stem, and choice point. An ANOVA for the no infusion session revealed a significant effect of maze location ($F(2,188) = 5.616, p = .004$), no epoch x location interaction ($F(2,188) = 1.629, p = .199$), and no effect of epoch ($F(1,94) = .099, p = .781$). Post-hoc analyses revealed that firing rate on the start box ($M = 1.031, SD = 1.16$) was significantly higher than firing rate on the maze choice point ($M = .74, SD = .83; p = .001$), but firing rate on the start box was not significantly different from firing rate at the maze stem ($M = .87, SD = 1.01; p = .190$), nor was stem firing rate significantly different from choice point firing rate ($p = .280$). The same analysis for the saline session again revealed a main effect of maze location ($F(2,176) = 6.871, p = .001$), but no epoch x location interaction ($F(2,176) = .102, p = .903$), and no main effect of epoch ($F(1,88) = 1.495, p = .225$). Post-hoc analyses revealed that mean start box firing rate ($M = 1.31, SD = 1.54$) was significantly higher than mean stem firing rate ($M = .82, SD = 1.02; p = .001$), but mean start box firing rate did not significantly differ from mean choice point firing rate ($M = 1.05, SD = 1.37; p = .298$). Mean stem firing rate and mean choice point firing rate did not significantly differ from one another ($p = .061$). For muscimol sessions, the ANOVA revealed a significant main effect of maze location ($F(2,154) = 3.736, p = .026$), and no epoch x maze location interaction ($F(2,154) = .114, p = .892$). However, a significant main effect of epoch was found ($F(1,77) = 7.432, p = .008$),

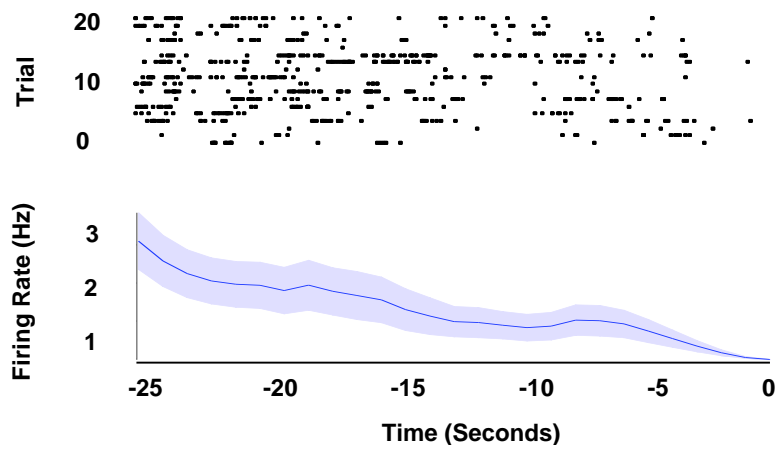
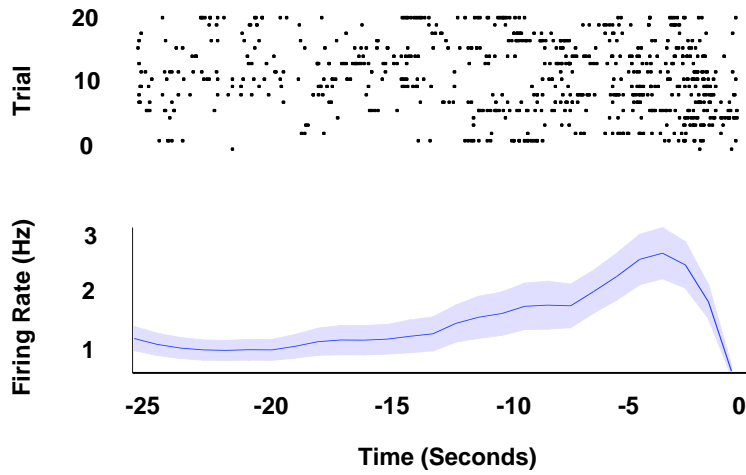
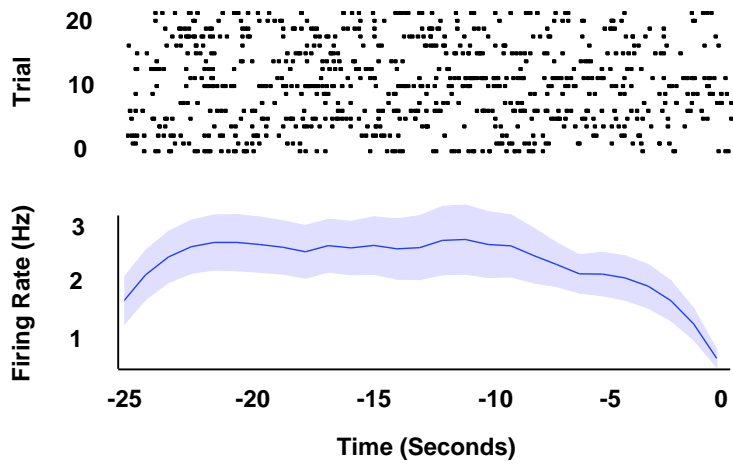


Figure 7.6. Firing Rate Over Time During the Delay Period

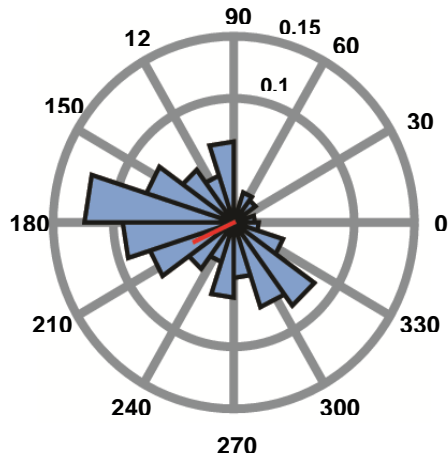
Example raster and trial-averaged firing rate plots for three pyramidal neurons during the delay period. For all three plots, time 0 at the far right of the x-axis represents start box exit. The top-most panel shows a representative neuron that did not display “ramping” or “decay” activity during the delay period, but rather showed a sustained firing rate throughout the duration of the delay. The majority of pyramidal neurons exhibited this type of delay period activity. The middle panel shows an example of a “ramping” neuron that significantly increased its firing rate as a function of time throughout the delay. The bottom-most panel shows a “decay” neuron that significantly decreased its firing rate as a function of time. “Ramping” and “decay” neurons were relatively rare in the recorded population of mPFC pyramidal neurons. Individual squares on raster plots are equal to individual spikes, shaded lines in rate plots equal SEM.

as mean firing rate during baseline epochs was significantly higher than mean firing rate during muscimol epochs. Post-hoc analyses revealed that mean firing rate on the start box ($M = .94$, $SD = .87$) was significantly higher than mean firing rate on the choice point ($M = .72$, $SD = .86$; $p = .047$), but that start box firing rate did not significantly differ from stem firing rate ($M = .84$, $SD = .94$; $p = .277$). Stem firing rate did not significantly differ from choice point firing rate ($p = .608$) (see Figure 7.5).

In order to analyze “ramping” (increases in firing rate) and “decay” (decreases in firing rate) activity during the delay period, a Poisson regression model was used with time as the predictor variable and firing rate as the outcome variable. The model was run for each single unit, and each single unit was assigned a regression coefficient and a p-value. An alpha level of .05 was used as a threshold for statistically significant “ramping” (positive regression coefficient) or “decay” (negative regression coefficient) activity. Relatively few neurons showed significant ramping or decay activity during the delay period (3/44 cells for no infusion baseline, 5/55 cells for no infusion testing, 4/50 for saline baseline, 2/40 for saline testing, 2/36 for muscimol baseline, and 3/45 for muscimol testing). Instead, most putative pyramidal neurons showed firing rates that remained elevated throughout the duration of the delay period (see Figure 7.6).

In summary, muscimol infusions into RE/Rh appeared to decrease firing rates of single units in the mPFC across all maze locations (start box, stem, and choice point). The firing rates of most single units in the mPFC remained

A



B

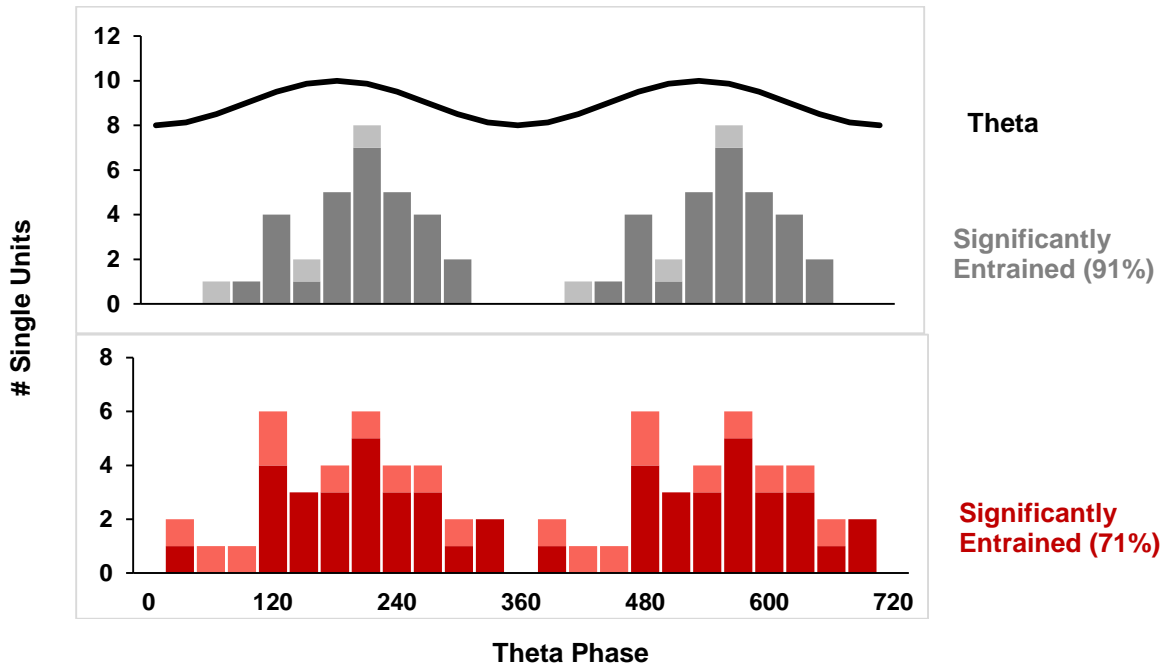


Figure 7.7. Entrainment of mPFC Single Units to Hippocampal Theta

(A) Rose plot from a representative pyramidal neuron recorded during a muscimol baseline epoch in mPFC showing significant entrainment to the hippocampal theta oscillation. Numbers on circumference are equal to theta phase (degrees), and bin height (blue bars) is equal to proportion of total spikes emitted by that neuron. The red line extending from the center of the plot is the mean resultant vector. Its direction indicates the neuron's preferred spiking phase (~205 degrees), and its length indicates magnitude of entrainment. (B) Linearized distribution of preferred spiking phases for all mPFC pyramidal neurons recorded during muscimol baseline (grey bars) and testing (red bars) epochs. Two theta cycles are included in black for reference. Y-axis represents the number of pyramidal neurons that showed a preference for each theta phase bin (x-axis). Darker colors equal significantly entrained neurons, lighter colors equal neurons that were not significantly entrained. mPFC neurons showed phase-locking that was modulated by theta peaks during baseline epochs. This phase-locking relationship was diminished following RE/Rh inactivation.

consistent across the duration of the delay period, with a small percentage of single units in each session showing firing rates that increased or decreased as a function of time while the rat occupied the start box.

7.3.3: Single Unit Entrainment

For *no-infusion* sessions, a total of 75 single units were included in entrainment analyses based on number of spikes emitted during the delay period (> 50 spikes). 72 single units were included for saline sessions, and 66 single units were included for muscimol sessions (see Table 7.2 for distribution of single units across rats and epochs). A Rayleigh's z-statistic was assigned to each single unit, and Kolmogorov-Smirnov tests revealed that z-statistic distributions did not significantly differ between *no- infusion* baseline and testing epochs ($p = .10$), nor between saline baseline and testing epochs ($p = .10$), but distributions between muscimol baseline and testing epochs were significantly different from one another ($p = .004$) (see Figure 7.8). A spike-normalized mean resultant vector length (MRL) value was calculated for each single unit in order to control for differences in number of spikes between epochs (see chapter 4 for detailed methods). Wilcoxon rank-sum tests revealed that MRL values were not significantly different between no infusion baseline and testing epochs ($p = .44$), nor were they significantly different between saline baseline and testing epochs ($p = .65$). MRL values were, however, significantly lower during muscimol testing epochs than muscimol baseline epochs ($p = .005$) (see Figure 7.9). These results confirm that RE/Rh inactivation significantly decreased the likelihood that neurons

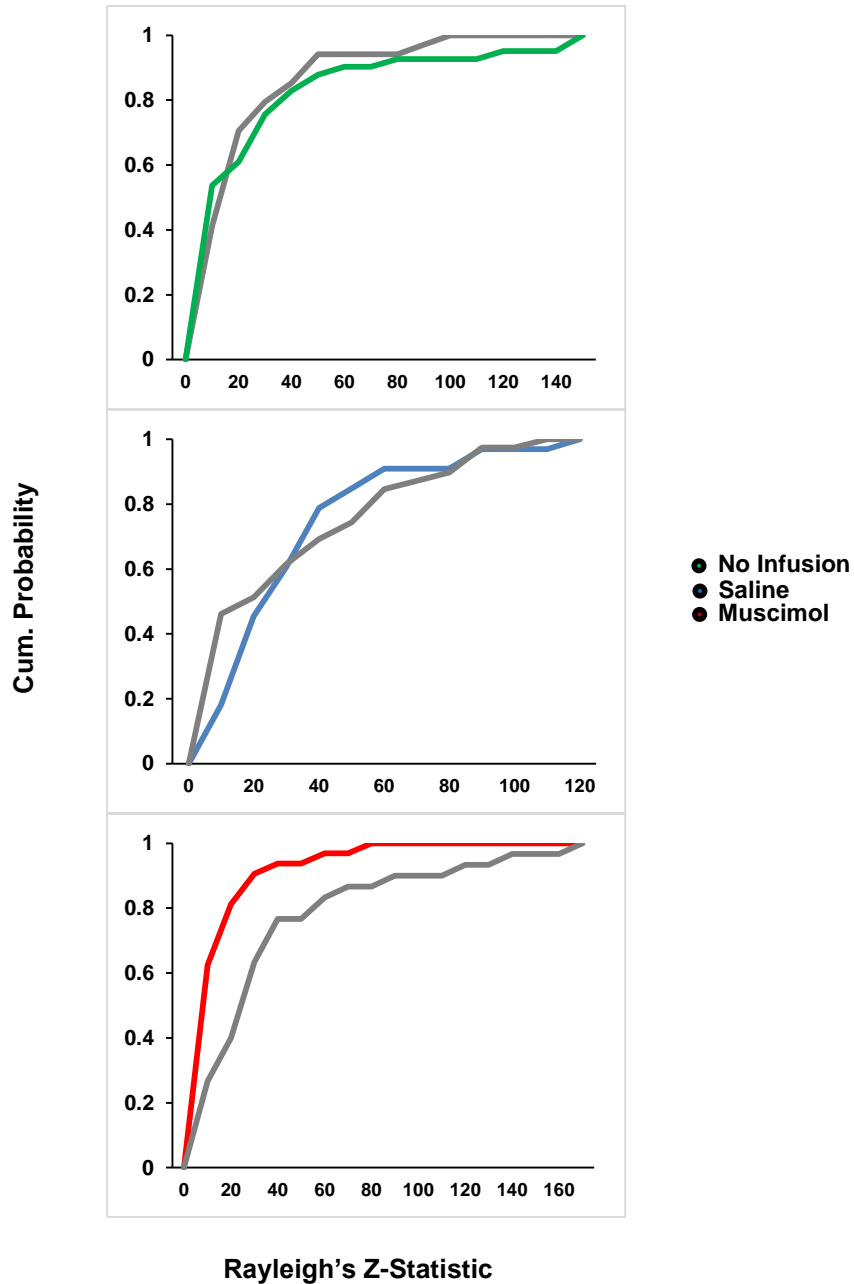


Figure 7.8. Rayleigh's Z-Statistic Distributions Across Sessions

Cumulative density plots of Rayleigh's z-statistic values (the higher the z-statistic, the higher the entrainment) for all three sessions. Distributions between baseline and testing epochs did not significantly differ for no infusion and saline sessions, but did significantly differ for muscimol sessions.

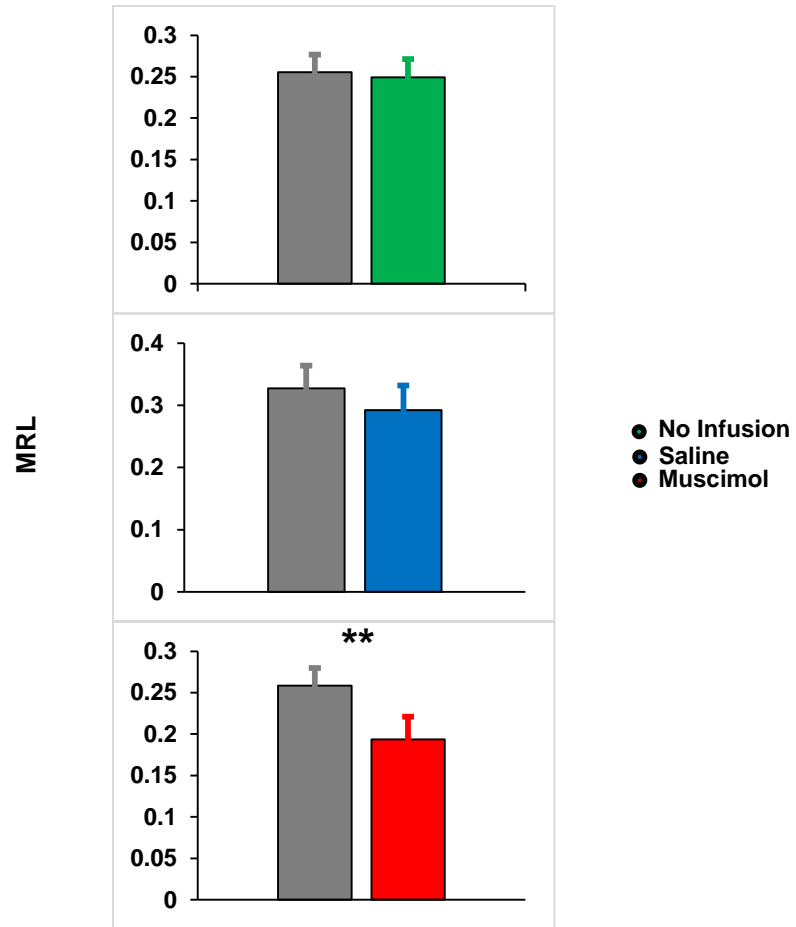


Figure 7.9. Mean-Resultant Vector Lengths Across Sessions

Subsampled mean resultant vector length (MRL) values for all sessions. RE/Rh inactivation significantly decreased MRL scores as compared to the pre-muscimol baseline epoch. ** $p < .01$, error bars = SEM.

in the mPFC would fire in phase with the hippocampal theta oscillation. It is unlikely that differences in firing rate between muscimol baseline and testing epochs influenced differences in entrainment because spike-phase distributions were subsampled in order to account for differences in number of spikes emitted between epochs. Furthermore, the median firing rate of mPFC single units was significantly increased following saline infusions, but no difference in entrainment was seen between saline baseline and testing epochs, suggesting that firing rate differences did not drive differences in single unit entrainment. The entrainment of mPFC neurons to hippocampal theta has previously been shown to increase during the choice phase of discrete-trials delayed alternation tasks in both rats (Jones & Wilson, 2005), and mice (Sigurdsson et al., 2010; O'Neill et al., 2013), suggesting that this form of hippocampal-prefrontal synchrony is important for spatial working memory.

7.3.4: Phase Coherence

Inactivation of RE/Rh significantly decreased phase coherence in the theta frequency band selectively while the rat passed through the maze choice point prior to making a reward arm decision. A 2 (epoch) x 3 (maze location) ANOVA for theta coherence during the muscimol session revealed no main effect of maze location ($F(2,24) = .023, p = .977$), no main effect of epoch ($F(1,12) = 2.79, p = .121$), and a significant epoch x maze location interaction ($F(2,24) = 4.391, p = .02$). Normalized theta coherence scores (testing coherence – baseline coherence) during the muscimol session were not significantly different from zero in the start

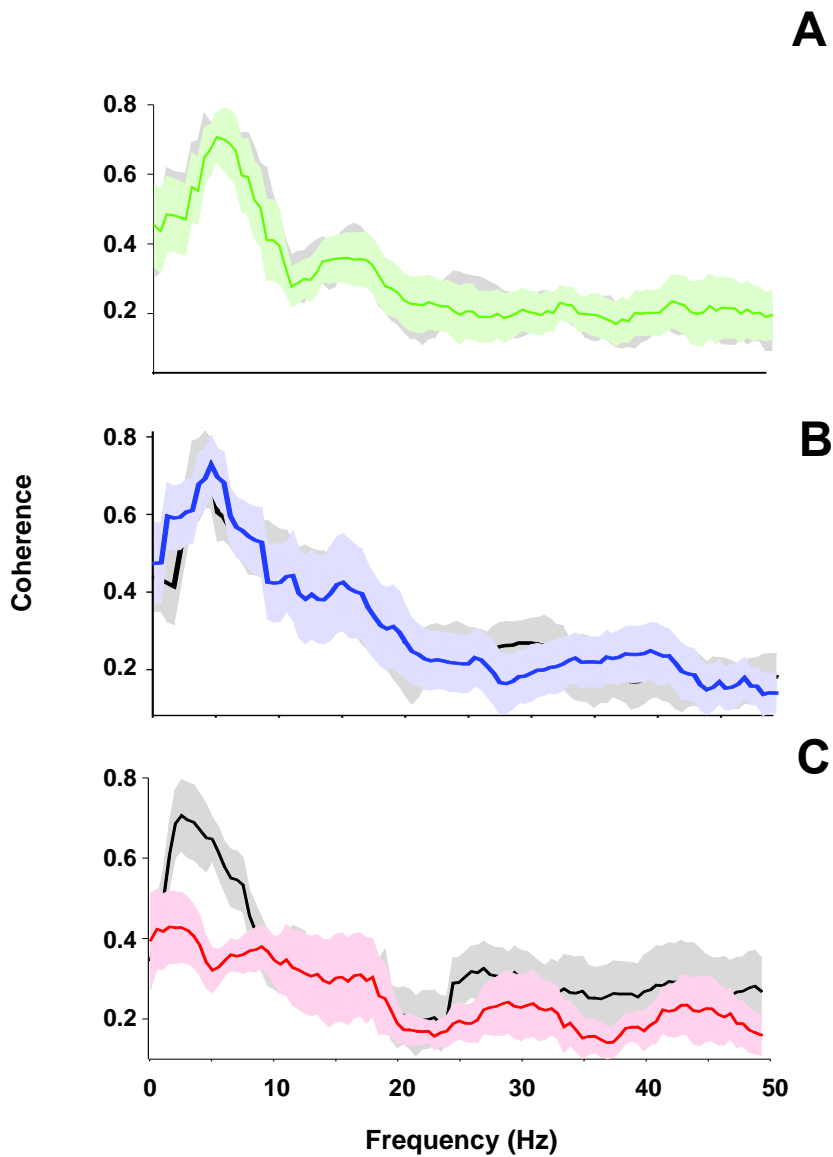


Figure 7.10. Phase Coherence at the Maze Choice Point

Phase coherence between the hippocampus and mPFC in the theta frequency band is lowered at the maze choice point following RE/Rh inactivation. Grey lines are equal to baseline epochs, colored lines are equal to testing epochs (A = no infusion session, B = saline session, C = muscimol session). Shaded lines = SEM.

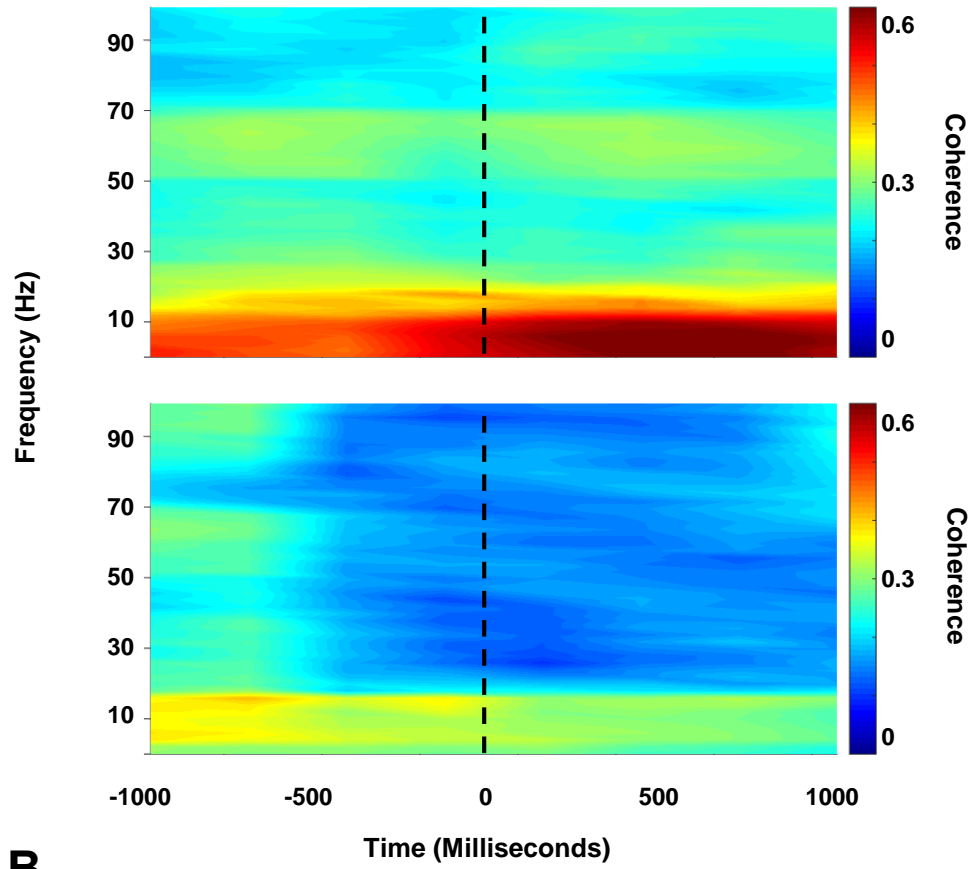
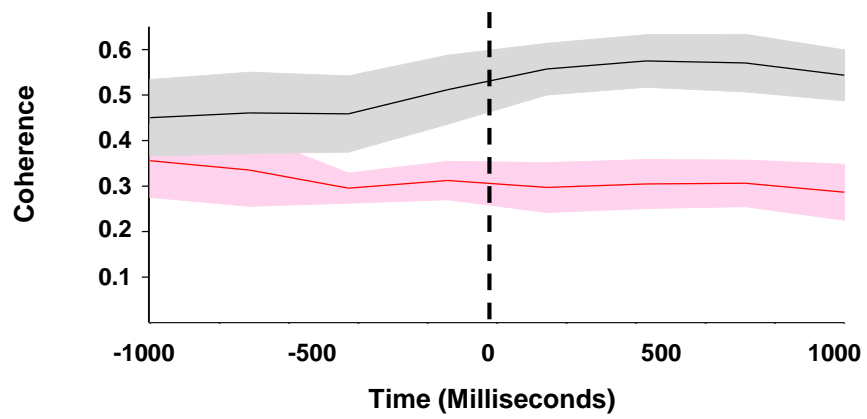
A**B**

Figure 7.11. Coherence Across Time During Choice Point Traversals

Averaged coherograms show coherence across frequency bands as a function of time as rats move through the choice point. (A) Top coherogram = muscimol baseline epochs, bottom coherogram = muscimol testing epochs. Dashed line indicates choice point entry. Note the prominent band of high coherence in the theta frequency range that appears directly following choice point entry during baseline epochs. This band of coherence is not present during muscimol testing epochs. (B) Theta coherence across time during choice point entry for muscimol sessions. Grey equals baseline epoch, red equals testing epoch. Shaded lines = SEM.

box ($M = -.018$, $SD = .04$, $t(6) = -1.08$, $p = .32$), nor were they significantly different from zero on the maze stem ($M = .008$, $SD = .05$, $t(6) = .378$, $p = .719$), but were significantly lower than zero for the choice point ($M = -.13$, $SD = .08$, $t(6) = -4.11$, $p = .006$) (see Figure 7.12b). Coherence drops following RE/Rh inactivation at the maze choice point were also selective for the theta frequency band. A 2 (epoch) x 4 (frequency) revealed a significant main effect of frequency band ($F(3,36) = 29.672$, $p < .001$), no significant epoch x frequency interaction ($F(3,36) = 2.444$, $p = .08$), and a significant main effect of epoch ($F(1,12) = 5.168$, $p = .04$). One-sample t-tests revealed that normalized delta ($M = -.08$, $SD = .12$, $t(6) = -1.723$, $p = .136$), beta ($M = -.06$, $SD = .09$, $t(6) = -1.926$, $p = .102$), and slow gamma ($M = -.03$, $SD = .07$, $t(6) = -1.124$, $p = .304$) coherence at the maze choice point for muscimol sessions were not significantly different from zero. However, normalized theta coherence ($M = -.13$, $SD = .08$, $t(6) = -4.11$, $p = .006$) was significantly lower than zero at the maze choice point (see Figure 7.12a).

Decreases in theta coherence at the maze choice point were selective for muscimol sessions. A 2 (epoch) x 3 (session) ANOVA for theta coherence revealed a main effect of session ($F(2,24) = 3.760$, $p = .038$), but no epoch x session interaction ($F(2,24) = 1.198$, $p = .319$), and no main effect of epoch ($F(1,12) = 2.711$, $p = .126$). Normalized theta coherence scores at the maze choice point were not significantly different from zero for no infusion sessions ($M = 0$, $SD = .112$, $t(6) = 0$, $p = 1$) or saline sessions ($M = -.03$, $SD = .04$, $t(6) = -1.930$, $p = .102$), but were significantly different than zero for muscimol sessions ($M = -.13$,

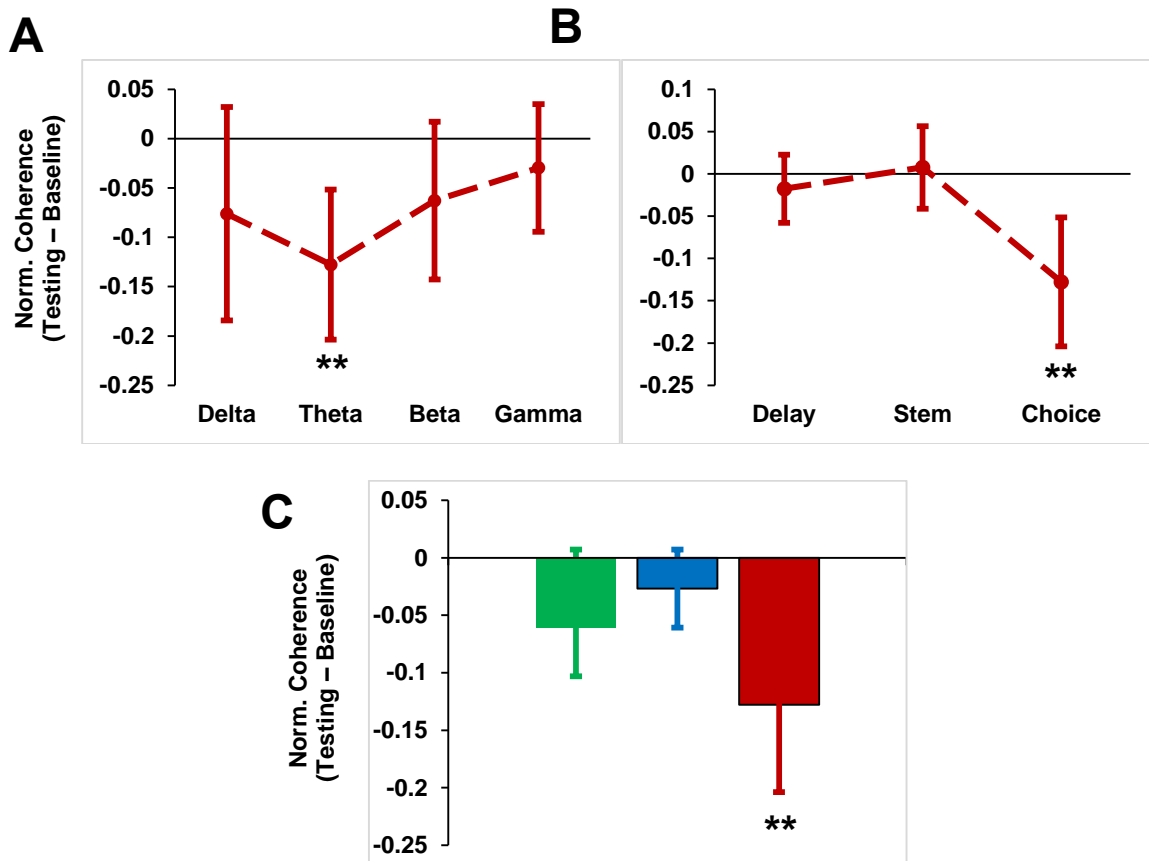


Figure 7.12. Theta Coherence Across Maze Locations and Sessions

(A) Normalized coherence (testing – baseline) across frequency bands for muscimol sessions during choice point occupancy. Normalized theta coherence is significantly different from zero. ****** $p < .01$. Error bars equal 95% confidence intervals. (B) Decrease in theta coherence following RE/Rh inactivation is specific to the maze choice point. Normalized theta coherence is significantly lower than zero only for choice point occupancy during muscimol sessions. ****** $p < .01$. Error bars equal 95% confidence intervals. (C) Normalized theta coherence at the maze choice point is significantly lower than zero only during muscimol sessions. ****** $p < .01$. Error bars equal 95% confidence intervals.

$SD = .08$, $t(6) = -4.11$, $p = .006$) (see Figure 7.12c). These results demonstrate that RE/Rh inactivation significantly decreased theta phase coherence between the hippocampus and mPFC selectively during maze choice point traversals.

7.3.5: Phase-Amplitude Coupling

Phase-amplitude coupling between theta and gamma oscillations was compared between sessions and maze locations. RE/Rh inactivation induced a selective decrease in theta-gamma coupling for slow gamma oscillations (30 – 80 Hz) while the rat traversed the maze choice point (see Figure 7.14). For investigation of theta-gamma coupling between the hippocampus and mPFC, a 2 (epoch) x 3 (session) ANOVA on MI scores revealed a main effect of session ($F(2,24) = 6.131$, $p = .007$), an epoch x session interaction ($F(2,24) = 4.601$, $p = .02$), and no effect of epoch ($F(1,12) = .579$, $p = .461$). Post-hoc analyses revealed that no-infusion MI was not significantly different from saline MI ($p = 1$) or muscimol MI ($p = .061$), but saline MI was significantly different from muscimol MI ($p = .032$). One-sample t-tests for normalized hippocampal-prefrontal theta-gamma MI score at the maze choice point revealed that no- infusion normalized MI was not significantly different from zero ($M = .001$, $SD = .003$, $t(6) = .425$, $p = .686$), nor was normalized MI for saline sessions ($M = .002$, $SD = .004$, $t(6) = 1.299$, $p = .242$). Normalized MI score for muscimol sessions was significantly lower than zero ($M = -.006$, $SD = .005$, $t(6) = -3.729$, $p = .01$), indicating that RE/Rh inactivation significantly lowered theta-gamma coupling between the

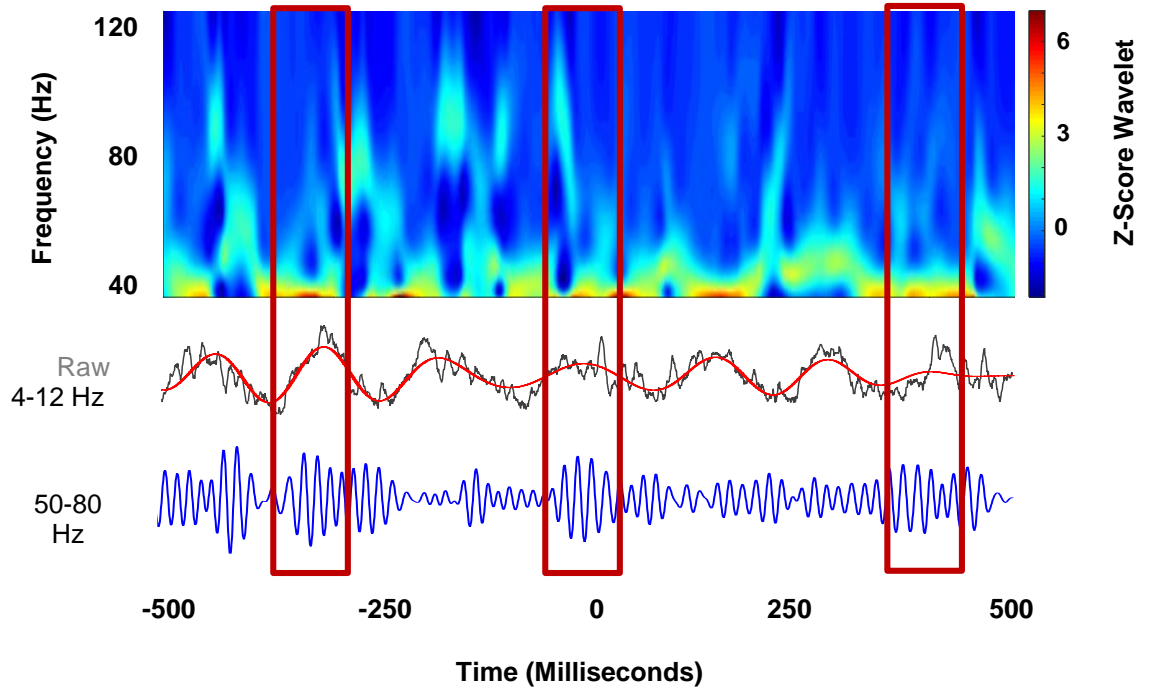


Figure 7.13. Single-Trial Schematic of Phase-Amplitude Coupling

Example of phase-amplitude coupling from one trial during choice point entry from a muscimol baseline epoch. Periods of high amplitude gamma (bottom blue trace) tend to coincide with the ascending phase of hippocampal theta peaks (middle grey and red traces). Slow mPFC gamma power is represented as heat in the top spectrogram.

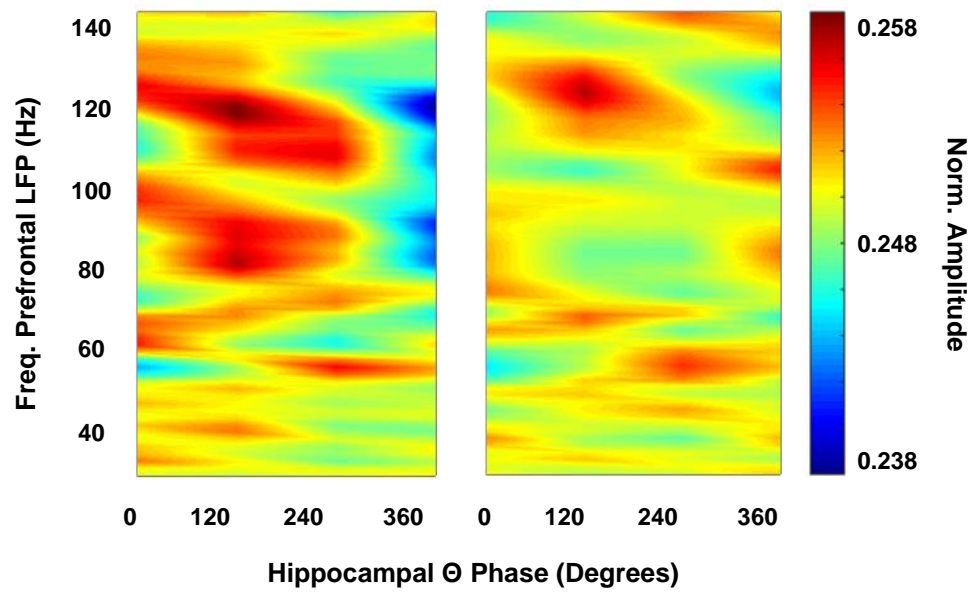
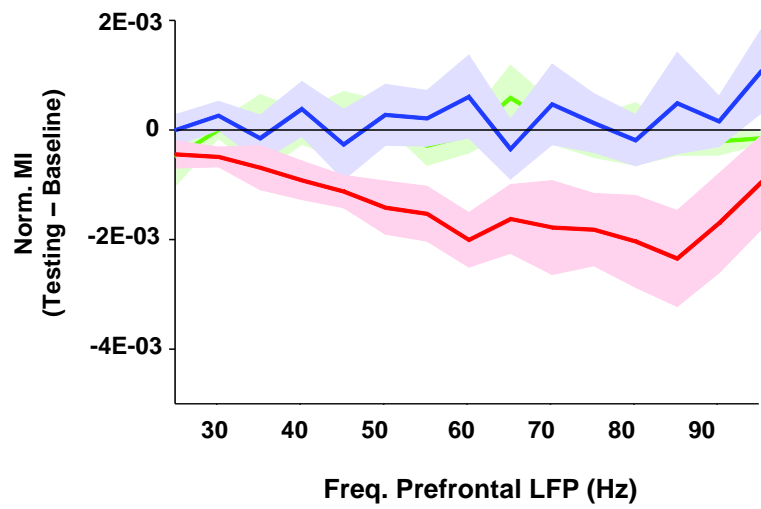
A**B**

Figure 7.14. Theta-Gamma Coupling Across Phases and Frequencies

(A) Co-modulograms showing preferred phase-amplitude pairs between hippocampal theta and mPFC gamma during muscimol baseline (left panel) and muscimol testing (right panel) sessions while the rat occupies the maze choice point. During baseline sessions, mPFC slow gamma (~60 – 80 Hz) is modulated by the ascending phase of hippocampal theta peaks (~120 degrees). Phase-amplitude coupling between hippocampal theta and mPFC slow gamma is diminished during testing sessions. (B) Normalized modulation index (MI) scores for hippocampal-prefrontal theta-gamma coupling at the maze choice point across a range of gamma frequencies. Green = no infusion, blue = saline, and red = muscimol sessions. Note the drop in theta-gamma coupling for slow gamma (~40 – 80 Hz) frequencies during muscimol sessions.

hippocampus and mPFC at the maze choice point. Similar 2 (epoch) x 3 (session) ANOVAs were performed for hippocampal-prefrontal theta-gamma MI score on the start box and maze stem, and these ANOVAs revealed no main effect of session ($F(2,24) = .664, p = .524$ for stem; $F(2,24) = 1.120, p = .343$ for start box), no epoch x session interaction ($F(2,24) = 1.134, p = .338$ for stem; $F(2,24) = .185, p = .832$ for start box), and no main effect of epoch ($F(1,12) = 1.625, p = .227$ for stem; $F(1,12) = .665, p = .431$ for start box). These results demonstrate that decreases in hippocampal-prefrontal theta-gamma coupling were unique to choice point traversals for the muscimol session.

Similar analyses were performed for theta-gamma coupling within the mPFC and within the dorsal hippocampus. The results for mPFC theta-gamma coupling paralleled those for hippocampal-prefrontal coupling, as a 2 (epoch) x 3 (session) ANOVA for MI scores at the maze choice point revealed a significant main effect of session ($F(2,24) = 4.559, p = .021$), a significant epoch x session interaction ($F(2,24) = 5.701, p = .009$), and no main effect of epoch ($F(1,12) = .657, p = .433$). One-sample t-tests revealed that normalized mPFC MI scores at the choice point were not significantly different than zero for no-infusion sessions ($M = -.0004, SD = .002, t(6) = -.758, p = .477$), nor were they significantly different for saline sessions ($M = .002, SD = .003, t(6) = 2.299, p = .061$). Normalized MI scores were significantly lower than zero for muscimol sessions ($M = -.006, SD = .004, t(6) = -3.603, p = .011$). 2 (epoch) x 3 (session) mixed-

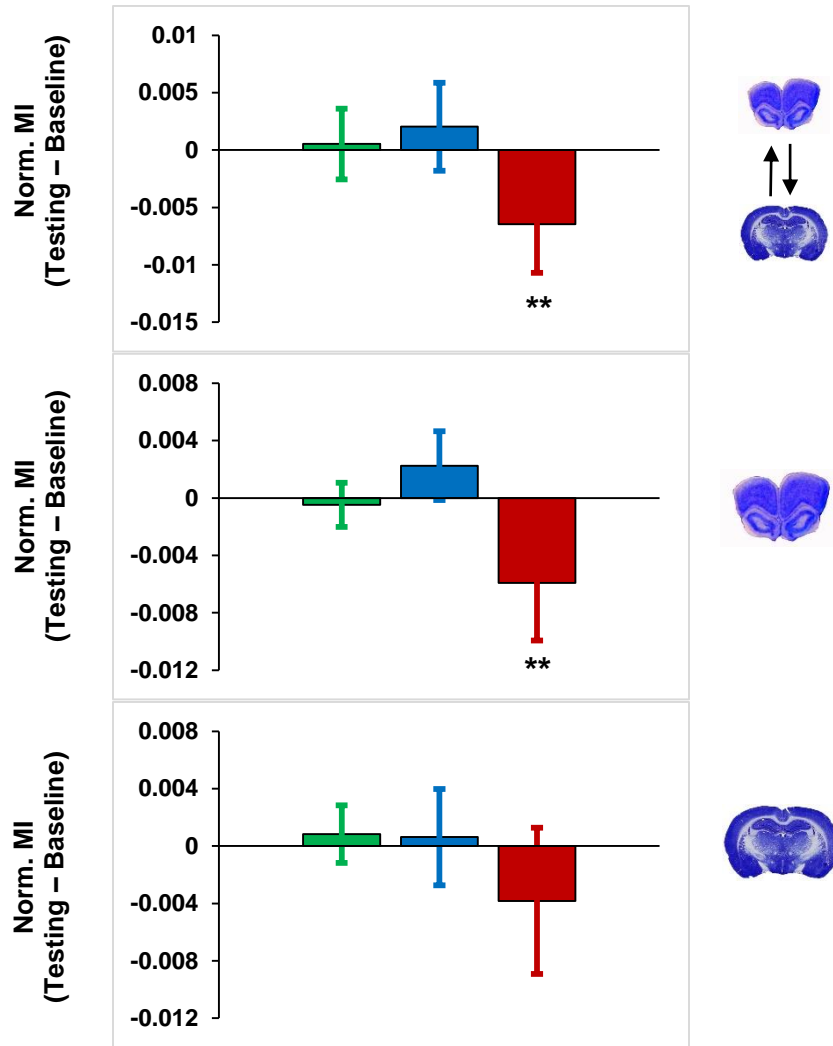


Figure 7.15. Theta-Gamma Coupling at the Maze Choice Point

Normalized MI scores across sessions for hippocampal-prefrontal theta-gamma coupling (top panel), mPFC theta-gamma coupling (middle panel), and hippocampal theta-gamma coupling (bottom panel) during choice point occupancy. Choice point theta-gamma coupling was severely decreased between the hippocampus and mPFC, and within the mPFC, following RE/Rh inactivation. ** $p < .01$. Error bars equal 95% confidence intervals.

factorial ANOVAs for mPFC theta-gamma MI scores on the maze stem and start box revealed no main effect of session ($F(2,24) = .524, p = .599$ for stem; $F(2,24) = 1.434, p = .258$ for start box), no epoch x session interaction ($F(2,24) = .395, p = .678$ for stem; $F(2,24) = .148, p = .863$ for start box), and no main effect of epoch ($F(1,12) = .997, p = .338$ for stem; $F(1,12) = .618, p = .447$ for start box). These results reveal that decreases in theta-gamma coupling within the mPFC were also selective for choice point occupancy during the muscimol session.

Finally, a 2 (epoch) x 3 (session) ANOVA for theta-gamma MI scores within the dorsal hippocampus at the maze choice point revealed a significant main effect of session ($F(2,24) = 10.440, p = .001$), but no significant epoch x session interaction ($F(2,24) = 3.067, p = .065$), and no main effect of epoch ($F(1,12) = .208, p = .656$). Post-hoc analyses revealed that MI scores for muscimol sessions were significantly different from MI scores for no infusion ($p = .006$) and saline ($p = .011$) sessions, but no significant difference between no infusion and saline sessions ($p = 1$). One-sample t-tests revealed that normalized hippocampal MI scores were not significantly different from zero for no infusion sessions ($M = .001, SD = .002, t(6) = 1.017, p = .348$), saline sessions ($M = .001, SD = .004, t(6) = .455, p = .665$), or muscimol sessions ($M = -.004, SD = .006, t(6) = -1.832, p = .117$). Similar 2 (epoch) x 3 (session) ANOVAs for hippocampal MI scores on the maze stem and start box revealed no main effect of session ($F(2,24) = .414, p = .666$ for stem; $F(2,24) = 1.249, p = .326$ for start box), no epoch x session interaction ($F(2,24) = .376, p = .690$ for stem; $F(2,24) = .239, p = .789$ for start

box), and no main effect of epoch ($F(1,12) = .002, p = .967$ for stem; $F(1,12) = .117, p = .738$ for start box) (see Figure 7.15). Although there was a trend of decreases in hippocampal theta-gamma coupling at the maze choice point following muscimol infusions, the effect did not reach statistical significance. Together, the cross-frequency coupling analysis revealed significant decreases in theta-gamma coupling in the mPFC and between the hippocampus and mPFC during choice point occupancy.

7.3.6: Power, Coherence, and Phase-Amplitude Coupling as a Function of Stem Position

In order to compare changes in power spectral density, phase coherence, and phase-amplitude coupling as a function of stem position, the maze stem was binned into 3 equally spaced segments (early stem, mid-stem, and late stem), and power, coherence, and MI scores were calculated for each segment and compared with choice-point and reward arm values. For theta power in the hippocampus, a 2 (epoch) x 5 (maze location) ANOVA for the muscimol session revealed a main effect of maze location ($F(4,48) = 14.389, p < .001$), but no epoch x maze location interaction ($F(4,48) = .883, p = .77$), and no effect of epoch ($F(1,12) = .122, p = .733$). A similar ANOVA for mPFC theta power revealed a main effect of maze location ($F(4,48) = 4.483, p = .004$), no epoch x maze location interaction ($F(4,48) = 2.351, p = .07$), and no effect of epoch ($F(1,12) = .057, p = .816$) (see Figure 7.17). These results demonstrate that theta power increased in both brain regions

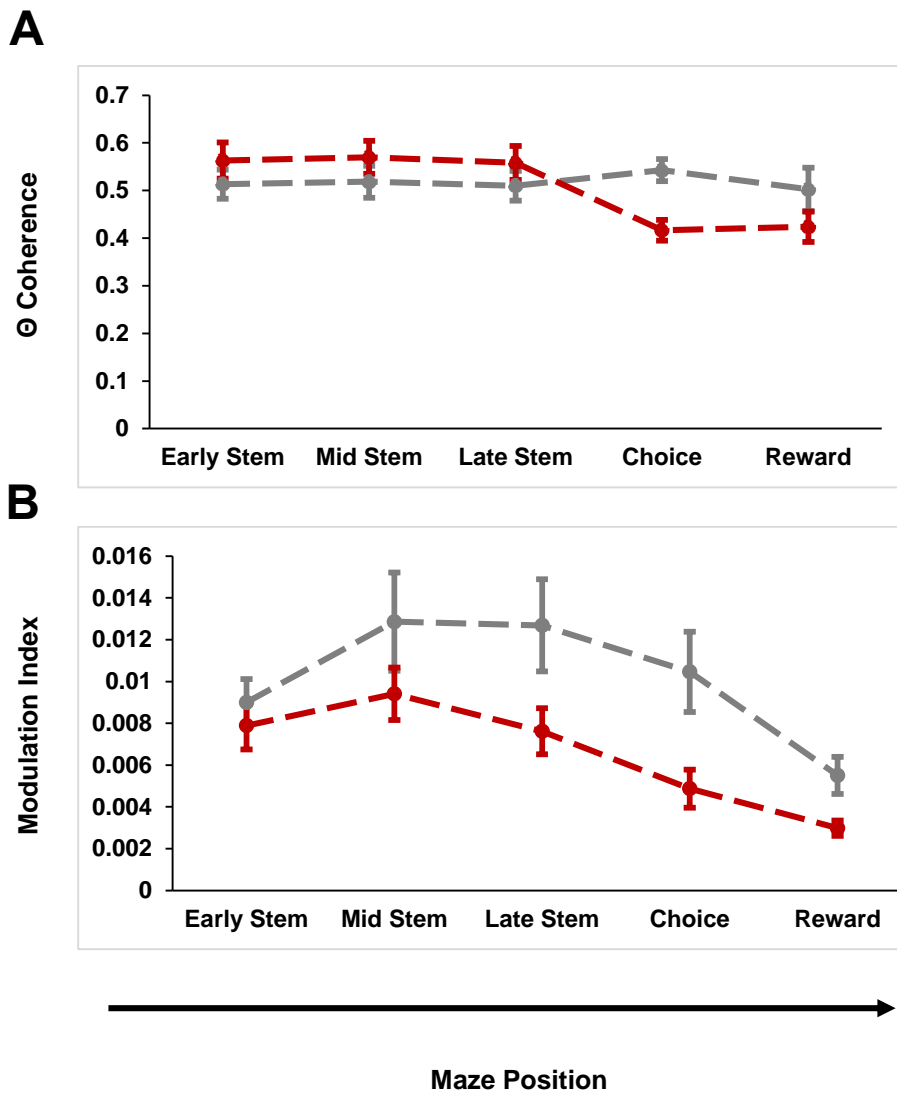


Figure 7.16. Coherence and Theta-Gamma Coupling Along the Maze

(A) Theta coherence as a function of maze location during muscimol sessions. Theta coherence is selectively disrupted at the maze choice point following RE/Rh inactivation. **(B)** Hippocampal-prefrontal theta-gamma coupling as a function of maze location during muscimol sessions. Theta-gamma coupling is disrupted as the rat moves closer to the choice point following RE/Rh inactivation. Note the timeline of theta-gamma coupling deficits as compared to the timeline of coherence deficits. Grey = baseline, red = testing.

during choice point and reward arm occupancy, but did not differ as a function of RE/Rh inactivation, confirming that corresponding decreases in theta phase coherence and theta-gamma phase-amplitude coupling were not a result of changes in theta power in either brain region.

A similar ANOVA for theta phase coherence revealed a significant main effect of maze location ($F(4,48) = 3.167, p = .002$), a significant epoch x maze location interaction ($F(4,48) = 4.048, p = .007$), and no significant main effect of epoch ($F(1,12) = .154, p = .701$) (see Figure 7.16a). This result further shows that decreases in choice point theta coherence are a result of RE/Rh inactivation, and are not due to differences in maze segment size. The same ANOVA for hippocampal-prefrontal theta-gamma coupling revealed a main effect of maze location ($F(4,48) = 20.512, p < .001$), no interaction ($F(4,48) = 2.447, p = .06$), and no main effect of epoch ($F(1,12) = 4.033, p = .07$) (see Figure 7.16b). Taken together, these results suggest that RE/Rh inactivation disrupts hippocampal-prefrontal theta-gamma coupling as the rat moves through the second half of the stem and into the choice point, and corresponding decreases in theta phase coherence between the hippocampus and mPFC do not occur until after the rat has entered the T-intersection of the maze.

7.4: Discussion

The results from this experiment show that inactivation of RE/Rh not only disrupts spatial working memory-guided choice accuracy, but also causes

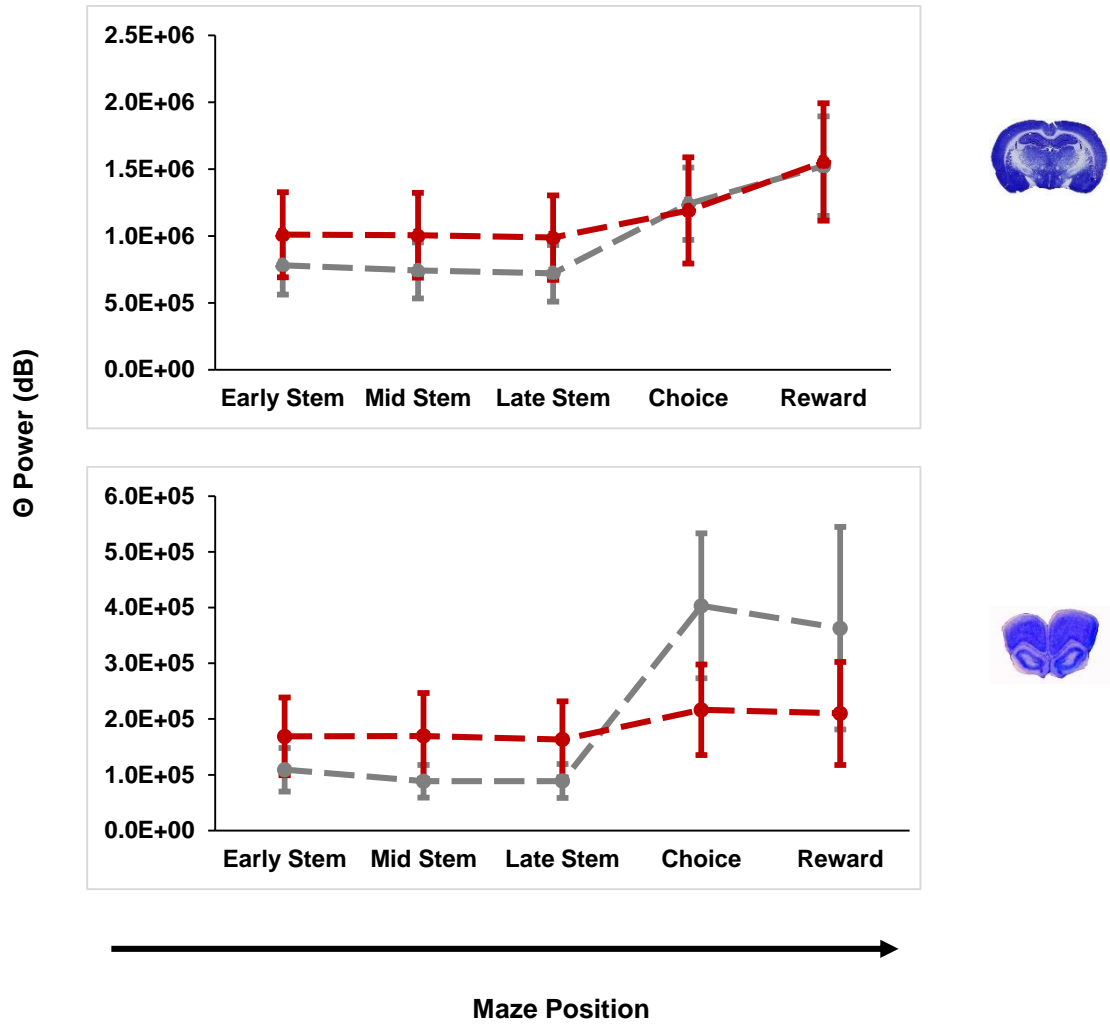


Figure 7.17. Theta Power Along the Maze

Theta power in the hippocampus (top panel) and mPFC (bottom panel) as a function of maze location. RE/Rh inactivation does not cause a significant decrease in theta power in either brain region at any section of the maze.

corresponding decreases in several measures of hippocampal-prefrontal synchrony. Decreases in single unit entrainment to hippocampal theta oscillations, theta-gamma phase-amplitude coupling, and theta phase coherence were all observed following muscimol infusions into RE/Rh. Furthermore, decreases in synchrony were confined to specific areas of the maze, such that entrainment reductions were observed during the delay period, reductions in phase-amplitude coupling occurred on portions of the stem closest to the choice point, and theta phase coherence decreased only while the rat moved through the choice point directly prior to choosing a reward arm. These results strongly implicate RE/Rh as orchestrators of hippocampal-prefrontal synchrony during spatial working memory, and further support the hypothesis that hippocampal-prefrontal synchrony is critically important for spatial working memory in mammalian species (Colgin, 2011; Gordon, 2011).

Differences in firing rate between saline baseline and testing sessions may have been due to the fact that different populations of neurons were recorded between epochs (rats were unplugged and plugged back in between epochs, and different single units with different waveform properties were isolated). Differences in firing rate may also have been due to the influence of the saline infusion on RE/Rh neurons directly adjacent to the tip of the internal cannula. One other possibility is that stress associated with the infusion procedure itself contributed to differences in firing rate profiles of prefrontal neurons between epochs. Differences in mean firing rate between epochs did not affect levels of

entrainment, however, as z-statistic distributions and mean MRL scores were not significantly different between baseline and saline epochs.

Decreases in hippocampal-prefrontal synchrony occurred in the absence of changes in the rat's overt behavior, as stem velocity and time spent at the choice point did not differ as a function of epoch. Similarly, theta power in both the hippocampus and mPFC was not significantly different between baseline and muscimol epochs, making it unlikely that differences in phase coherence and phase-amplitude coupling were due to shifts in power spectral density following muscimol infusions. Phase-amplitude coupling between the hippocampus and mPFC was disrupted following RE/Rh inactivation, but not within the hippocampus itself, suggesting that RE/Rh is not necessary for maintaining phase synchrony within the hippocampus. However, RE/Rh inactivation did significantly disrupt phase-amplitude coupling in the mPFC, indicating that RE/Rh may be important for functionally synchronizing cortical networks during memory tasks, consistent with a general role for thalamic nuclei in cortico-cortical synchronization (Saalmann, 2014). Phase-amplitude coupling deficits were seen directly prior to decreases in theta phase coherence following RE/Rh inactivation. One possible interpretation of this result is that the hippocampal theta oscillation synchronizes with networks of interneurons in the mPFC directly prior to memory-guided decision making (phase-amplitude coupling), and that this synchronization promotes prefrontal-hippocampal communication (phase coherence) while the rat is making a decision.

In summary, these results provide strong evidence that the ventral midline thalamus is critical for regulating cortico-limbic synchrony, which itself is necessary for spatial working memory. One outstanding issue that remains is the nature of the relationship between different components of the prefrontal-thalamo-hippocampal circuit and different phases of the memory-guided decision making process. Future experiments using optogenetics could elucidate the separate roles of the prefrontal-thalamic, thalamo-hippocampal, hippocampal-thalamic, and thalamo-cortical connections during spatial working memory, which would provide further insight into how this “memory circuit” functions at the intersection of cognition and action.

Table 7.1: Distribution of mPFC Pyramidal Neurons Across Rats

Rat	No Infusion	Saline	Muscimol
14-18	Baseline: 17 Testing: 16	Baseline: 19 Testing: 11	Baseline: 11 Testing: 17
14-19	Baseline: 6 Testing: 18	Baseline: 3 Testing: 3	Baseline: 5 Testing: 5
14-20	Baseline: 6 Testing: 6	Baseline: 10 Testing: 9	Baseline: 5 Testing: 5
14-22	Baseline: 6 Testing: 5	Baseline: 4 Testing: 6	Baseline: 8 Testing: 9
14-23	Baseline: 5 Testing: 9	Baseline: 9 Testing: 7	Baseline: 5 Testing: 7
14-24	Baseline: 4 Testing: 1	Baseline: 5 Testing: 4	Baseline: 4 Testing: 2
14-25	None	None	None

Table 7.2: Number of mPFC Pyramidal Neurons Included in Entrainment Analyses Across Rats

Rat	No Infusion	Saline	Muscimol
14-18	Baseline: 15 Testing: 14	Baseline: 18 Testing: 9	Baseline: 11 Testing: 14
14-19	Baseline: 3 Testing: 11	Baseline: 3 Testing: 3	Baseline: 3 Testing: 4
14-20	Baseline: 4 Testing: 3	Baseline: 7 Testing: 6	Baseline: 4 Testing: 3
14-22	Baseline: 4 Testing: 5	Baseline: 4 Testing: 6	Baseline: 4 Testing: 8
14-23	Baseline: 4 Testing: 7	Baseline: 4 Testing: 5	Baseline: 5 Testing: 3
14-24	Baseline: 4 Testing: 1	Baseline: 3 Testing: 4	Baseline: 3 Testing: 2
14-25	None	None	None

Chapter 8

CONCLUSIONS

The experiments outlined in this dissertation support the hypothesis that synchrony between neuronal populations in the prefrontal cortex and hippocampus is important for spatial working memory. Furthermore, this synchrony is modulated by the ventral midline thalamus, a brain area that has direct reciprocal projections to both the dorsal hippocampus and medial prefrontal cortex (mPFC) in the rodent. These results dovetail with previous research showing that hippocampal-prefrontal synchrony is correlated with spatial working memory (Jones & Wilson, 2005; Hyman et al., 2010; Sigurdsson et al., 2010; O'Neill et al., 2013), as well as with previous research showing that the ventral midline thalamus is necessary for spatial working memory (Hembrook & Mair, 2011; Hembrook et al., 2012; Hallock et al., 2013a). The current results contribute to the literature by showing that hippocampal-prefrontal synchrony increases during the successful performance of a hippocampus and ventral midline thalamic-dependent spatial working memory task, as compared to a task that takes place in the same behavioral apparatus, but is not dependent on either of these brain areas. Furthermore, the results contained within this thesis demonstrate, for the first time,

that the ventral midline thalamus contributes to spatial working memory by mediating hippocampal-prefrontal synchrony.

What does oscillatory synchrony between disparate brain areas tell us about what is happening at the cellular level in those brain areas? Phase relationships between LFPs determine the timing of action potentials in neural networks (Fell & Axmacher, 2011), as neuronal excitability is influenced by the phase of an oscillation (Elbert & Rockstroh, 1987; Frohlich & McCormick, 2010). Phase synchronization also enables synaptic inputs on a postsynaptic neuron to arrive simultaneously, which causes rapid membrane depolarization within the postsynaptic neuron (Konig et al., 1996). Phase synchronization can also promote long-term potentiation (LTP) by facilitating temporally proximate activation of pre- and post-synaptic neurons (Markram et al., 1997; Abbott & Nelson, 2000; Caporale, & Dan, 2008). Neurons tend to fire action potentials on specific phases of an LFP oscillation (Fries, 2005), and phase synchronization between brain regions would ensure that neurons with similar phase preferences would fire together. In the hippocampus, electrical stimulation during theta peaks induces LTP, whereas stimulation at theta troughs induces long-term depression (LTD) (Pavlidis et al., 1988; Huerta & Lisman, 1993). Phase synchronization between the hippocampus and mPFC may therefore facilitate neural plasticity on a timescale

that is relevant for information encoding, maintenance, or retrieval during spatial working memory tasks. The current results show that mPFC neurons are entrained to hippocampal theta peaks during spatial working memory task performance, and gamma amplitude in the mPFC is increased during the ascending phase of hippocampal theta oscillations during working memory-guided decision making. These results suggest that neuronal excitability in cortical brain regions could also be modulated by the phase of hippocampal theta oscillations when hippocampal-cortical synchrony is required. Further research could extend these results by optogenetically inhibiting cortical networks during distinct hippocampal theta phases, and observing whether differences in neural plasticity or behavior are tied to theta phase (see Siegle & Wilson, 2014 for an example of such an experiment in the hippocampus).

In experiments 2 & 3 of the thesis, different types of synchrony were observed on different locations throughout the T-maze during the performance of the working memory-dependent delayed alternation (DA) task. The design of the DA task makes it difficult to separate encoding and retrieval phases during each trial, as both processes presumably take place over the course of a single maze traversal. One possibility is that information encoding predominately takes place over the delay period when the animal needs to bind details about its previous

location with route planning for the upcoming trial. This process could also happen on the stem of the T-maze; however, differences in synchrony were not observed on the maze stem in experiments 1 & 2, suggesting that the processing of task-relevant information occurs primarily during the delay period. Differences in phase coherence and theta-gamma coupling were also seen while the rat passed through the maze choice point, with the onset of theta-gamma coupling differences preceding the onset of phase coherence differences following thalamic inactivation. During choice point traversal, the rat could be retrieving information about the previous trial in order to make his goal arm decision. If this is the case, then theta phase coherence and theta-gamma coupling in the hippocampal-prefrontal network could be particularly important for the retrieval of trial-relevant information during spatial working memory. Information encoding could be dependent on hippocampal to prefrontal communication, consistent with the classical role of the hippocampus in memory formation (Scoville & Milner, 1957; Eichenbaum, 2013). Previous research has shown that spikes from single units in the rodent mPFC fire to hippocampal theta cycles of the past, indicating that the hippocampus leads the mPFC during single unit entrainment (Siapas et al., 2005). These results suggest that the hippocampal theta oscillation synchronizes single unit activity in the prefrontal cortex, which possibly supports information encoding

during spatial working memory. During choice point traversals, trial-specific information may be retrieved by the hippocampus from the mPFC, allowing the rat to make a goal-directed decision. The fact that ventral midline thalamic inactivation disrupted entrainment, phase coherence, and phase-amplitude coupling suggests that the ventral midline thalamus is important for supporting both hippocampal to prefrontal, and prefrontal to hippocampal, communication. Future experiments could test the hypothesis that hippocampal-to-prefrontal communication supports encoding during the delay period, and prefrontal-to-hippocampal communication supports retrieval during choice point traversals, by optogenetically targeting either hippocampal afferents in the thalamus, or thalamic afferents in the mPFC, and inactivating them during the delay period. Either prefrontal afferents in the thalamus, or thalamic afferents in the hippocampus, could then be targeted and inactivated selectively during choice point traversals. The expectation would be that optogenetic inactivation of hippocampal-to-prefrontal axons selectively during the delay period, but not during choice point traversals, would disrupt spatial working memory task performance. In contrast, prefrontal-to-hippocampal inactivation selectively during choice point traversals, but not during the delay period, should disrupt spatial working memory task performance. Optogenetic inhibition could also be performed during the

performance of a discrete-trials delayed alternation task, which would allow for the separation of encoding and retrieval phases during a single trial. In this experiment, the expectation would be that hippocampal-to-prefrontal inactivation during the *encoding* phase would disrupt performance, while prefrontal-to-hippocampal inactivation during the *retrieval* phase would disrupt performance.

Another question generated by the available data is how the ventral midline thalamus modulates hippocampal-prefrontal synchrony. The ventral midline thalamus may itself generate theta oscillations, which could then simultaneously synchronize with theta oscillations in the hippocampus and mPFC. Theta oscillations in the ventral midline thalamus could also be influenced by fluctuations in prefrontal gamma power, allowing for directionally-specific phase-amplitude coupling in hippocampal-prefrontal networks to take place. Alternatively, gamma generated in the ventral midline thalamus could functionally synchronize with prefrontal gamma, which would then be modulated by hippocampal theta phases. One other possibility, which is most strongly supported by the data, is that the ventral midline thalamus directly regulates cortical theta-gamma coupling via reciprocal projections with the mPFC. Prefrontal theta-gamma coupling could then promote hippocampal-prefrontal theta-gamma coupling through prefrontal-to-hippocampal theta phase coherence. Ventral

midline thalamic inactivation caused disruptions in both hippocampal-prefrontal theta-gamma coupling and prefrontal theta-gamma coupling, but not hippocampal theta-gamma coupling, indicating that intrinsic cortico-cortical synchrony parallels synchrony in cortico-limbic networks during memory retrieval and decision making. In order to answer these questions directly, however, recordings of LFP and single unit activity will need to be taken in the ventral midline thalamus. Simultaneous recordings of mPFC, hippocampal, and ventral midline thalamic activity will lend direct insight into how the ventral midline thalamus orchestrates hippocampal-prefrontal synchrony during working memory tasks.

Firing rates of mPFC neurons increase during the delay period of the working memory-dependent DA task as compared to the non-working memory-dependent CD task. This increase in firing rate may reflect a working memory-specific function for mPFC neurons, which is consistent with primate data demonstrating that neurons in the functionally homologous dorsolateral PFC elevate their firing rates selectively during the delay period of working memory tasks (Fuster et al., 1982; Goldman-Rakic, 1995). The firing rate of many mPFC neurons remained consistent throughout the extent of the delay period during the DA task, which is in agreement with imaging studies in humans that have shown elevations in BOLD activity that begins directly after stimulus offset and persists

until a response is made (Courtney et al., 1996; Cohen et al., 1997). A small subset of mPFC neurons linearly increased or decreased their firing rates as a function of time throughout the delay period, and this “ramping” and “decay” behavior was observed during both the DA and CD tasks. One interpretation of this result is that the mPFC is capable of maintaining representations of time during task performance, and that this representation is distinct from the working memory-specific processes that take place in the structure. The fact that mPFC neurons show firing rate patterns that are not specifically tied to working memory may not be surprising in light of the extensive connections between the mPFC and other areas of the brain, including the hypothalamus, medulla, striatum, and amygdala (Vertes, 2006). Given this diversity of connectivity, an understanding of how populations of mPFC neurons may code for working memory-specific behavior will likely depend on high-dimensional analyses that are capable of extracting information from large populations of simultaneously recorded single units within multiple disparate brain regions (Cunningham & Yu, 2014).

The prefrontal-thalamo-hippocampal circuit has been tied to working memory, and theta oscillations throughout the circuit appear to play a prominent role in synchronizing the three structures during working memory-guided decision making. The hippocampus, ventral midline thalamus, and mPFC also play a role in

memory consolidation (Maviel et al., 2004; Nakashiba et al., 2009; Loureiro et al., 2012), indicating that this pathway is capable of supporting memory-related processes during both active behavior and periods of rest or quiescence (Thierry et al., 2000). During awake behavior, the hippocampal LFP is dominated by theta oscillations, which synchronize with the mPFC during working memory tasks. During rest, the hippocampal LFP is dominated by large-irregular amplitude (LIA) activity, during which “replay” events occur (see chapter 2). These two hippocampal “states” may promote different patterns of synchronous activation in thalamic and prefrontal networks, which may in turn separately facilitate encoding, consolidation, and retrieval. Oscillatory synchrony between the mPFC, RE/Rh, and hippocampus during waking states may also underlie the prefrontal-thalamo-hippocampal pathway’s contribution to interference reduction and contextual fear memory specificity (Xu & Sudhof, 2013; Navawongse & Eichenbaum, 2013; Preston & Eichenbaum, 2013). Recordings from the ventral midline thalamus during hippocampal theta states and LIA states will answer the question of whether thalamic activity is differentially modulated by shifts in oscillatory profiles in the hippocampal LFP.

In summary, phase synchrony in the hippocampal-prefrontal network is selectively important for spatial working memory. Synchronization in this network

is directly influenced by inactivation of the ventral midline thalamus, indicating that this brain region plays a critical role in the regulation of cortico-limbic interactions.

REFERENCES

- Abbott, L. F., & Nelson, S. B. (2000). Synaptic plasticity: taming the beast. *Nature Neuroscience*, **3**: 1178-1183.
- Aggleton, J. P., Hunt, P. R., & Rawlins, J. N. P. (1986). The effects of hippocampal lesions upon spatial and non-spatial tests of working memory. *Behavioural brain research*, **19**: 133-146.
- Ainge, J. A., van der Meer, M. A., Langston, R. F., & Wood, E. R. (2007). Exploring the role of context-dependent hippocampal activity in spatial alternation behavior. *Hippocampus*, **17**: 988-1002.
- Allen TA, Narayanan NS, Kholodar-Smith DB, Zhao Y, Laubach M, & Brown TH. (2008). Imaging the spread of reversible brain inactivations using fluorescent muscimol. *Journal of Neuroscience Methods*, **171**: 30–38.
- Arnsten, A.F.T., & Goldman-Rakic, P.S. (1998). Noise stress impairs prefrontal cortical cognitive function in monkeys: Evidence for a hyperdopaminergic mechanism. *JAMA Psychiatry*, **55**: 362-368.
- Atkinson, R.C., & Shiffrin, R.M. (1968). Human memory: A proposed system and its control processes. In *The Psychology of Learning and Motivation: Advances in Research and Theory* (Spence, K.W., ed.), pp. 89-195, Academic Press.
- Axmacher, N., Mormann, F., Fernández, G., Elger, C. E., & Fell, J. (2006). Memory formation by neuronal synchronization. *Brain research reviews*, **52**: 170-182.
- Baddeley, A., & Hitch, G. (1974). Working memory. In *The Psychology of Learning and Motivation* (Bower, G.A., ed), pp. 48-79, Academic Press.
- Baddeley, A.D. (1986). *Working Memory*. Oxford University Press: Oxford.
- Baddeley, A. (1992). Working memory. *Science*, **255**: 556-559.
- Baddeley, A. (1998). Recent developments in working memory. *Current Opinion in Neurobiology*, **8**: 234-238.

- Baddeley, A. (2000). The episodic buffer: A new component of working memory? *Trends in Cognitive Sciences*, **4**: 417-423.
- Baddeley, A. (2003). Working memory: Looking back and looking forward. *Nature Reviews Neuroscience*, **4**: 829-839.
- Baeg, E. H., Kim, Y. B., Huh, K., Mook-Jung, I., Kim, H. T., & Jung, M. W. (2003). Dynamics of population code for working memory in the prefrontal cortex. *Neuron*, **40**: 177-188.
- Barbas, H., & Pandya, D.N. (1989). Architecture and intrinsic connections of the prefrontal cortex in the rhesus monkey. *Journal of Comparative Neurology*, **286**: 353-375.
- Bartos, M., Vida, I., & Jonas, P. (2007). Synaptic mechanisms of synchronized gamma oscillations in inhibitory interneuron networks. *Nature reviews neuroscience*, **8**: 45-56.
- Battaglia, F. P., Sutherland, G. R., & McNaughton, B. L. (2004). Hippocampal sharp wave bursts coincide with neocortical “up-state” transitions. *Learning & Memory*, **11**: 697-704.
- Becker, J. T., Walker, J. A., Olton, D. S., & O'Connell, B. C. (1978). Neuroanatomical bases of short-term spatial memory in the rat. *Society for Neuroscience Abstracts*, *4*, 73.
- Belluscio MA, Mizuseki K, Schmidt R, Kempter R, & Buzsaki G. (2012). *The Journal of Neuroscience*, **32**: 423-435.
- Benchenane K, Peyrache A, Khamassi M, Tierney PL, Gioanni Y, Battaglia FP, & Wiener SI. (2010). Coherent theta oscillations and reorganization of spike timing in the hippocampal- prefrontal network upon learning. *Neuron*, **66**: 921-936.
- Bertram, E. H., & Zhang, D. X. (1999). Thalamic excitation of hippocampal CA1 neurons: a comparison with the effects of CA3 stimulation. *Neuroscience*, **92**: 15-26.
- Bisley, J.W., Zaksas, D., Droll, J., & Pasternak, T. (2004). Activity of neurons in cortical area MT during a memory for motion task. *Journal of Neurophysiology*, **91**: 286-300.
- Bower MR, Euston DR, & McNaughton BL. (2005). Sequential-context-dependent hippocampal activity is not necessary to learn sequences with repeated elements. *The Journal of Neuroscience*, **25**: 1313-1323.

- Bragin A, Jando G, Nadasdy Z, Hetke J, Wise K, & Buzsaki G. (1995). Gamma (40-100 Hz) oscillation in the hippocampus of the behaving rat. *The Journal of Neuroscience*, **15**: 47-60.
- Brandon, M. P., Bogaard, A. R., Libby, C. P., Connerney, M. A., Gupta, K., & Hasselmo, M. E. (2011). Reduction of theta rhythm dissociates grid cell spatial periodicity from directional tuning. *Science*, **332**: 595-599.
- Brito, G. N., & Brito, L. S. (1990). Septohippocampal system and the prelimbic sector of frontal cortex: a neuropsychological battery analysis in the rat. *Behavioural brain research*, **36**: 127-146.
- Buhl, D. L., & Buzsáki, G. (2005). Developmental emergence of hippocampal fast-field “ripple” oscillations in the behaving rat pups. *Neuroscience*, **134**: 1423-1430.
- Buzsáki, G. (1986). Hippocampal sharp waves: their origin and significance. *Brain research*, **398**: 242-252.
- Buzsaki G. (2002). Theta oscillations in the hippocampus. *Neuron*, **33**: 325-340.
- Buzsaki, G. (2006). *Rhythms of the Brain*. Oxford University Press.
- Buzsáki, G., & da Silva, F. L. (2012). High frequency oscillations in the intact brain. *Progress in Neurobiology*, **98**: 241-249.
- Buzsáki, G., Anastassiou, C. A., & Koch, C. (2012). The origin of extracellular fields and currents—EEG, ECoG, LFP and spikes. *Nature reviews neuroscience*, **13**: 407-420.
- Cai, J.X., & Arnsten, A.F.T. (1997). Dose-dependent effects of the dopamine D1 receptor agonists A77636 or SKF81297 on spatial working memory in aged monkeys. *Journal of Pharmacology*, **283**: 183-189.
- Canolty, R. T., Edwards, E., Dalal, S. S., Soltani, M., Nagarajan, S. S., Kirsch, H. E., & Knight, R. T. (2006). High gamma power is phase-locked to theta oscillations in human neocortex. *Science*, **313**: 1626-1628.
- Caporale, N., & Dan, Y. (2008). Spike timing-dependent plasticity: a Hebbian learning rule. *Annu. Rev. Neurosci.*, **31**: 25-46.

- Castner, S.A., & Goldman-Rakic, P.S. (1999). Long-lasting psychotomimetic consequences of repeated low-dose amphetamine exposure in rhesus monkeys. *Neuropsychopharmacology*, **20**: 10-28.
- Cavada, C., & Goldman-Rakic, P.S. (1989). Posterior parietal cortex in rhesus monkey: II. Evidence for segregated corticocortical networks linking sensory and limbic areas with the frontal lobe. *Journal of Comparative Neurology*, **287**: 422-445.
- Chafee, M.V., & Goldman-Rakic, P.S. (1998). Matching patterns of activity in primate prefrontal area 8a and parietal area 7ip neurons during a spatial working memory task. *Journal of Neurophysiology*, **79**: 2919-2940.
- Cholvin, T., Loureiro, M., Cassel, R., Cosquer, B., Geiger, K., Nogueira, D. D. S., & Cassel, J. C. (2013). The ventral midline thalamus contributes to strategy shifting in a memory task requiring both prefrontal cortical and hippocampal functions. *The Journal of Neuroscience*, *33*(20), 8772-8783.
- Churchwell, J. C., & Kesner, R. P. (2011). Hippocampal-prefrontal dynamics in spatial working memory: interactions and independent parallel processing. *Behavioural brain research*, **225**: 389-395.
- Cohen, J. D., Perlstein, W. M., Braver, T. S., Nystrom, L. E., Noll, D. C., Jonides, J., & Smith, E. E. (1997). Temporal dynamics of brain activation during a working memory task. *Nature*, **386**: 604-608.
- Cohen MX, Elger CE, & Fell J. (2009). Oscillatory activity and phase–amplitude coupling in the human medial frontal cortex during decision making. *Journal of Cognitive Neuroscience*, **21**: 390-402.
- Cohen, M. X. (2014). *Analyzing neural time series data: theory and practice*. MIT Press.
- Colgin, L. L., Moser, E. I., & Moser, M. B. (2008). Understanding memory through hippocampal remapping. *Trends in neurosciences*, **31**: 469-477.
- Colgin, L. L., & Moser, E. I. (2010). Gamma oscillations in the hippocampus. *Physiology*, **25**: 319-329.
- Colgin LL. (2011). Oscillations and hippocampal-prefrontal synchrony. *Current Opinion in Neurobiology*, **21**: 467-474.

- Conrad, R., & Hull, A.J. (1964). Information, acoustic confusion and memory span. *British Journal of Psychology*, **55**: 429-432.
- Constantinidis, C., & Steinmetz, M.A. (1996). Neuronal activity in posterior parietal area 7a during the delay periods of a spatial memory task. *Journal of Neurophysiology*, **76**: 1352-1355.
- Courtney, S. M., Ungerleider, L. G., Keil, K., & Haxby, J. V. (1996). Object and spatial visual working memory activate separate neural systems in human cortex. *Cerebral Cortex*, **6**: 39-49.
- Courtney, S. M., Ungerleider, L. G., Keil, K., & Haxby, J. V. (1997). Transient and sustained activity in a distributed neural system for human working memory. *Nature*, **386**: 608-611.
- Courtney, S. M., Petit, L., Maisog, J. M., Ungerleider, L. G., & Haxby, J. V. (1998). An area specialized for spatial working memory in human frontal cortex. *Science*, **279**: 1347-1351.
- Cowen SL, & McNaughton BL. (2007). Selective delay activity in the medial prefrontal cortex of the rat: Contribution of sensorimotor information and contingency. *Journal of Neurophysiology*, **98**: 303-316.
- Csicsvari, J., Hirase, H., Czurko, A., Mamiya, A., & Buzsáki, G. (1999). Fast network oscillations in the hippocampal CA1 region of the behaving rat. *J Neurosci*, **19**: 1-4.
- Cunningham, J. P., & Byron, M. Y. (2014). Dimensionality reduction for large-scale neural recordings. *Nature Neuroscience*, **17**: 1500-1509.
- Czerniawski, J., Yoon, T., & Otto, T. (2009). Dissociating space and trace in dorsal and ventral hippocampus. *Hippocampus*, **19**: 20-32.
- d'Esposito, M., Aguirre, G. K., Zarahn, E., Ballard, D., Shin, R. K., & Lease, J. (1998). Functional MRI studies of spatial and nonspatial working memory. *Cognitive Brain Research*, **7**: 1-13.
- Dalley, J. W., Cardinal, R. N., & Robbins, T. W. (2004). Prefrontal executive and cognitive functions in rodents: neural and neurochemical substrates. *Neuroscience & Biobehavioral Reviews*, **28**: 771-784.

- Davidson TJ, Kloosterman F, & Wilson MA. (2009). Hippocampal replay of extended experience. *Neuron*, **63**: 497-507.
- Day, M., Carr, D.B., Ulrich, S., Ilijic, E., Tkatch, T., & Surmeier, D.J. (2005). Dendritic excitability of mouse frontal cortex pyramidal neurons is shaped by the interaction among HCN, kir2, and leak channels. *Journal of Neuroscience*, **25**: 8776-8787.
- Delatour, B., & Gisquet-Verrier, P. (1996). Prelimbic cortex specific lesions disrupt delayed-variable response tasks in the rat. *Behavioral neuroscience*, **110**: 1282.
- Della Sala, S., Gray, C., Baddeley, A.D., Allamano, N., & Wilson, L. (1999). Pattern span: A tool for unwinding visuo-spatial memory. *Neuropsychologia*, **37**: 1189-1199.
- Demiralp, T., Bayraktaroglu, Z., Lenz, D., Junge, S., Busch, N. A., Maess, B., & Herrmann, C. S. (2007). Gamma amplitudes are coupled to theta phase in human EEG during visual perception. *International Journal of Psychophysiology*, **64**: 24-30.
- Di Prisco, G. V., & Vertes, R. P. (2006). Excitatory actions of the ventral midline thalamus (rhomboid/reuniens) on the medial prefrontal cortex in the rat. *Synapse*, **60**: 45-55.
- Diba K, & Buzsaki G. (2007). Forward and reverse hippocampal place-cell sequences during ripples. *Nature Neuroscience*, **10**: 1241-1242.
- Dolleman-Van der Weel, M. J., & Witter, M. P. (2000). Nucleus reuniens thalami innervates γ aminobutyric acid positive cells in hippocampal field CA1 of the rat. *Neuroscience letters*, **278**: 145-148.
- Dolleman-van der Weel MJ, Morris RGM, & Witter MP. (2009). Neurotoxic lesions of the thalamic reuniens or mediodorsal nucleus in rats affect non-mnemonic aspects of watermaze learning. *Brain Structure and Function*, **213**: 329-342.
- Douchamps, V., Jeewajee, A., Blundell, P., Burgess, N., & Lever, C. (2013). Evidence for encoding versus retrieval scheduling in the hippocampus by theta phase and acetylcholine. *The Journal of Neuroscience*, **33**: 8689-8704.
- Dudchenko, P. A., Wood, E. R., & Eichenbaum, H. (2000). Neurotoxic hippocampal lesions have no effect on odor span and little effect on odor recognition memory but produce significant impairments on spatial span, recognition, and alternation. *The Journal of Neuroscience*, **20**: 2964-2977.

- Dudchenko, P. A. (2001). How do animals actually solve the T maze?. *Behavioral neuroscience*, **115**: 850.
- Dudchenko, P. A., & Davidson, M. (2002). Rats use a sense of direction to alternate on T-mazes located in adjacent rooms. *Animal cognition*, **5**: 115-118.
- Dudchenko, P. A. (2004). An overview of the tasks used to test working memory in rodents. *Neuroscience & Biobehavioral Reviews*, **28**: 699-709.
- Ego-Stengel, V., & Wilson, M. A. (2010). Disruption of ripple-associated hippocampal activity during rest impairs spatial learning in the rat. *Hippocampus*, **20**: 1-10.
- Eichenbaum H. (2000). Hippocampus: Mapping or memory? *Current Biology*, **10**: 785-787.
- Eichenbaum, H. (2013). What HM taught us. *Journal of cognitive neuroscience*, **25**: 14-21.
- Elbert, T., & Rockstroh, B. (1987). Threshold regulation-a key to the understanding of the combined dynamics of EEG and event-related potentials.
- Fanselow, M. S., & Dong, H. W. (2010). Are the dorsal and ventral hippocampus functionally distinct structures?. *Neuron*, **65**: 7-19.
- Fell, J., & Axmacher, N. (2011). The role of phase synchronization in memory processes. *Nature reviews neuroscience*, **12**: 105-118.
- Fellows BJ. (1967). Chance stimulus sequences for discrimination tasks. *Psychology Bulletin*, **67**: 87-92.
- Ferbinteanu J, & Shapiro ML. (2003). Prospective and retrospective memory coding in the hippocampus. *Neuron*, **40**: 1227-1239.
- Ferbinteanu J, Shirvalkar P, & Shapiro ML. (2011). Memory modulates journey-dependent coding in the rat hippocampus. *The Journal of Neuroscience*, **31**: 9135-9146.
- Ferino, F., Thierry, A. M., & Glowinski, J. (1987). Anatomical and electrophysiological evidence for a direct projection from Ammon's horn to the medial prefrontal cortex in the rat. *Experimental Brain Research*, **65**: 421-426.

- Ferrera, V.P., Rudolph, K.K., & Maunsell, J.H. (1994). Responses of neurons in the parietal and temporal visual pathways during a motion task. *Journal of Neurophysiology*, **14**: 6171-6186.
- Foster DJ, & Wilson MA. (2006). Reverse replay of behavioural sequences in hippocampal place cells during the awake state. *Nature*, **440**: 680-683.
- Frank LM, Brown EN, & Wilson M. (2000). Trajectory encoding in the hippocampus and entorhinal cortex. *Neuron*, **27**: 169-178.
- Freund, T. F., & Antal, M. (1988). GABA-containing neurons in the septum control inhibitory interneurons in the hippocampus. *Nature*, **336**: 170-173.
- Fries, P. (2005). A mechanism for cognitive dynamics: neuronal communication through neuronal coherence. *Trends in Cognitive Sciences*, **9**: 474-480.
- Fröhlich, F., & McCormick, D. A. (2010). Endogenous electric fields may guide neocortical network activity. *Neuron*, **67**: 129-143.
- Funahashi, S., Bruce, C.J., & Goldman-Rakic, P.S. (1989). Mnemonic coding of visual space in the monkey's dorsolateral prefrontal cortex. *Journal of Neurophysiology*, **61**: 331-349.
- Funahashi, S., Bruce, C.J., & Goldman-Rakic, P.S. (1990). Visuo-spatial coding in primate prefrontal neurons revealed by oculomotor paradigms. *Journal of Neurophysiology*, **63**: 814-831.
- Funahashi, S., Bruce, C.J., & Goldman-Rakic, P.S. (1991). Neuronal activity related to saccadic eye movements in the monkey's dorsolateral prefrontal cortex. *Journal of Neurophysiology*, **65**: 1464-1483.
- Fuster, J.M., & Alexander, G.E. (1971). Neuron activity related to short-term memory. *Science*, **173**: 652-654.
- Fuster, J.M., Bauer, R.H., & Jervey, J.P. (1981). Effects of cooling inferotemporal cortex on performance of visual memory tasks. *Experimental Neurology*, **71**: 398-409.

- Fuster, J.M., Bauer, R.H., & Jervey, J.P. (1982). Cellular discharge in the dorsolateral prefrontal cortex of the monkey in cognitive tasks. *Experimental Neurology*, **77**: 679-694.
- Fuster, J.M., Bauer, R.H., & Jervey, J.P. (1985). Functional interactions between inferotemporal and prefrontal cortex in a cognitive task. *Brain Research*, **330**: 299-307.
- Fuster, J.M. (1990). Inferotemporal units in selective visual attention and short-term memory. *Journal of Neurophysiology*, **64**: 681-697.
- Fuster, J.M. (2001). The prefrontal cortex – an update: Time is of the essence. *Neuron*, **30**: 319-333.
- Gill PR, Mizumori SJ, & Smith DM. (2011). Hippocampal episode fields develop with learning. *Hippocampus*, **21**: 1240-1249.
- Goldman-Rakic, P. S. (1987). Circuitry of primate prefrontal cortex and regulation of behavior by representational memory. *Comprehensive Physiology*
- Goldman-Rakic, P.S., Leranth, C., Williams, S.M., Mons, N., & Geffard, M. (1989). Dopamine synaptic complex with pyramidal neurons in primate cerebral cortex. *Proceedings of the National Academy of Sciences*, **86**: 9015-9019.
- Goldman-Rakic, P.S. (1995). Cellular basis of working memory. *Neuron*, **14**: 477-485.
- Goldman-Rakic, P.S., Muly, E.C., & Williams, G.V. (2000). D1 receptors in prefrontal cells and circuits. *Brain Research Reviews*, **31**: 295-301.
- Gordon JA. (2011). Oscillations and hippocampal-prefrontal synchrony. *Current Opinion in Neurobiology*, **21**: 486-491.
- Gottlieb, Y., Vaadia, E., & Abeles, M. (1989). Single unit activity in the auditory cortex of a monkey performing a short-term memory task. *Experimental Brain Research*, **74**: 139-148.
- Granon, S., Vidal, C., Thinus-Blanc, C., Changeux, J. P., & Poucet, B. (1994). Working memory, response selection, and effortful processing in rats with medial prefrontal lesions. *Behavioral neuroscience*, **108**: 883.

- Griffin, A. L., Eichenbaum, H., & Hasselmo, M. E. (2007). Spatial representations of hippocampal CA1 neurons are modulated by behavioral context in a hippocampus-dependent memory task. *The Journal of Neuroscience*, **27**: 2416-2423.
- Griffin AL, Owens CB, Peters GJ, Adelman PC, & Cline KM. (2012). Spatial representations in dorsal hippocampal neurons during a tactile-visual conditional discrimination task. *Hippocampus*, **22**: 299-308.
- Griffin, A. L., & Hallock, H. L. (2013). Hippocampal signatures of episodic memory: evidence from single-unit recording studies. *Frontiers in behavioral neuroscience*, **7**.
- Gupta, A. S., van der Meer, M. A., Touretzky, D. S., & Redish, A. D. (2010). Hippocampal replay is not a simple function of experience. *Neuron*, **65**: 695-705.
- Gupta AS, van der Meer MAA, Touretzsky DS, & Redish AD. (2012). Segmentation of spatial experience by hippocampal theta sequences. *Nature Neuroscience*, **15**: 1032-1039.
- Hallock, H. L., Arreola, A. C., Shaw, C. L., & Griffin, A. L. (2013a). Dissociable roles of the dorsal striatum and dorsal hippocampus in conditional discrimination and spatial alternation T-maze tasks. *Neurobiology of learning and memory*, **100**: 108-116.
- Hallock, H. L., Wang, A., Shaw, C. L., & Griffin, A. L. (2013b). Transient inactivation of the thalamic nucleus reuniens and rhomboid nucleus produces deficits of a working-memory dependent tactile-visual conditional discrimination task. *Behavioral neuroscience*, **127**: 860.
- Hallock, H. L., & Griffin, A. L. (2013). Dynamic coding of dorsal hippocampal neurons between tasks that differ in structure and memory demand. *Hippocampus*, **23**: 169-186.
- Hasselmo, M., Bodelón, C., & Wyble, B. (2002). A proposed function for hippocampal theta rhythm: separate phases of encoding and retrieval enhance reversal of prior learning. *Neural computation*, **14**: 793-817.
- Hasselmo, M. E. (2005). What is the function of hippocampal theta rhythm?—Linking behavioral data to phasic properties of field potential and unit recording data. *Hippocampus*, **15**: 936-949.
- Hebb, D.O. (1949). *The Organization of Behavior*. Wiley: New York.

- Hembrook JR, & Mair RG. (2011). Lesions of reuniens and rhomboid thalamic nuclei impair radial maze win-shift performance. *Hippocampus*, **21**: 815-826.
- Hembrook JR, Onos KD, & Mair RG. (2012). Inactivation of ventral midline thalamus produces selective spatial delayed conditional discrimination impairment in the rat. *Hippocampus*, **22**: 853-860.
- Herkenham, M. (1979). The afferent and efferent connections of the ventromedial thalamic nucleus in the rat. *Journal of Comparative Neurology*, **183**: 487-517.
- Hernandez, A., Zainos, A., & Romo, R. (2000). Neuronal correlates of sensory discrimination in the somatosensory cortex. *Proceedings of the National Academy of Sciences*, **97**: 6191-6196.
- Huerta, P. T. & Lisman, J. E. (1993). Heightened synaptic plasticity of hippocampal CA1 neurons during a cholinergically induced rhythmic state. *Nature*, **364**: 723-725.
- Huerta, P. T., & Lisman, J. E. (1995). Bidirectional synaptic plasticity induced by a single burst during cholinergic theta oscillation in CA1 in vitro. *Neuron*, **15**: 1053-1063.
- Hyman, J. M., Zilli, E. A., Paley, A. M., & Hasselmo, M. E. (2005). Medial prefrontal cortex cells show dynamic modulation with the hippocampal theta rhythm dependent on behavior. *Hippocampus*, **15**: 739-749.
- Hyman, J. M., Zilli, E. A., Paley, A. M., & Hasselmo, M. E. (2010). Working memory performance correlates with prefrontal-hippocampal theta interactions but not with prefrontal neuron firing rates. *Frontiers in integrative neuroscience*, **4**.
- della Rocchetta, A. I., & Milner, B. (1993). Strategic search and retrieval inhibition: The role of the frontal lobes. *Neuropsychologia*, **31**: 503-524.
- Jadhav, S. P., Kemere, C., German, P. W., & Frank, L. M. (2012). Awake hippocampal sharp-wave ripples support spatial memory. *Science*, **336**: 1454-1458.
- Jarvis MR, & Mitra PP. (2001). Sampling properties of the spectrum and coherency of sequences of action potentials. *Neural Computation*, **13**: 717-749.
- Jay TM, Glowinski J, & Thierry AM. (1989). Selectivity of the hippocampal projection to the prelimbic area of the prefrontal cortex in the rat. *Brain Research*, **505**: 337-340.

- Jay, T. M., & Witter, M. P. (1991). Distribution of hippocampal CA1 and subicular efferents in the prefrontal cortex of the rat studied by means of anterograde transport of Phaseolus vulgaris-leucoagglutinin. *Journal of Comparative Neurology*, **313**: 574-586.
- Jay, T. M., Burette, F., & Laroche, S. (1996). Plasticity of the hippocampal-prefrontal cortex synapses. *Journal of Physiology-Paris*, **90**: 361-366.
- Jensen O, & Lisman JE. (1996). Novel lists of 7 +/- 2 known items can be reliably stored in an oscillatory short-term memory network: Interaction with long-term memory. *Learning and Memory*, **3**: 257-263.
- Jezeq K, Henrikson EJ, Treves A, Moser EI, & Moser MB. (2011). Theta-paced flickering between place-cell maps in the hippocampus. *Nature*, **478**: 246-249.
- Jones, M. W., & Wilson, M. A. (2005). Theta rhythms coordinate hippocampal–prefrontal interactions in a spatial memory task. *PLoS biology*, **3**: e402.
- Jonides, J., Smith, E. E., Koeppe, R. A., Awh, E., Minoshima, S., & Mintun, M. A. (1993). Spatial working-memory in humans as revealed by PET. *Nature*, **363**: 623-625.
- Jung MW, Qin Y, McNaughton BL, & Barnes, CA. (1998). Firing characteristics of deep layer neurons in prefrontal cortex in rats performing spatial working memory tasks. *Cerebral Cortex*, **8**: 437-450.
- Jutras, M. J., & Buffalo, E. A. (2010). Synchronous neural activity and memory formation. *Current opinion in neurobiology*, **20**: 150-155.
- Kapur, S., & Remington, G. (1996). Serotonin-dopamine interaction and its relevance to schizophrenia. *American Journal of Psychiatry*, **153**: 466-476.
- Kesner RP, Hunt ME, Williams JM, & Long JM. (1996). Prefrontal cortex and working memory for spatial response, spatial location and visual object information in the rat. *Cerebral Cortex*, **6**: 311-318.
- Kim J, Delcasso S, & Lee I. (2011). Neural correlates of object-in-place learning in hippocampus and prefrontal cortex. *The Journal of Neuroscience*, **31**: 16991-17006.
- Kirchhoff, B. A., Wagner, A. D., Maril, A., & Stern, C. E. (2000). Prefrontal–temporal circuitry for episodic encoding and subsequent memory. *The Journal of Neuroscience*, **20**: 6173-6180.

- Köhler, C., Chan-Palay, V., & Wu, J. Y. (1984). Septal neurons containing glutamic acid decarboxylase immunoreactivity project to the hippocampal region in the rat brain. *Anatomy and embryology*, **169**: 41-44.
- Kolb, B. (1984). Functions of the frontal cortex of the rat: a comparative review. *Brain Research Reviews*, **8**: 65-98.
- Komorowski RW, Manns JR, & Eichenbaum H. (2009). Robust conjunctive item–place coding by hippocampal neurons parallels learning what happens where. *The Journal of Neuroscience*, **29**: 9918-9921.
- Komorowski RW, Garcia CG, Wilson A, Hattori S, Howard MW, & Eichenbaum H. (2013). Ventral hippocampal neurons are shaped by experience to represent behaviorally relevant contexts. *The Journal of Neuroscience*, **33**: 8079-8087.
- König, P., Engel, A. K., & Singer, W. (1996). Integrator or coincidence detector? The role of the cortical neuron revisited. *Trends in Neurosciences*, **19**: 130-137.
- Kopp, F., Schröger, E., & Lipka, S. (2006). Synchronized brain activity during rehearsal and short-term memory disruption by irrelevant speech is affected by recall mode. *International Journal of Psychophysiology*, **61**: 188-203.
- Kraus BJ, Robinson RJ, White JA, Eichenbaum H, & Hasselmo ME. (2013). Hippocampal “time cells”: Time versus path integration. *Neuron*, **78**: 1090-1101.
- Lacaille, J. C., Mueller, A. L., Kunkel, D. D., & Schwartzkroin, P. A. (1987). Local circuit interactions between oriens/alveus interneurons and CA1 pyramidal cells in hippocampal slices: electrophysiology and morphology. *The Journal of neuroscience*, **7**: 1979-1993.
- Lansink CS, Jackson JC, Lankelma JV, Ito R, Robbins TW, Everitt BJ, & Pennartz CMA. (2012). Reward cues in space: Commonalities and differences in neural coding by hippocampal and ventral striatal ensembles. *The Journal of Neuroscience*, **32**: 12444-12459.
- Lawrie, S. M., Buechel, C., Whalley, H. C., Frith, C. D., Friston, K. J., & Johnstone, E. C. (2002). Reduced frontotemporal functional connectivity in schizophrenia associated with auditory hallucinations. *Biological Psychiatry*, **51**: 1008-1011.

- Lee, I., & Kesner, R. P. (2003). Time-dependent relationship between the dorsal hippocampus and the prefrontal cortex in spatial memory. *The Journal of Neuroscience*, **23**: 1517-1523.
- Lee, I., Yoganarasimha, D., Rao, G., & Knierim, J. J. (2004). Comparison of population coherence of place cells in hippocampal subfields CA1 and CA3. *Nature*, **430**: 456-459.
- Lee I, Griffin AL, Zilli EA, Eichenbaum H, & Hasselmo ME. (2006). Gradual translocation of spatial correlates of neuronal firing in the hippocampus toward prospective reward locations. *Neuron*, **51**: 639-650.
- Leutgeb S, Leutgeb JK, Moser MB, & Moser EI. (2005a). Place cells, spatial maps and the population code for memory. *Current Opinion in Neurobiology*, **15**: 738-746.
- Leutgeb S, Leutgeb JK, Barnes CA, Moser EI, McNaughton BL, & Moser MB. (2005b). Independent codes for spatial and episodic memory in hippocampal neuronal ensembles. *Science*, **309**: 619-623.
- Lewis, P. A., & Miall, R. C. (2006). A right hemispheric prefrontal system for cognitive time measurement. *Behavioural Processes*, **71**: 226-234.
- Lisman, J. E., & Idiart, M. A. (1995). Storage of 7 \pm 2 short-term memories in oscillatory subcycles. *Science*, **267**: 1512-1515.
- Lisman J. (2005). The theta/gamma discrete phase code occurring during the hippocampal phase precession may be a more general brain coding scheme. *Hippocampus*, **15**: 913-922.
- Lorente de Nó, R. (1934). Studies on the structure of the cerebral cortex. II. Continuation of the study of the ammonic system. *Journal für Psychologie und Neurologie*, **46**: 113-177.
- Loureiro, M., Cholvin, T., Lopez, J., Merienne, N., Latreche, A., Cosquer, B., & de Vasconcelos, A. P. (2012). The ventral midline thalamus (reuniens and rhomboid nuclei) contributes to the persistence of spatial memory in rats. *The Journal of Neuroscience*, **32**: 9947-9959.
- MacDonald CJ, Lepage KQ, Eden UT, & Eichenbaum, H. (2011). Hippocampal “time cells” bridge the gap in memory for discontinuous events. *Neuron*, **71**: 737-749.

- MacDonald CJ, Carrow S, Place R, & Eichenbaum H. (2013). Distinct hippocampal time cell sequences represent odor memories in immobilized rats. *The Journal of Neuroscience*, **33**: 14607-14616.
- Maglóczy, Z., Acsády, L., & Freund, T. F. (1994). Principal cells are the postsynaptic targets of supramammillary afferents in the hippocampus of the rat. *Hippocampus*, **4**: 322-334.
- Manns JR, Howard MW, & Eichenbaum H. (2007). Gradual changes in hippocampal activity support remembering the order of events. *Neuron*, **56**: 530-540.
- Manseau, F., Goutagny, R., Danik, M., & Williams, S. (2008). The hippocamposeptal pathway generates rhythmic firing of GABAergic neurons in the medial septum and diagonal bands: an investigation using a complete septohippocampal preparation in vitro. *The Journal of Neuroscience*, **28**: 4096-4107.
- Markram, H., Lübke, J., Frotscher, M., & Sakmann, B. (1997). Regulation of synaptic efficacy by coincidence of postsynaptic APs and EPSPs. *Science*, **275**: 213-215.
- Maviel, T., Durkin, T. P., Menzaghi, F., & Bontempi, B. (2004). Sites of neocortical reorganization critical for remote spatial memory. *Science*, **305**: 96-99.
- McCarthy, G., Blamire, A. M., Puce, A., Nobre, A. C., Bloch, G., Hyder, F., & Shulman, R. G. (1994). Functional magnetic resonance imaging of human prefrontal cortex activation during a spatial working memory task. *Proceedings of the National Academy of Sciences*, **91**: 8690-8694.
- McKenzie S, Robinson NTM, Herrera L, Churchill JC, & Eichenbaum H. (2013). Learning causes reorganization of neuronal firing patterns to represent related experiences within a hippocampal schema. *The Journal of Neuroscience*, **33**: 10243-10256.
- Mehta MR, Barnes CA, & McNaughton BL. (1997). Experience-dependent, asymmetric expansion of hippocampal place fields. *Proceedings of the National Academy of Sciences*, **94**: 8918-8921.
- Meyer-Lindenberg, A. S., Olsen, R. K., Kohn, P. D., Brown, T., Egan, M. F., Weinberger, D. R., & Berman, K. F. (2005). Regionally specific disturbance of dorsolateral prefrontal-hippocampal functional connectivity in schizophrenia. *Archives of General Psychiatry*, **62**: 379-386.
- Miller, E.K., Li, L., & Desimone, R. (1993). Activity of neurons in anterior inferior temporal cortex during a short-term memory task. *Journal of Neurophysiology*, **13**: 1460-1478.

- Miller, G.A., Galanter, E., & Pribram, K. (1960). *Plans and the Structure of Behavior*. Holt: New York.
- Mishkin, M., Ungerleider, L.G., & Macko, K.A. (1983). Object vision and spatial vision: Two cortical pathways. *Trends in Neurosciences*, **6**: 414-417.
- Miyashita, Y., & Chang, H.S. (1988). Neuronal correlate of pictorial short-term memory in the primate temporal cortex. *Nature*, **331**: 68-70.
- Moita MAP, Rosis S, Zhou Y, LeDoux JE, & Blair HT. (2004). Putting fear in its place: Remapping of hippocampal place cells during fear conditioning. *The Journal of Neuroscience*, **24**: 7015-7023.
- Mormann, F., Fell, J., Axmacher, N., Weber, B., Lehnertz, K., Elger, C. E., & Fernández, G. (2005). Phase/amplitude reset and theta–gamma interaction in the human medial temporal lobe during a continuous word recognition memory task. *Hippocampus*, **15**: 890-900.
- Morris, R. G. M., Garrud, P., Rawlins, J. N. P., & O'Keefe, J. (1982). Place navigation impaired in rats with hippocampal lesions. *Nature*, **297**: 681-683.
- Moser, M. B., Moser, E. I., Forrest, E., Andersen, P., & Morris, R. G. (1995). Spatial learning with a minislab in the dorsal hippocampus. *Proceedings of the National Academy of Sciences*, **92**: 9697-9701.
- Motter, B.C. (1994). Neural correlates of feature selective memory and pop-out in extrastriate area V4. *Journal of Neuroscience*, **14**: 2190-2199.
- Nakashiba, T., Buhl, D. L., McHugh, T. J., & Tonegawa, S. (2009). Hippocampal CA3 output is crucial for ripple-associated reactivation and consolidation of memory. *Neuron*, **62**: 781-787.
- Navawongse, R., & Eichenbaum, H. (2013). Distinct pathways for rule-based retrieval and spatial mapping of memory representations in hippocampal neurons. *The Journal of Neuroscience*, **33**: 1002-1013.
- Neunuebel, J. P., & Knierim, J. J. (2012). Spatial firing correlates of physiologically distinct cell types of the rat dentate gyrus. *The Journal of Neuroscience*, **32**: 3848-3858.

- Neunuebel, J. P., & Knierim, J. J. (2014). CA3 retrieves coherent representations from degraded input: direct evidence for CA3 pattern completion and dentate gyrus pattern separation. *Neuron*, **81**: 416-427.
- Newman, E. L., Gillet, S. N., Climer, J. R., & Hasselmo, M. E. (2013). Cholinergic blockade reduces theta-gamma phase amplitude coupling and speed modulation of theta frequency consistent with behavioral effects on encoding. *The Journal of Neuroscience*, **33**: 19635-19646.
- O'Keefe, J., & Dostrovsky, J. (1971). The hippocampus as a spatial map. Preliminary evidence from unit activity in the freely-moving rat. *Brain research*, **34**: 171-175.
- O'Keefe, J. O., & Nadel, L. (1978). *The hippocampus as a cognitive map*. Oxford: Clarendon Press.
- O'Keefe J, & Recce ML. (1993). Phase relationship between hippocampal place units and the EEG theta rhythm. *Hippocampus*, **3**: 317-330.
- O'Neill, P. K., Gordon, J. A., & Sigurdsson, T. (2013). Theta oscillations in the medial prefrontal cortex are modulated by spatial working memory and synchronize with the hippocampus through its ventral subregion. *The Journal of Neuroscience*, **33**: 14211-14224.
- Olton, D.S., & Wertz, M.A. (1978). Hippocampal function and behavior: Spatial discrimination and response inhibition. *Physiology of Behavior*, **20**: 597-605.
- Olton, D. S., Becker, J. T., & Handelmann, G. E. (1979). Hippocampus, space, and memory. *Behavioral and Brain Sciences*, **2**: 313-322.
- Olton, D. S., & Collison, C. (1979). Intramaze cues and "odor trails" fail to direct choice behavior on an elevated maze. *Animal Learning & Behavior*, **7**: 221-223.
- Olton, D. S., Becker, J. T., & Handelmann, G. E. (1980). Hippocampal function: working memory or cognitive mapping?. *Physiological psychology*, **8**: 239-246.
- Owen, A.M., Downes, J.J., Sahakian, B.J., Plkey, C.E., & Robbins, T.W. (1990). Planning and spatial working memory following frontal lobe lesions in man. *Neuropsychologia*, **28**: 1021-1034.

- Pastalkova, E., Itskov, V., Amarasingham, A., & Buzsáki, G. (2008). Internally generated cell assembly sequences in the rat hippocampus. *Science*, **321**: 1322-1327.
- Paulesu, E., Frith, C., & Frackowiak, R.S. (1993). The neural correlates of the verbal component of working memory. *Nature*, **362**: 342-345.
- Paulesu, E., Connelly, A., Frith, C. D., Friston, K. J., Heather, J., Myers, R., & Frackowiak, R. S. (1995). Functional MR imaging correlations with positron emission tomography. Initial experience using a cognitive activation paradigm on verbal working memory. *Neuroimaging Clinics of North America*, **5**: 207-225.
- Pavrides, C., Greenstein, Y. J., Grudman, M., & Winson, J. (1988). Long-term potentiation in the dentate gyrus is induced preferentially on the positive phase of θ -rhythm. *Brain research*, **439**: 383-387.
- Payne, L., & Kounios, J. (2009). Coherent oscillatory networks supporting short-term memory retention. *Brain Research*, **1247**: 126-132.
- Paxinos J., & Watson C. (2005). The rat brain in stereotaxic coordinates, 5th ed. New York: Elsevier.
- Peters, G. J., David, C. N., Marcus, M. D., & Smith, D. M. (2013). The medial prefrontal cortex is critical for memory retrieval and resolving interference. *Learning & Memory*, **20**: 201-209.
- Petrides, M., & Milner, B. (1982). Deficits on subject-ordered tasks after frontal-and temporal-lobe lesions in man. *Neuropsychologia*, **20**: 249-262.
- Petsche, H., Stumpf, C., & Gogolak, G. (1962). The significance of the rabbit's septum as a relay station between the midbrain and the hippocampus I. The control of hippocampus arousal activity by the septum cells. *Electroencephalography and clinical neurophysiology*, **14**: 202-211.
- Peyrache A, Khamassi M, Benchenane K, Wiener SI, & Battaglia FP. (2009). Replay of rule-learning related neural patterns in the prefrontal cortex during sleep. *Nature Neuroscience*, **12**: 919-926.
- Pfeiffer, B. E., & Foster, D. J. (2013). Hippocampal place-cell sequences depict future paths to remembered goals. *Nature*, **497**: 74-79.

- Pikkarainen, M., Rönkkö, S., Savander, V., Insausti, R., & Pitkänen, A. (1999). Projections from the lateral, basal, and accessory basal nuclei of the amygdala to the hippocampal formation in rat. *Journal of Comparative Neurology*, **403**: 229-260.
- Pitkänen, A., Pikkarainen, M., Nurminen, N., & Ylinen, A. (2000). Reciprocal connections between the amygdala and the hippocampal formation, perirhinal cortex, and postrhinal cortex in rat: a review. *Annals of the New York Academy of Sciences*, **911**: 369-391.
- Poolos, N.P., Migliore, M., & Johnston, D. (2002). Pharmacological upregulation of h-channels reduces the excitability of pyramidal neuron dendrites. *Nature Neuroscience*, **5**: 767-774.
- Porter MC, & Mair RG. (1997). The effects of frontal cortical lesions on remembering depend on the procedural demands of tasks performed in the radial arm maze. *Behavioural Brain Research*, **87**: 115-125.
- Prasad JA, Macgregor EM, & Chudasama Y. (2013). Lesions of the thalamic reuniens cause impulsive but not compulsive responses. *Brain Structure and Function*, **218**: 85-96.
- Preston, A. R., & Eichenbaum, H. (2013). Interplay of hippocampus and prefrontal cortex in memory. *Current Biology*, **23**: 764-773.
- Racine, R. J., & Kimble, D. P. (1965). Hippocampal lesions and delayed alternation in the rat. *Psychonomic science*, **3**: 285-286.
- Rainer, G., Asaad, W.F., & Miller, E.K. (1998). Selective representation of relevant information by neurons in the primate prefrontal cortex. *Nature*, **393**: 577-579.
- Rao, S.C., Rainer, G., & Miller, E.K. (1997). Integration of what and where in the primate prefrontal cortex. *Science*, **276**: 821-824.
- Romo, R., & Salinas, E. (2001). Touch and go: Decision-making mechanisms in somatosensation. *Annual Review of Neuroscience*, **24**: 107-137.

- Romo, R., Hernandez, A., Zainos, A., Lemus, L., & Brody, C.D. (2002). Neuronal correlates of decision-making in secondary somatosensory cortex. *Nature Neuroscience*, **5**: 1217-1225.
- Rowe, J. B., Toni, I., Josephs, O., Frackowiak, R. S., & Passingham, R. E. (2000). The prefrontal cortex: response selection or maintenance within working memory?. *Science*, **288**: 1656-1660.
- Saalmann, Y. B. (2014). Intralaminar and medial thalamic influence on cortical synchrony, information transmission and cognition. *Frontiers in Systems Neuroscience*, **8**.
- Salmon, E., Van der Linden, M., Collette, F., Delfiore, G., Maquet, P., Degueldre, C., & Franck, G. (1996). Regional brain activity during working memory tasks. *Brain*, **119**: 1617-1625.
- Santoro, A. (2013). Reassessing pattern separation in the dentate gyrus. *Frontiers in behavioral neuroscience*, **7**.
- Sarnthein, J., Petsche, H., Rappelsberger, P., Shaw, G. L., & Von Stein, A. (1998). Synchronization between prefrontal and posterior association cortex during human working memory. *Proceedings of the National Academy of Sciences*, **95**: 7092-7096.
- Sauseng, P., Klimesch, W., Doppelmayr, M., Hanslmayr, S., Schabus, M., & Gruber, W. R. (2004). Theta coupling in the human electroencephalogram during a working memory task. *Neuroscience letters*, **354**: 123-126.
- Sauseng, P., Klimesch, W., Heise, K. F., Gruber, W. R., Holz, E., Karim, A. A., & Hummel, F. C. (2009). Brain oscillatory substrates of visual short-term memory capacity. *Current biology*, **19**: 1846-1852.
- Sawaguchi, T., Matsumura, M., & Kubota, K. (1990). Effects of dopamine antagonists on neuronal activity related to a delayed response task in monkey prefrontal cortex. *Journal of Neurophysiology*, **63**: 1401-1412.
- Schmitzer-Torbert N, Jackson J, Henze D, Harris K, & Redish AD. (2005). Quantitative measures of cluster quality for use in extracellular recordings. *Neuroscience*, **131**: 1-11.
- Scoville, W. B., & Milner, B. (1957). Loss of recent memory after bilateral hippocampal lesions. *Journal of neurology, neurosurgery, and psychiatry*, **20**: 11.

- Seamans, J. K., Floresco, S. B., & Phillips, A. G. (1995). Functional differences between the prelimbic and anterior cingulate regions of the rat prefrontal cortex. *Behavioral neuroscience*, **109**: 1063.
- Seidenbecher T, Laxmi TR, Stork O, & Pape HC. (2003). Amygdalar and hippocampal theta rhythm synchronization during fear memory retrieval. *Science*, **301**: 846-850.
- Serrien, D. J., Pogosyan, A. H., & Brown, P. (2004). Influence of working memory on patterns of motor related cortico-cortical coupling. *Experimental brain research*, **155**: 204-210.
- Shallice, T., & Warrington, E.K. (1970). Independent functioning of verbal memory stores: A neuropsychological study. *Quarterly Journal of Experimental Psychology*, **22**: 261-273.
- Shaw CL, Watson GDR, Hallock HL, Cline KM, & Griffin, AL. (2013). The role of the medial prefrontal cortex in the acquisition, retention, and reversal of a tactile visuospatial conditional discrimination task. *Behavioural Brain Research*, **236**: 94-101.
- Sherry, D.F., & Shacter, D.L. (1987). The evolution of multiple memory systems. *Psychological Review*, **94**: 439-454.
- Siapas, A. G., Lubenov, E. V., & Wilson, M. A. (2005). Prefrontal phase locking to hippocampal theta oscillations. *Neuron*, **46**: 141-151.
- Siegel M, Warden MR, & Miller EK. (2009). Phase-dependent neuronal coding of objects in short-term memory. *Proceedings of the National Academy of Sciences*, **106**: 21341-21346.
- Siegle, J. H., & Wilson, M. A. (2014). Enhancement of encoding and retrieval functions through theta phase-specific manipulation of hippocampus. *Elife*, **3**, e03061
- Sigurdsson, T., Stark, K. L., Karayiorgou, M., Gogos, J. A., & Gordon, J. A. (2010). Impaired hippocampal–prefrontal synchrony in a genetic mouse model of schizophrenia. *Nature*, **464**(7289), 763-767.

- Singer, A. C., Carr, M. F., Karlsson, M. P., & Frank, L. M. (2013). Hippocampal SWR activity predicts correct decisions during the initial learning of an alternation task. *Neuron*, **77**: 1163-1173.
- Skaggs WE, & McNaughton BL. (1996). Replay of neuronal firing sequences in rat hippocampus during sleep following spatial experience. *Science*, **271**: 1870-1873.
- Skaggs WE, McNaughton BL, Wilson MA, & Barnes CA. (1996). Theta phase precession in hippocampal neuronal populations and the compression of temporal sequences. *Hippocampus*, **6**: 149-172.
- Smiley, J.F., & Goldman-Rakic, P.S. (1993). Heterogeneous targets of dopamine synapses in monkey prefrontal cortex demonstrated by serial section electron microscopy: A laminar analysis using the silver-enhanced diaminobenzidine sulfide (SEDS) immunolabeling technique. *Cerebral Cortex*, **3**: 223-238.
- Smith DM, & Mizumori SJ. (2006a). Hippocampal place cells, context, and episodic memory. *Hippocampus*, **16**: 716-729.
- Smith DM, & Mizumori SJ. (2006b). Learning-related development of context-specific neuronal responses to places and events: The hippocampal role in context processing. *The Journal of Neuroscience*, **26**: 3154-3163.
- Smith, E. E., Jonides, J., & Koeppe, R. A. (1996). Dissociating verbal and spatial working memory using PET. *Cerebral Cortex*, **6**: 11-20.
- Smith, M. L., Leonard, G., Crane, J., & Milner, B. (1995). The effects of frontal-or temporal-lobe lesions on susceptibility to interference in spatial memory. *Neuropsychologia*, **33**: 275-285.
- Squire, L.R. (1992). Memory and the hippocampus: A synthesis from findings with rats, monkeys, and humans. *Psychological Review*, **99**: 195-231.
- Squire, L.R. (2004). Memory systems of the brain: A brief history and current perspective. *Neurobiology of Learning and Memory*, **82**: 171-177.

- Stark, E., Roux, L., Eichler, R., Senzai, Y., Royer, S., & Buzsáki, G. (2014). Pyramidal cell-interneuron interactions underlie hippocampal ripple oscillations. *Neuron*, **83**: 467-480.
- Steward, O., & Scoville, S. A. (1976). Cells of origin of entorhinal cortical afferents to the hippocampus and fascia dentata of the rat. *Journal of Comparative Neurology*, **169**: 347-370.
- Stewart, M., & Fox, S. E. (1990). Do septal neurons pace the hippocampal theta rhythm?. *Trends in neurosciences*, **13**: 163-169.
- Strange, B. A., Witter, M. P., Lein, E. S., & Moser, E. I. (2014). Functional organization of the hippocampal longitudinal axis. *Nature Reviews Neuroscience*, **15**: 655-669.
- Swanson, L. W., & Cowan, W. M. (1977). An autoradiographic study of the organization of the efferent connections of the hippocampal formation in the rat. *Journal of Comparative Neurology*, **172**: 49-84.
- Swanson, L. W. (1981). A direct projection from Ammon's horn to prefrontal cortex in the rat. *Brain research*, **217**: 150-154.
- Tamamaki, N., & Nojyo, Y. (1995). Preservation of topography in the connections between the subiculum, field CA1, and the entorhinal cortex in rats. *Journal of Comparative Neurology*, **353**: 379-390.
- Thierry A, Gioanni Y, Degenetais E, Glowinski J. (2000) Hippocampo-prefrontal cortex pathway: Anatomical and electrophysiological characteristics. *Hippocampus*, **10**: 411-19.
- Tort ABL, Kramer MA, Thorn C, Gibson DJ, Kubota Y, Graybiel AM, & Kopell NJ. (2008). Dynamic cross-frequency couplings of local field potential oscillations in rat striatum and hippocampus during performance of a T-maze task. *Proceedings of the National Academy of Sciences*, **105**: 20517-20522.
- Tort ABL, Komorowski R, Eichenbaum H, & Kopell N. (2010). Measuring phase-amplitude coupling between neuronal oscillations of different frequencies. *Journal of Neurophysiology*, **104**: 1195-1210.

- Traub, R. D., Kopell, N., Bibbig, A., Buhl, E. H., LeBeau, F. E., & Whittington, M. A. (2001). Gap junctions between interneuron dendrites can enhance synchrony of gamma oscillations in distributed networks. *The Journal of Neuroscience*, **21**: 9478-9486.
- Vallar, G., & Papagno, C. (2002). Neuropsychological impairments of verbal short-term memory. In *Handbook of Memory Disorders* (Baddeley, A.D., Kopelman, M.D., & Wilson, B.A., eds), pp. 249-270, Wiley: Chichester.
- van der Meer MAA, & Redish AD. (2011). Theta phase precession in rat ventral striatum links place and reward information. *The Journal of Neuroscience*, **31**: 2843-2854.
- Varela, C., Kumar, S., Yang, J. Y., & Wilson, M. A. (2014). Anatomical substrates for direct interactions between hippocampus, medial prefrontal cortex, and the thalamic nucleus reuniens. *Brain Structure and Function*, **219**: 911-929.
- Vertes, R. P. (2006). Interactions among the medial prefrontal cortex, hippocampus and midline thalamus in emotional and cognitive processing in the rat. *Neuroscience*, **142**: 1-20.
- Vertes, R. P., Hoover, W. B., Do Valle, A. C., Sherman, A., & Rodriguez, J. J. (2006). Efferent projections of reuniens and rhomboid nuclei of the thalamus in the rat. *Journal of Comparative Neurology*, **499**: 768-796.
- Vertes, R. P., Hoover, W. B., Szigeti-Buck, K., & Leranth, C. (2007). Nucleus reuniens of the midline thalamus: link between the medial prefrontal cortex and the hippocampus. *Brain research bulletin*, **71**: 601-609.
- Viana Di Prisco G, & Vertes RP. (2006) Excitatory actions of the ventral midline thalamus (Rhomboid/Reuniens) on the medial prefrontal cortex in the rat. *Synapse*, **60**: 45-55.
- Vijayraghavan, S., Wang, M., Birnbaum, S.G., Williams, G.V., & Arnsten, A.F.T. (2007). Inverted-U dopamine D1 receptor actions on prefrontal neurons engaged in working memory. *Nature Neuroscience*, **10**: 376-384.
- Wager, T. D., & Smith, E. E. (2003). Neuroimaging studies of working memory. *Cognitive, Affective, & Behavioral Neuroscience*, **3**: 255-274.

- Walker, J. A., & Olton, D. S. (1979). Spatial memory deficit following fimbria-fornix lesions: Independent of time for stimulus processing. *Physiology & behavior*, **23**: 11-15.
- Wang, M., Ramos, B.P., Paspalas, C.D., Shu, Y., Simen, A., Duque, A., & Arnsten, A.F.T. (2007). A2A-adrenoreceptors strengthen working memory networks by inhibiting cAMP-HCN channel signaling in prefrontal cortex. *Cell*, **129**: 397-410.
- Wikenheiser, A. M., & Redish, A. D. (2015). Hippocampal theta sequences reflect current goals. *Nature Neuroscience*, **18**: 289-294.
- Williams, G.V., & Goldman-Rakic, P.S. (1995). Modulation of memory fields by dopamine D1 receptors in prefrontal cortex. *Nature*, **376**: 572-575.
- Williams, S.M., & Goldman-Rakic, P.S. (1993). Characterization of the dopaminergic innervation of the primate frontal cortex using a dopamine-specific antibody. *Cerebral Cortex*, **3**: 199-222.
- Williams, S.M., & Goldman-Rakic, P.S. (1998). Widespread origin of the primate mesofrontal dopamine system. *Cerebral Cortex*, **8**: 321-345.
- Wilson, F.A., Scalaidhe, S.P., & Goldman-Rakic, P.S. (1993). Dissociation of object and spatial processing domains in primate prefrontal cortex. *Science*, **260**: 1955-1958.
- Wilson MA, & McNaughton BL. (1994). Reactivation of hippocampal ensemble memories during sleep. *Science*, **265**: 676-679.
- Witter, M. P., Groenewegen, H. J., Da Silva, F. L., & Lohman, A. H. M. (1989). Functional organization of the extrinsic and intrinsic circuitry of the parahippocampal region. *Progress in neurobiology*, **33**: 161-253.
- Wood ER, Dudchenko PA, Robitsek RJ, & Eichenbaum H. (2000). Hippocampal neurons encode information about different types of memory episodes occurring in the same location. *Neuron*, **27**: 623-633.
- Xu, W., & Südhof, T. C. (2013). A neural circuit for memory specificity and generalization. *Science*, **339**: 1290-1295.
- Yamamoto, J., Suh, J., Takeuchi, D., & Tonegawa, S. (2014). Successful execution of working memory linked to synchronized high-frequency gamma oscillations. *Cell*, **157**: 845-857.

- Yassa, M. A., & Stark, C. E. (2011). Pattern separation in the hippocampus. *Trends in neurosciences*, **34**: 515-525.
- Ylinen, A., Bragin, A., Nádasdy, Z., Jandó, G., Szabo, I., Sik, A., & Buzsáki, G. (1995). Sharp wave-associated high-frequency oscillation (200 Hz) in the intact hippocampus: network and intracellular mechanisms. *The Journal of neuroscience*, **15**: 30-46.
- Young, J. J., & Shapiro, M. L. (2011). Dynamic coding of goal-directed paths by orbital prefrontal cortex. *The Journal of neuroscience*, **31**: 5989-6000.

Appendix A

LIST OF CODE

A1: Int_DA.m

```
%This script creates an "Int" variable for DA sessions.

clear all, clc

dir = 'X:' %Input field name
datafolder = strcat(dir);
clear dir;

%Load position data
load(strcat(datafolder, 'VT1.mat'));
pos_x = ExtractedX; pos_y = ExtractedY; pos_t = TimeStamps;
clear ExtractedX ExtractedY TimeStamps

%Load event strings
load(strcat(datafolder, 'Events.mat'));

%Define the beginning and end of the session
start = TimeStamps (1,2); %If event timestamps for beginning and
end of session differ from those defined in this script, manually
input event timestamp values
finish = TimeStamps(1,3);
Int = [];
clear EventStrings TimeStamps

%Define the Int variable
ind = find(pos_t>start & pos_t<finish);
pos_t1=pos_t(ind); pos_x1=pos_x(ind); pos_y1=pos_y(ind);
[Int] = whereishe(pos_x1,pos_y1,pos_t1);

Int_ind = find(Int(:,1)>start & Int(:,8)<finish);
starttrials = Int_ind(1,1);
endtrials = Int_ind(end);
Int = Int(1:endtrials,:);

%Populate column 4 of the Int variable
% 0 = Correct, 1 = Incorrect
numtrials = length(Int(:,1)); %Omit the first free-choice trial
```

```

for i = 2:numtrials;
    if(Int(i,3)== Int(i-1,3));
        Int(i,4)= 1;
    else Int(i,4) = 0;
    end
end

percentCorrect = ((numtrials-1) - sum(Int(:,4)))/(numtrials-1)

save(strcat(datafolder, 'Int.mat'), 'Int');

```

A2: cleaningscript.m

```

function[cleaneeg] = cleaningscript(eeg, params)

[cleaneeg, datafit] = rmlinesmovingwinc(eeg, [1 0.5], 10, params, 'n');
cleaneeg = locdetrend(cleaneeg, params.Fs, [1 0.5]);
cleaneeg = cleaneeg';

end

```

A3: Detrend_LFP.m

```

function [Detrended_Signal] = Detrend_LFP(Sample)
%This function detrends continuously sampled data by fitting a low
order
%polynomial to the original signal.

%Inputs - Sample (Continuously sampled data in Samples x Trials
format)

for i = 1:size(Sample,2);
    [p,s,mu] = polyfit((1:numel(Sample(:,i)))', Sample(:,i), 6);
    f_y(:,i) = polyval(p, (1:numel(Sample(:,i)))', [], mu);

    Detrended_Signal(:,i) = Sample(:,i) - f_y(:,i);
end

end

```

A4: PETH_Delay.m

```
function [FR_Stem,FR_CP,FR_Reward,FR_Return,n, nAvg, n_allTrials,
nAvg_Smooth, SEM_Smooth p b FR_Delay] = PETH_Delay(spk, Int)
%This function creates a peri-event time histogram, raster plot, and
%average firing rate plot over time for a single unit recorded during
delay
%pedestal occupancy.

%The function also detects changes in firing rate over time
("ramping"
%activity) by fitting a log-transformed (to account for non-normal
%distributions of firing rate) OLS regression model to the data.

%Inputs
% -spk = 1 x nSamples array of spike timestamps
% -Int = nTrials x 8 matrix of timestamps values for maze occupancy

%Outputs
% -n = Matrix of raw spike counts during delay pedestal occupancy
% -nAvg = Averaged spike counts per 1 second time bin across trials
% -n_allTrials = Summed spike counts per 1 second time bin across
trials
% -nAvg_Smooth = Smoothed firing rate over time
% -SEM_Smooth = Smoothed standard error of the mean estimates for
each
% data point in nAvg_Smooth
% -p = P value for regression coefficient
% -b = Regression coefficient (R)
% -FR_Delay = Mean firing rate during delay pedestal occupancy for
entire
% session

nTrials=length(Int(:,1));
spksec=spk/1e6;
TrialStart = (Int(2:nTrials,1)-26*1e6)/1e6;
TrialEnd = Int(2:nTrials,1)/1e6;
DelayCenter = (Int(2:nTrials,1)-13*1e6)/1e6;
intsec = Int/1e6;
ntrials = size(Int,1);

edges = (-13:1:13);
bin=1;
```

```

for i = 2:ntrials
    spk_new = find(spksec>intsec(i,1) & spksec<intsec(i,5));
    time_spent = (intsec(i,5)) - (intsec(i,1));
    nspikes = length(spk_new);
    FR_Stem(i) = nspikes/time_spent;
end

FR_Stem = mean(FR_Stem);

for i = 2:ntrials
    spk_new = find(spksec>intsec(i,5) & spksec<intsec(i,6));
    time_spent = (intsec(i,6)) - (intsec(i,5));
    nspikes = length(spk_new);
    FR_CP(i) = nspikes/time_spent;
end

FR_CP = mean(FR_CP);

for i = 2:ntrials
    spk_new = find(spksec>intsec(i,6) & spksec<intsec(i,2));
    time_spent = (intsec(i,2)) - (intsec(i,6));
    nspikes = length(spk_new);
    FR_Reward(i) = nspikes/time_spent;
end

FR_Reward = mean(FR_Reward);

for i = 2:ntrials
    spk_new = find(spksec>intsec(i,7) & spksec<intsec(i,8));
    time_spent = (intsec(i,8)) - (intsec(i,7));
    nspikes = length(spk_new);
    FR_Return(i) = nspikes/time_spent;
end

FR_Return = mean(FR_Return);

for i = 2:nTrials
    s=spksec(find(spksec>TrialStart(i-1) & spksec<TrialEnd(i-1)));
    ev=DelayCenter(i-1);
    s0=s-ev; %Designate middle of delay as time zero
    n(:,i-1) = histc(s0,edges);
    if isempty(s)==0, subplot(311), plot(s0,i, 'k.'), end
    axis([-13 13 0 nTrials+1])
    hold on
end

```

```

n_allTrials = sum(n,2)*bin; %Sum spike counts across trials for each
bin
max_n_allTrials = max(n_allTrials);
subplot(312), bar(edges,n_allTrials), axis([-13 13 0
max_n_allTrials+1])

%Create data for firing rate plot
nAvg = mean(n,2); %Average spike counts across trials for each bin
nAvg_Smooth = sgolayfilt(nAvg,3,11); %Apply 3rd degree Savitzky-Golay
filter to averaged spike counts
Std = std(n,0,2);
SEM = Std/sqrt(nTrials); %Calculate standard error of the mean across
trials for each bin
SEM_Smooth = sgolayfilt(SEM,3,11); %Smooth standard error values to
correspond to smoothed spike count averages
max_data = max(nAvg_Smooth) + max(SEM_Smooth);
max_graph = max_data + 0.05;
subplot(313)
varargout=shadedErrorBar(edges,nAvg_Smooth,SEM_Smooth,'b',0)
%plot(edges, nAvg_Smooth) %Plot smoothed firing rate plot
%hold on
%plot(edges,nAvg_Smooth + SEM_Smooth,'b--')
%hold on
%plot(edges,nAvg_Smooth - SEM_Smooth,'b--')
axis tight

%Calculate correlation coefficient of firing rate over time
nAvg(19,:) = [];
x = linspace(1,18,18);
x = x';
[b, dev, stats] = glmfit(x,nAvg,'poisson');
p = stats.p(2,1);
b = stats.beta(2,1);
FR_Delay = mean(nAvg,1);

end

```

A5: Entrainment_Delay.m

```

function [mrl pval mrl_subsampled z n xout nSpikes] =
Entrainment_Delay(Int, Timestamps, Samples, Spk)
%This function calculates the spike-phase distribution between a
single

```

```

%unit and simultaneously recorded theta oscillations during delay
pedestal
%occupancy.

%Inputs:
%Int - nTrials x 8 matrix (see function "Int_DA.m")
%Timestamps - 1 x nSamples array (continuously sampled data)
%Samples - 512 x nSamples matrix (continuously sampled data)
%Spk - Array of spike times in nSamples x 1 format

%Outputs:
%mrl - Length of mean resultant length vector (ranges from 0 to 1)
%pval - Rayleigh's p-value (based on Rayleigh's z statistic)
%mr1_subsampled - Length of mean resultant length vector calculated
from a bootstrapped
%   sampling distribution of n = 50 spike-phase pairs (partially
controls
%   for differences in spike count between single units)
%z - Rayleigh's z statistic (z value relative to null hypothesis of
uniform
%   spike-phase distribution)
%n - Phase-binned spike counts
%xout - Phase axis for histogram
%nSpikes - Number of spikes assigned a phase value (should be >50)

%This function calls the functions "Chronux_LFP.m",
"Skaggs_filter.m",
%"Detrend_LFP.m", and "PhaseFreqDetect.m"

%Isolate LFP samples occurring during delay pedestal occupancy
[data1_delay data1_stem data1_choice_point] =
Chronux_LFP(Int,Samples,Timestamps);
data1_delay = data1_delay(:)';
data1_delay = data1_delay';
data1_delay = Detrend_LFP(data1_delay); %Get rid of drifting
artifacts in CSC data
[signal_filtered] = Skaggs_filter(data1_delay); %Filter theta from
raw signal

%Isolate CSC timestamps for delay pedestal occupancy
Samples = Samples(:)';
Timestamps =
linspace(Timestamps(1,1),Timestamps(1,end),length(Samples));
numtrials = size(Int,1);
signal_ts = cell(numtrials,1);

```

```

for i = 2:numtrials %Create timestamp index
signal_ts{i} = find(Timestamps>Int(i,1)-25*1e6 &
Timestamps<Int(i,1));
end
maxLength=max(cellfun(@(x) numel(x), signal_ts));
signal_ts = cell2mat(cellfun(@(x) cat(2,x,zeros(1,maxLength-
length(x))),...
    signal_ts, 'UniformOutput', false)); %Convert cell array of indexed
timestamp values to numeric array
signal_ts(1,:) = [];
signal_ts = signal_ts';
signal_ts(length(signal_ts),:) = [];
signal_ts = Timestamps(signal_ts);
signal_ts = signal_ts(:)';
signal_filtered = signal_filtered';

[Phase, InstCycleFrequency, PerCycleFreq, signal_filtered] = ...
    PhaseFreqDetect(signal_filtered, signal_ts); %Isolate theta
phases (degrees) for each CSC timestamp
PhaseRadians = Phase*(pi/180); %Convert theta phase degree values to
radians

Spk = Spk';
for i = 2:numtrials; %Create index of spike timestamps occurring
during delay pedestal occupancy
    s{i} = find(Spk>Int(i,1)-25*1e6 & Spk<Int(i,1));
end
ix = cellfun(@isempty,s);
s(ix) = {nan}; %Get rid of empty cells (trials during which no spikes
occurred)
spk_new = cell2mat(s); %Convert cell array index to numeric array
spk_new(isnan(spk_new)) = []; %Get rid of cells containing NaN values
spk_phase = Phase(spk_new); %Phase value, in degrees, for each spike
timestamp
spk_phase_radians = PhaseRadians(spk_new); %Phase value, in radians,
for each spike timestamp
spk_phase(isnan(spk_phase)) = []; %Get rid of spikes that could not
be assigned a theta phase (due to low theta amplitude)
spk_phase_radians(isnan(spk_phase_radians)) = [];

nSpikes = length(spk_phase);

%for i = 2:numtrials;
%    sCP{i} = find(Spk>Int(i,5)-1*1e6 & Spk<Int(i,5)+1*1e6);
%end
%ixCP = cellfun(@isempty,sCP);

```

```

%sCP(ixCP) = {nan};
%spk_CPnew = cell2mat(sCP);
%spk_CPnew(isnan(spik_CPnew)) = [];
%nSpikesCP = length(spik_CPnew);
%FR_CP = (nSpikesCP/size(Int,1))/2;

%In order to control for effect of number of spikes on mean resultant
%length vector, randomly subsample 50 spikes from the spike-phase
%distribution 1000 times and take the mean MRL value of the
subsampled
%distribution
permnum = 1000;
for i = 1:permnum
    random_spikes = randsample(spik_phase_radians,50);
    mrl(i) = circ_r(random_spikes);
end
mrl_subsampled = mean(mrl,2);
mrl = circ_r(spik_phase_radians); %Calculate cluster's mean resultant
length vector
[pval, z] = circ_rtest(spik_phase_radians); %Calculate Rayleigh's z
statistic and resulting p value (deviance from a uniform
distribution)
[n xout] = hist(spik_phase,[0:30:360]); %Create histogram of spike
counts per phase bin

subplot(121)
circ_plot(spik_phase_radians,'hist')
subplot(122)
bar(xout,n)
xlim ([0 360])
xlabel ('Theta Phase')
ylabel ('Spike Count')

end

```

A6: Skaggs_filter.m

```

%Input is the eeg values and output is the filtered eeg values.
%Uses a butterworth filter, 3rd order. Can change filter limits in
lines 7
%and 8.

```

```

function filteredeeg=Skaggs_filter(eegval)
nfq=2034/2; %Niquist frequency (nfq)=sampling rate/2
par1=4/nfq;

```

```

par2=12/nfq;
[b,a]=butter(3,[par1 par2]);
filteredeeg=filtfilt(b,a,eegval);

```

A7: PhaseFreqDetect.m

```

function [Phase, InstCycleFrequency, PerCycleFreq, signal_filtered] =
DetectPhase(signal_filtered, signal_ts)

% signal_filtered should be bandpass filtered (filtfilt). It's most
% important to get high frequency oscillations out - so 1-60 is okay,
% 1-30
% or even 4-12Hz might be better, depending on your need.

% Ensure that you have 'signal' processing toolbox added to your
% path.
% Otherwise matlab will use the wrong version of the function
% 'findpeaks'

% Set parameters for allowed peak and trough detection. These can be
% changed to whatever you want. 6-10 is about standard. This will
% not
% filter your signal - it will only constrain this code to find
% cycles
% within this range.
MinFreq = 6;
MaxFreq = 10;

%%
fs = 2034;
MPD = 1/MaxFreq*fs;

[~, peaks] = findpeaks(signal_filtered, 'MINPEAKDISTANCE',
round(MPD));
[~, troughs] = findpeaks(signal_filtered.*-1, 'MINPEAKDISTANCE',
round(MPD));

Test = 0;
PerCycleFreq = [];

Phase = NaN(length(signal_filtered),1);
InstCycleFrequency = NaN(length(signal_filtered),1);

for i = 1:length(peaks)-1

```

```

    valley = troughs(find(troughs > peaks(i) & troughs <
peaks(i+1)));
    if length(valley) ~= 1, continue, end % Makes sure there is one
valley between the peaks
    % find zero crossings for descending zero and ascending zero
    [~, ZeroCross270] = min(abs(signal_filtered(peaks(i):valley) -
[(signal_filtered(peaks(i)) + signal_filtered(valley)) / 2]));
    ZeroCross270 = ZeroCross270+peaks(i)-1;
    [~, ZeroCross90] = min(abs(signal_filtered(valley:peaks(i+1)) -
[(signal_filtered(peaks(i+1)) + signal_filtered(valley)) / 2]));
    ZeroCross90 = ZeroCross90+valley-1 ;

    ThetaCyclePhase = [];
    % peak to ZeroCross 270
    x = [peaks(i) ZeroCross270];
    if length(unique(x)) == 1, Test = Test+1; continue, end
    y = [180 270];
    xi = peaks(i):1:ZeroCross270;
    yi = interp1(x,y,xi);

    ThetaCyclePhase(peaks(i)-peaks(i)+1:1:ZeroCross270-peaks(i)+1) =
yi;

    % ZeroCross270 to trough
    x = [ZeroCross270 valley];
    if length(unique(x)) == 1, Test = Test+1; continue, end
    y = [270 360];
    xi = ZeroCross270:1:valley;
    yi = interp1(x,y,xi);

    ThetaCyclePhase(ZeroCross270-peaks(i)+1:1:valley-peaks(i)+1) =
yi;

    % trough to ZeroCross90 - not huge problem
    x = [valley ZeroCross90];
    if length(unique(x)) == 1, Test = Test+1; continue, end
    y = [0 90];
    xi = valley:1:ZeroCross90;
    yi = interp1(x,y,xi);

    ThetaCyclePhase(valley-peaks(i)+1:1:ZeroCross90-peaks(i)+1) = yi;

    % ZeroCross90 to peak
    x = [ZeroCross90 peaks(i+1)];
    if length(unique(x)) == 1, Test = Test+1;continue, end

```

```

y = [90 180];
xi = ZeroCross90:1:peaks(i+1);
yi = interp1(x,y,xi);

ThetaCyclePhase(ZeroCross90-peaks(i)+1:1:peaks(i+1)-peaks(i)+1) =
yi;

Phase(peaks(i):peaks(i+1)) = ThetaCyclePhase;
InstCycleFrequency(peaks(i):peaks(i+1)) = 1/((peaks(i+1)-
peaks(i))/fs);
PerCycleFreq(i) = 1/((peaks(i+1)-peaks(i))/fs);
end
PerCycleFreq(PerCycleFreq == 0) = NaN;

```

A8: OneTrialPAC.m (used to construct wavelet-filtered spectrograms)

```

function [tfZ, EEGTheta, EEGGamma] = OneTrialPAC(PhaseSample,
PowerSample, srate)
%One-trial visualization of theta-gamma phase-amplitude coupling

min_freq = 30;
max_freq = 120;
num_frex = 91;

Ldata = length(PowerSample);
Ltapr = length(PowerSample);
Lconv1 = Ldata+Ltapr-1;
Lconv = pow2(nextpow2(Lconv1));
frex=30:120;

tf=zeros(91,length(PowerSample));
datspctra = fft(PowerSample,Lconv);
s=4./(2*pi.*frex);
t=-((length(PowerSample)-1)/2)/srate:1/srate:((length(PowerSample)-
2)/2)/srate+1/srate;

for fi=1:length(frex);
wavelet=exp(2*i*pi*frex(fi).*t).*exp(-t.^2./(2*s(fi)^2));
m = ifft(datspctra.*fft(wavelet,Lconv),Lconv);
m = m(1:Lconv1);
m = m(floor((Ltapr-1)/2):end-1-ceil((Ltapr-1)/2));
tf(fi,:) = abs(m).^2;
end

tfZ = zscore(tf);

```

```

times = linspace(-500,500,length(PowerSample));

nfq=srate/2;
par1=6/nfq;
par2=10/nfq;
[b,a]=butter(3,[par1 par2]);
EEGTheta=filtfilt(b,a,PhaseSample);

nfq=srate/2;
par1=50/nfq;
par2=80/nfq;
[b,a]=butter(3,[par1 par2]);
EEGGamma=filtfilt(b,a,PowerSample);

%subplot(311)
%imagesc(times,frex,tfZ)

%subplot(312)
%plot(times,PhaseSample,'k')
%axis tight
%hold on
%plot(times,EEGTheta,'r')

%subplot(313)
plot(times,EEGGamma,'b')
axis tight

end

```

A9: coherence_master.m

```

function
[Delay,Stem,Choice_Point,C_ChoicePoint,Cohgram,CP_Theta,CP_ThetaMap]
= coherence_master(Int,EEG1,EEG2,Timestamps,srate)
%UNTITLED Summary of this function goes here
% Detailed explanation goes here

[data1_delay, data1_stem, CP_EEG1] = Chronux_LFP(Int, EEG1,
Timestamps);
[data1_delay, data1_stem, CP_EEG2] = Chronux_LFP(Int, EEG2,
Timestamps);

CP_EEG1 = Detrend_LFP(CP_EEG1);

```

```

CP_EEG2 = Detrend_LFP(CP_EEG2);

EEG1 = EEG1(:)';
EEG2 = EEG2(:)';
Timestamps = linspace(Timestamps(1,1),Timestamps(1,end),
length(EEG1));

params.tapers = [5 9];
params.pad = 0;
params.Fs = srate;
params.fpass = [0 100];
params.err = [2 .05];
params.trialave = 0;

[EEG1] = cleaningscript(EEG1, params);
[EEG2] = cleaningscript(EEG2, params);

ntrials = size(Int,1);

for i = 2:ntrials
    Timestamps_new = Timestamps(Timestamps>Int(i-1,8) &
Timestamps<Int(i,1));
    EEG1_new = EEG1(Timestamps>Int(i-1,8) & Timestamps<Int(i,1));
    EEG2_new = EEG2(Timestamps>Int(i-1,8) & Timestamps<Int(i,1));
    EEG1_new = EEG1_new';
    EEG2_new = EEG2_new';
    EEG1_new = Detrend_LFP(EEG1_new);
    EEG2_new = Detrend_LFP(EEG2_new);
    EEG1_new = EEG1_new';
    EEG2_new = EEG2_new';

    params.fpass = [0 4];

[C,phi,S12,S1,S2,f,confC,phistd,Cerr]=coherencyc(EEG1_new,EEG2_new,pa
rams);
    C_Delta(i-1) = mean(C);

    params.fpass = [4 12];

[C,phi,S12,S1,S2,f,confC,phistd,Cerr]=coherencyc(EEG1_new,EEG2_new,pa
rams);
    C_Theta(i-1) = mean(C);

    params.fpass = [15 30];

```

```

[C,phi,S12,S1,S2,f,confC,phistd,Cerr]=coherencyc (EEG1_new,EEG2_new,pa
rams);
    C_Beta(i-1) = mean(C);

    params.fpass = [30 80];

[C,phi,S12,S1,S2,f,confC,phistd,Cerr]=coherencyc (EEG1_new,EEG2_new,pa
rams);
    C_Gamma(i-1) = mean(C);
end

Delay.Delta = mean(C_Delta);
Delay.Theta = mean(C_Theta);
Delay.Beta = mean(C_Beta);
Delay.Gamma = mean(C_Gamma);

%permnum = 20;

%for k = 1:permnum

%   shuffle_index_EEG1 = randperm(length(EEG1));
%   shuffled_EEG1 = EEG1(shuffle_index_EEG1);
%   shuffle_index_EEG2 = randperm(length(EEG2));
%   shuffled_EEG2 = EEG2(shuffle_index_EEG2);

%   for i = 2:ntrials
%   Timestamps_new = Timestamps(Timestamps>Int(i-1,8) &
Timestamps<Int(i,1));
%   EEG1_new = shuffled_EEG1(Timestamps>Int(i-1,8) &
Timestamps<Int(i,1));
%   EEG2_new = shuffled_EEG2(Timestamps>Int(i-1,8) &
Timestamps<Int(i,1));
%   EEG1_new = EEG1_new';
%   EEG2_new = EEG2_new';
%   EEG1_new = Detrend_LFP(EEG1_new);
%   EEG2_new = Detrend_LFP(EEG2_new);
%   EEG1_new = EEG1_new';
%   EEG2_new = EEG2_new';

%   params.fpass = [4 12];
%
[C,phi,S12,S1,S2,f,confC,phistd,Cerr]=coherencyc (EEG1_new,EEG2_new,pa
rams);
%   C_Theta(i-1) = mean(C);

```

```

% end

% shuffled_theta(k) = mean(C_Theta);

%end

%Delay.Theta_Shuffled = mean(shuffled_theta);

for i = 2:ntrials
    Timestamps_new = Timestamps(Timestamps>Int(i,1) &
Timestamps<Int(i,5));
    EEG1_new = EEG1(Timestamps>Int(i,1) & Timestamps<Int(i,5));
    EEG2_new = EEG2(Timestamps>Int(i,1) & Timestamps<Int(i,5));
    EEG1_new = EEG1_new';
    EEG2_new = EEG2_new';
    EEG1_new = Detrend_LFP(EEG1_new);
    EEG2_new = Detrend_LFP(EEG2_new);
    EEG1_new = EEG1_new';
    EEG2_new = EEG2_new';

    params.fpass = [0 4];

[C,phi,S12,S1,S2,f,confC,phistd,Cerr]=coherencyc(EEG1_new,EEG2_new,pa
rams);
    C_Delta(i-1) = mean(C);

    params.fpass = [4 12];

[C,phi,S12,S1,S2,f,confC,phistd,Cerr]=coherencyc(EEG1_new,EEG2_new,pa
rams);
    C_Theta(i-1) = mean(C);

    params.fpass = [15 30];

[C,phi,S12,S1,S2,f,confC,phistd,Cerr]=coherencyc(EEG1_new,EEG2_new,pa
rams);
    C_Beta(i-1) = mean(C);

    params.fpass = [30 80];

[C,phi,S12,S1,S2,f,confC,phistd,Cerr]=coherencyc(EEG1_new,EEG2_new,pa
rams);
    C_Gamma(i-1) = mean(C);
end

```

```

Stem.Delta = mean(C_Delta);
Stem.Theta = mean(C_Theta);
Stem.Beta = mean(C_Beta);
Stem.Gamma = mean(C_Gamma);

%for k = 1:length(permnum)

%   shuffle_index_EEG1 = randperm(length(EEG1));
%   shuffled_EEG1 = EEG1(shuffle_index_EEG1);
%   shuffle_index_EEG2 = randperm(length(EEG2));
%   shuffled_EEG2 = EEG2(shuffle_index_EEG2);

%   for i = 2:ntrials
%   Timestamps_new = Timestamps(Timestamps>Int(i,1) &
Timestamps<Int(i,5));
%   EEG1_new = shuffled_EEG1(Timestamps>Int(i,1) &
Timestamps<Int(i,5));
%   EEG2_new = shuffled_EEG2(Timestamps>Int(i,1) &
Timestamps<Int(i,5));
%   EEG1_new = EEG1_new';
%   EEG2_new = EEG2_new';
%   EEG1_new = Detrend_LFP(EEG1_new);
%   EEG2_new = Detrend_LFP(EEG2_new);
%   EEG1_new = EEG1_new';
%   EEG2_new = EEG2_new';

%   params.fpass = [4 12];
%
[C,phi,S12,S1,S2,f,confC,phistd,Cerr]=coherencyc(EEG1_new,EEG2_new,pa
rams);
%   C_Theta(i-1) = mean(C);

%   end

%   shuffled_theta(k) = mean(C_Theta);

%end

%Stem.Theta_Shuffled = mean(shuffled_theta);

for i = 2:ntrials
    Timestamps_new = Timestamps(Timestamps>Int(i,5) &
Timestamps<Int(i,6));

```

```

    EEG1_new = EEG1(Timestamps>Int(i,5) & Timestamps<Int(i,6));
    EEG2_new = EEG2(Timestamps>Int(i,5) & Timestamps<Int(i,6));
    EEG1_new = EEG1_new';
    EEG2_new = EEG2_new';
    EEG1_new = Detrend_LFP(EEG1_new);
    EEG2_new = Detrend_LFP(EEG2_new);
    EEG1_new = EEG1_new';
    EEG2_new = EEG2_new';

    params.fpass = [0 4];

[C,phi,S12,S1,S2,f,confC,phistd,Cerr]=coherencyc(EEG1_new,EEG2_new,pa
rams);
    C_Delta(i-1) = mean(C);

    params.fpass = [4 12];

[C,phi,S12,S1,S2,f,confC,phistd,Cerr]=coherencyc(EEG1_new,EEG2_new,pa
rams);
    C_Theta(i-1) = mean(C);

    params.fpass = [15 30];

[C,phi,S12,S1,S2,f,confC,phistd,Cerr]=coherencyc(EEG1_new,EEG2_new,pa
rams);
    C_Beta(i-1) = mean(C);

    params.fpass = [30 80];

[C,phi,S12,S1,S2,f,confC,phistd,Cerr]=coherencyc(EEG1_new,EEG2_new,pa
rams);
    C_Gamma(i-1) = mean(C);
end

C_Theta(isnan(C_Theta)) = [];

Choice_Point.Delta = mean(C_Delta);
Choice_Point.Theta = mean(C_Theta);
Choice_Point.Beta = mean(C_Beta);
Choice_Point.Gamma = mean(C_Gamma);

%for k = 1:length(permnum)

%    shuffle_index_EEG1 = randperm(length(EEG1));

```

```

% shuffled_EEG1 = EEG1(shuffle_index_EEG1);
% shuffle_index_EEG2 = randperm(length(EEG2));
% shuffled_EEG2 = EEG2(shuffle_index_EEG2);

% for i = 2:ntrials
% Timestamps_new = Timestamps(Timestamps>Int(i,5) &
Timestamps<Int(i,6));
% EEG1_new = shuffled_EEG1(Timestamps>Int(i,5) &
Timestamps<Int(i,6));
% EEG2_new = shuffled_EEG2(Timestamps>Int(i,5) &
Timestamps<Int(i,6));
% EEG1_new = EEG1_new';
% EEG2_new = EEG2_new';
% EEG1_new = Detrend_LFP(EEG1_new);
% EEG2_new = Detrend_LFP(EEG2_new);
% EEG1_new = EEG1_new';
% EEG2_new = EEG2_new';

% params.fpass = [4 12];
%
[C,phi,S12,S1,S2,f,confC,phistd,Cerr]=coherencyc(EEG1_new,EEG2_new,pa
rams);
% C_Theta(i-1) = mean(C);

% end

% shuffled_theta(k) = mean(C_Theta);

%end

%Choice_Point.Theta_Shuffled = mean(shuffled_theta);

params.fpass = [0 100];
params.trialave = 1;

[C_ChoicePoint,phi,S12,S1,S2,f_Stat,confC,phistd,Cerr]=coherencyc(CP_
EEG1,CP_EEG2,params);
C_ChoicePoint = C_ChoicePoint';

movingwin = [.5 .2];

[Cohgram,phi,S12,S1,S2,t,f_Mov,confC,phistd,Cerr]=cohgramc(CP_EEG1,CP
_EEG2,movingwin,params);

```

```

params.fpass = [4 12];

[CP_ThetaMap,phi,S12,S1,S2,t,f_Mov_Theta,confC,phistd,Cerr]=cohgramc(
CP_EEG1,CP_EEG2,movingwin,params);

CP_Theta = mean(CP_ThetaMap,2);

CP_Theta = CP_Theta';

%for i = 2:ntrials
    %for j = 1:(size(IntStem,2))-1
        %Timestamps_new = Timestamps(Timestamps>IntStem(i,j) &
Timestamps<IntStem(i,j+1));
        %EEG1_new = EEG1(Timestamps>IntStem(i,j) &
Timestamps<IntStem(i,j+1));
        %EEG2_new = EEG2(Timestamps>IntStem(i,j) &
Timestamps<IntStem(i,j+1));
        %EEG1_new = EEG1_new';
        %EEG2_new = EEG2_new';
        %EEG1_new = Detrend_LFP(EEG1_new);
        %EEG2_new = Detrend_LFP(EEG2_new);
        %EEG1_new = EEG1_new';
        %EEG2_new = EEG2_new';

        %params.fpass = [0 4];

%[C,phi,S12,S1,S2,f,confC,phistd,Cerr]=coherencyc(EEG1_new,EEG2_new,p
arams);
        %C_Delta(i-1) = mean(C);

        %params.fpass = [4 12];

%[C,phi,S12,S1,S2,f,confC,phistd,Cerr]=coherencyc(EEG1_new,EEG2_new,p
arams);
        %C_Theta(i-1) = mean(C);

        %params.fpass = [15 30];

%[C,phi,S12,S1,S2,f,confC,phistd,Cerr]=coherencyc(EEG1_new,EEG2_new,p
arams);
        %C_Beta(i-1) = mean(C);

        %params.fpass = [30 80];

```

```

%[C,phi,S12,S1,S2,f,confC,phistd,Cerr]=coherencyc (EEG1_new,EEG2_new,p
arams);
    %C_Gamma(i-1) = mean(C);

    %muDelta(:,j) = mean(C_Delta);
    %muTheta(:,j) = mean(C_Theta);
    %muBeta(:,j) = mean(C_Beta);
    %muGamma(:,j) = mean(C_Gamma);
    %end
%end

%StemBinned.Delta = muDelta;
%StemBinned.Theta = muTheta;
%StemBinned.Beta = muBeta;
%StemBinned.Gamma = muGamma;

subplot(311)
plot(f_Stat,C_ChoicePoint)

subplot(312)
pcolor(t,f_Mov,Cohgram')
shading interp

subplot(313)
pcolor(t,f_Mov_Theta,CP_ThetaMap')
shading interp

colormap(jet)

end

```

A10: theta_mod_gamma.m

```

function [avgM,M,MI] =
theta_mod_gamma(eegtheta,eeggamma,Int,Timestamps,Type)

%This function creates a phase-amplitude distribution between theta
and
%slow gamma oscillations either within one signal, or between two
signals.

%The phase-amplitude distribution is then assigned a modulation index
value

```

```

%(see Tort et al., 2010). The original data are then shuffled and a
z-test
%is performed between the observed modulation index value and the
shuffled
%distribution of modulation index values.

%tic:toc(2) = 172.195810 seconds
%h1h 020515

%Input arguments:
% -Eegtheta: 512 x nSamples matrix of raw LFP values used for phase
% estimation
% -Eeggamma: 512 x nSamples matrix of raw LFP values used for
amplitude
% estimation
% -Int: nTrials x 8 matrix of maze timestamps values
% -Timestamps: 1 x nSamples array of LFP timesetamps values
% -Type: Either a 1, 2, or 3 depending on which areas of the maze
are to
% be analyzed
% -if Type = 1, theta-gamma coupling for delay pedestal
occupancy is
% analyzed
% -if Type = 2, theta-gamma coupling for stem occupancy is
analyzed
% -if Type = 3, theta-gamma coupling for choice point occupancy
is
% analyzed
%
%Output:
% -M: nTrials x 5 struct array with the following fields:
% 'MI', 'amp', 'NormAmp', 'PhaseAxis', 'phase'
% M.MI = modulation index value, M.amp = gamma amplitude for
each
% phase bin, M.NormAmp = normalized gamma amplitude for each
phase
% bin, M.PhaseAxis = theta phase bins, M.phase = theta phase
bin with
% highest gamma amplitude
% -avgM: Struct array with session averaged MI, amp, and NormAmp
values
% -MI_shuffled: 1 x 100 array of averaged MI values from 100
permutations
% of randomly shuffled data
% -MI_Z: Z-score of observed MI value within distribution of
shuffled MI

```

```

%         values
%   -p: p-value produced from z-test comparing the observed average
MI
%         value against the distribution of shuffled MI values

if nargin ~= 5
    error('theta_mod_gamma:argChk', 'Wrong number of input
arguments')
end

%if Type ~= [1 2 3]
    %error('theta_mod_gamma:argType', 'Final input argument must be
equal to 1, 2, or 3')
%end

%eegtheta = eegtheta(:)';
%eeggamma = eeggamma(:)';
%ts = linspace(Timestamps(1,1),Timestamps(1,end), length(eegtheta));
ts = Timestamps;

%params.tapers = [5 9];
%params.pad = 0;
%params.Fs = 2034;
%params.fpass = [0 100];
%params.err = [2 .05];
%params.trialave = 0;

%[eegtheta] = cleaningscript(eegtheta, params);
%[eeggamma] = cleaningscript(eeggamma, params);

lowpass1 = 6;
highpass1 = 11;
lowpass2 = 30;
highpass2 = 80;

ntrials = size(Int,1);

if Type == 1
    for i = 2:ntrials;
        ts_new = ts(ts>Int(i-1,8) & ts<Int(i,1));
    end
end

```

```

eegtheta_new = eegtheta(ts>Int(i-1,8) & ts<Int(i,1));
eeggamma_new = eeggamma(ts>Int(i-1,8) & ts<Int(i,1));
eegtheta_new = eegtheta_new';
eeggamma_new = eeggamma_new';
eegtheta_new = Detrend_LFP(eegtheta_new);
eeggamma_new = Detrend_LFP(eeggamma_new);
eegtheta_new = eegtheta_new';
eeggamma_new = eeggamma_new';

data =
makedatafile(ts_new,eegtheta_new,eeggamma_new,lowpass1,highpass1,lowp
ass2,highpass2);

M(i) = modindex(data, 'n', 18);
MI(i) = M(i).MI;

end

MI(:,1) = [];
MI(isnan(MI)) = [];
MI = mean(MI);
M(1) = [];
avgM.MI = M(1).MI;
avgM.amp = M(1).amp;
avgM.NormAmp = M(1).NormAmp;
avgM.PhaseAxis = M(1).PhaseAxis;

for i = 2:(ntrials-1);

    avgM.MI=avgM.MI+M(i).MI;
    avgM.amp=avgM.amp+M(i).amp;
    avgM.NormAmp=avgM.NormAmp+M(i).NormAmp;

end

avgM.MI = avgM.MI / (ntrials-1);
avgM.amp = avgM.amp / (ntrials-1);
avgM.NormAmp = avgM.NormAmp / (ntrials-1);

%permnum = 100;
%for k = 1:permnum
    %shuffle_index_theta = randperm(length(eegtheta));
    %shuffled_theta = eegtheta(shuffle_index_theta);
    %shuffle_index_gamma = randperm(length(eeggamma));
    %shuffled_gamma = eeggamma(shuffle_index_gamma);

```

```

%for i = 2:ntrials;
%ts_new = ts(ts>Int(i-1,8) & ts<Int(i,1));
%eegtheta_shuffled = shuffled_theta(ts>Int(i-1,8) & ts<Int(i,1));
%eeggamma_shuffled = shuffled_gamma(ts>Int(i-1,8) & ts<Int(i,1));
%eegtheta_shuffled = eegtheta_shuffled';
%eeggamma_shuffled = eeggamma_shuffled';
%eegtheta_shuffled = Detrend_LFP(eegtheta_shuffled);
%eeggamma_shuffled = Detrend_LFP(eeggamma_shuffled);
%eegtheta_shuffled = eegtheta_shuffled';
%eeggamma_shuffled = eeggamma_shuffled';

%data_shuffled =
makedatafile(ts_new,eegtheta_shuffled,eeggamma_shuffled,lowpass1,high
pass1,lowpass2,highpass2);

%M_shuffled(i) = modindex(data_shuffled,'n',18);

%end

%M_shuffled(1) = [];
%avgM_shuffled.MI = M_shuffled(1).MI;

%for i = 2:(ntrials-1);

%avgM_shuffled.MI=avgM_shuffled.MI+M_shuffled(i).MI;

%end

%avgM_shuffled.MI = avgM_shuffled.MI / (ntrials-1);

%MI_shuffled(k) = avgM_shuffled.MI;

%mu = mean(MI_shuffled);
%sigma = std(MI_shuffled);
%ZMI_Shuffled = zscore(MI_shuffled);
%MI_Z = bsxfun(@rdivide, bsxfun(@minus, avgM.MI, mu), sigma);

%[h p] = ztest(avgM.MI,mu,sigma);

%subplot(211)

```

```

phase=[avgM.PhaseAxis 360+avgM.PhaseAxis];
amp=[avgM.NormAmp avgM.NormAmp];
bar(phase,amp,'BarWidth',1);
xlim([0 720])

%subplot(212)

%hist(ZMI_Shuffled,18)
%hold on
%yL = get(gca,'YLim');
%line([MI_Z MI_Z],yL,'Color','r');

elseif Type == 2

for i = 2:ntrials;
    ts_new = ts(ts>Int(i,1) & ts<Int(i,5));
    eegtheta_new = eegtheta(ts>Int(i,1) & ts<Int(i,5));
    eeggamma_new = eeggamma(ts>Int(i,1) & ts<Int(i,5));
    eegtheta_new = eegtheta_new';
    eeggamma_new = eeggamma_new';
    eegtheta_new = Detrend_LFP(eegtheta_new);
    eeggamma_new = Detrend_LFP(eeggamma_new);
    eegtheta_new = eegtheta_new';
    eeggamma_new = eeggamma_new';

    data =
makedatafile(ts_new,eegtheta_new,eeggamma_new,lowpass1,highpass1,lowp
ass2,highpass2);

    M(i) = modindex(data,'n',18);
    MI(i) = M(i).MI;

end

MI(:,1) = [];
MI(isnan(MI)) = [];
MI = mean(MI);
M(1) = [];
avgM.MI = M(1).MI;
avgM.amp = M(1).amp;
avgM.NormAmp = M(1).NormAmp;
avgM.PhaseAxis = M(1).PhaseAxis;

for i = 2:(ntrials-1);

```

```

    avgM.MI=avgM.MI+M(i).MI;
    avgM.amp=avgM.amp+M(i).amp;
    avgM.NormAmp=avgM.NormAmp+M(i).NormAmp;

end

avgM.MI = avgM.MI / (ntrials-1);
avgM.amp = avgM.amp / (ntrials-1);
avgM.NormAmp = avgM.NormAmp / (ntrials-1);

%permnum = 100;
%for k = 1:permnum
    %shuffle_index_theta = randperm(length(eegtheta));
    %shuffled_theta = eegtheta(shuffle_index_theta);
    %shuffle_index_gamma = randperm(length(eeggamma));
    %shuffled_gamma = eeggamma(shuffle_index_gamma);

    %for i = 2:ntrials;
    %ts_new = ts(ts>Int(i,1) & ts<Int(i,5));
    %eegtheta_shuffled = shuffled_theta(ts>Int(i,1) & ts<Int(i,5));
    %eeggamma_shuffled = shuffled_gamma(ts>Int(i,1) & ts<Int(i,5));
    %eegtheta_shuffled = eegtheta_shuffled';
    %eeggamma_shuffled = eeggamma_shuffled';
    %eegtheta_shuffled = Detrend_LFP(eegtheta_shuffled);
    %eeggamma_shuffled = Detrend_LFP(eeggamma_shuffled);
    %eegtheta_shuffled = eegtheta_shuffled';
    %eeggamma_shuffled = eeggamma_shuffled';

    %data_shuffled =
    makedatafile(ts_new,eegtheta_shuffled,eeggamma_shuffled,lowpass1,high
    pass1,lowpass2,highpass2);

    %M_shuffled(i) = modindex(data_shuffled,'n',18);

    %end

%M_shuffled(1) = [];
%avgM_shuffled.MI = M_shuffled(1).MI;

%for i = 2:(ntrials-1);

    %avgM_shuffled.MI=avgM_shuffled.MI+M_shuffled(i).MI;

%end

```

```

%avgM_shuffled.MI = avgM_shuffled.MI / (ntrials-1);

%MI_shuffled(k) = avgM_shuffled.MI;

%mu = mean(MI_shuffled);
%sigma = std(MI_shuffled);
%ZMI_Shuffled = zscore(MI_shuffled);
%MI_Z = bsxfun(@divide, bsxfun(@minus, avgM.MI, mu), sigma);

%[h p] = ztest(avgM.MI,mu,sigma);

%subplot(211)

phase=[avgM.PhaseAxis 360+avgM.PhaseAxis];
amp=[avgM.NormAmp avgM.NormAmp];
bar(phase,amp, 'BarWidth',1);
xlim([0 720])

%subplot(212)

%hist(ZMI_Shuffled,18)
%hold on
%yL = get(gca,'YLim');
%line([MI_Z MI_Z],yL,'Color','r');

elseif Type == 3

    for i = 2:ntrials;
        ts_new = ts(ts>Int(i,5) & ts<Int(i,6));
        eegtheta_new = eegtheta(ts>Int(i,5) & ts<Int(i,6));
        eeggamma_new = eeggamma(ts>Int(i,5) & ts<Int(i,6));
        eegtheta_new = eegtheta_new';
        eeggamma_new = eeggamma_new';
        eegtheta_new = Detrend_LFP(eegtheta_new);
        eeggamma_new = Detrend_LFP(eeggamma_new);
        eegtheta_new = eegtheta_new';
        eeggamma_new = eeggamma_new';

        data =
        makedatafile(ts_new,eegtheta_new,eeggamma_new,lowpass1,highpass1,lowpass2,highpass2);

```

```

M(i) = modindex(data, 'n', 18);
MI(i) = M(i).MI;

end

MI(:,1) = [];
MI(isnan(MI)) = [];
MI = mean(MI);
M(1) = [];
avgM.MI = M(1).MI;
avgM.amp = M(1).amp;
avgM.NormAmp = M(1).NormAmp;
avgM.PhaseAxis = M(1).PhaseAxis;

for i = 2:(ntrials-1);

    avgM.MI=avgM.MI+M(i).MI;
    avgM.amp=avgM.amp+M(i).amp;
    avgM.NormAmp=avgM.NormAmp+M(i).NormAmp;

end

avgM.MI = avgM.MI / (ntrials-1);
avgM.amp = avgM.amp / (ntrials-1);
avgM.NormAmp = avgM.NormAmp / (ntrials-1);

end

%permnum = 100;
%for k = 1:permnum
    %shuffle_index_theta = randperm(length(eegtheta));
    %shuffled_theta = eegtheta(shuffle_index_theta);
    %shuffle_index_gamma = randperm(length(eeggamma));
    %shuffled_gamma = eeggamma(shuffle_index_gamma);

    %for i = 2:ntrials;
    %ts_new = ts(ts>Int(i,5) & ts<Int(i,6));
    %eegtheta_shuffled = shuffled_theta(ts>Int(i,5) & ts<Int(i,6));
    %eeggamma_shuffled = shuffled_gamma(ts>Int(i,5) & ts<Int(i,6));
    %eegtheta_shuffled = eegtheta_shuffled';
    %eeggamma_shuffled = eeggamma_shuffled';
    %eegtheta_shuffled = Detrend_LFP(eegtheta_shuffled);
    %eeggamma_shuffled = Detrend_LFP(eeggamma_shuffled);
    %eegtheta_shuffled = eegtheta_shuffled';

```

```

    %eeggamma_shuffled = eeggamma_shuffled';

    %data_shuffled =
    makedatafile(ts_new,eegtheta_shuffled,eeggamma_shuffled,lowpass1,high
    pass1,lowpass2,highpass2);

    %M_shuffled(i) = modindex(data_shuffled,'n',18);

    %end

%M_shuffled(1) = [];
%avgM_shuffled.MI = M_shuffled(1).MI;

%for i = 2:(ntrials-1);

    %avgM_shuffled.MI=avgM_shuffled.MI+M_shuffled(i).MI;

%end

%avgM_shuffled.MI = avgM_shuffled.MI / (ntrials-1);

%MI_shuffled(k) = avgM_shuffled.MI;

%mu = mean(MI_shuffled);
%sigma = std(MI_shuffled);
%ZMI_Shuffled = zscore(MI_shuffled);
%MI_Z = bsxfun(@rdivide, bsxfun(@minus, avgM.MI, mu), sigma);

%[h p] = ztest(avgM.MI,mu,sigma);

%subplot(211)

phase=[avgM.PhaseAxis 360+avgM.PhaseAxis];
amp=[avgM.NormAmp avgM.NormAmp];
bar(phase,amp,'BarWidth',1);
xlim([0 720])

%subplot(212)

```

```

%hist(ZMI_Shuffled,18)
%hold on
%yL = get(gca,'YLim');
%line([MI_Z MI_Z],yL,'Color','r');

```

```
end
```

A11: makedatafile_morlet.m (used to extract phase and power information for comodulograms)

```

function [data] =
makedatafile_morlet(timestamps,eeg1,eeg2,lowpass1,highpass1,lowpass2,
highpass2)
%UNTITLED2 Summary of this function goes here
% Detailed explanation goes here

data.FS = 2034;
data.ADChannel = 64;

ts = timestamps;

data.T = ts;
data.X = eeg1;

phase = [lowpass1 highpass1];
power = [lowpass2 highpass2];

phase_frequency = mean(phase);
power_frequency = mean(power);

time = -1:1/2034:1;
s_phase = 4/(2*pi*phase_frequency)^2;
s_power = 4/(2*pi*power_frequency)^2;
wavelet_phase = exp(2*1i*pi*phase_frequency.*time) .* exp(-
time.^2./(2*s_phase)/phase_frequency);
wavelet_power = exp(2*1i*pi*power_frequency.*time) .* exp(-
time.^2./(2*s_power)/power_frequency);

n_wavelet = length(wavelet_phase);
n_data = length(eeg1);

```

```

n_convolution      = n_wavelet+n_data-1;
half_of_wavelet_size = (length(wavelet_phase)-1)/2;

fft_wavelet_phase = fft(wavelet_phase,n_convolution);
fft_wavelet_power = fft(wavelet_power,n_convolution);
fft_theta        = fft(eeg1,n_convolution);
fft_gamma        = fft(eeg2,n_convolution);

convolution_result_fft_phase =
ifft(fft_wavelet_phase.*fft_theta,n_convolution) * sqrt(s_phase);
convolution_result_fft_power =
ifft(fft_wavelet_power.*fft_gamma,n_convolution) * sqrt(s_power);

convolution_result_fft_phase =
convolution_result_fft_phase(half_of_wavelet_size+1:end-
half_of_wavelet_size);
convolution_result_fft_power =
convolution_result_fft_power(half_of_wavelet_size+1:end-
half_of_wavelet_size);

data.Xt = real(convolution_result_fft_phase);
data.Xg = real(convolution_result_fft_power);

data.Xt_hil = hilbert(data.Xt);
data.Xg_hil = hilbert(data.Xg);

data.Xt_env = abs(convolution_result_fft_phase);
data.Xg_env = abs(convolution_result_fft_power);

data.Xt_phase = angle(convolution_result_fft_phase)*(180/pi)+180;
mPFC_phases = angle(convolution_result_fft_power)*(180/pi)+180;

data.Xt_freq = diff(data.Xt_phase)./diff(data.T);
data.Xg_freq = diff(mPFC_phases)./diff(data.T);

end

```

A12: stem_binner.m

```
%% Stem_Binner.m
% hlh 030415

function [IntStem] =
stem_binner(ExtractedX,ExtractedY,TimeStamps,numbins,xmin,xmax,ymin,y
max)

%This function finds boundaries for equally spaced bins along the
maze stem
%(size = numbins), and creates a modified "Int" variable containing
%timestamp values for occupancy of each bin during each trial

%Input arguments:
% -ExtractedX: Session x-coordinates (extracted from "VT1.mat")
% -ExtractedY: Session y-coordinates (extracted from "VT1.mat")
% -TimeStamps: Session timestamp values (extracted from "VT1.mat")
% -numbins: Number of desired bins (1x1 scalar)
% -xmin: X-coordinate equivalent to stem entrance
% -xmax: X-coordinate equivalent to stem exit
% -ymin: Y-coordinate equivalent to leftmost boundary of stem
% -ymax: Y-coordinate equivalent to rightmost boundary of stem
% (Note: xmin,xmax,ymin,ymax are variable for now, but can be
hardcoded
% into the function later if desired)

% Make sure that ymin,ymax values are generous and include all of
the
% maze stem. Make sure that xmin,xmax values are conservative and
include
% only portions of the maze stem where left/right turn trajectories
were
% overlapping.

%Output arguments:
% -IntStem: nTrials x numbins matrix of timestamp values
(IntStem(:,1) =
% stem entry, IntStem(:,size(IntStem,2)) = stem exit)

Bins = linspace(xmin,xmax,numbins);
Bins = round(Bins);

IntStem = [];
tolerance = 1000;
```

```

Y_ind = find(ExtractedY>ymin & ExtractedY<ymax);

for j = 1:length(Bins)
    X_ind = find(ExtractedX>(Bins(1,j))-20 &
ExtractedX<(Bins(1,j))+20);
    stem_ind = intersect(X_ind,Y_ind);
    mask = true(size(stem_ind));
    last = 1;
    for i = 2:length(stem_ind)
        if (abs(stem_ind(i)-stem_ind(last))<tolerance)
            mask(i) = false;
        else
            last = i;
        end
    end
    stem_temp = stem_ind(mask);
    stem_temp = TimeStamps(stem_temp);
    stem_temp = stem_temp';
    IntStem(:,j) = stem_temp;
end

end

```

A13: bin_my_data.m

```

function [Coherence,MI,Power] =
bin_my_data(IntStem,HippocampalLFP,PrefrontalLFP,TimeStamps,srate)
%UNTITLED4 Summary of this function goes here
% Detailed explanation goes here

EEG1 = HippocampalLFP(:);
EEG2 = PrefrontalLFP(:);
TimeStamps = linspace(TimeStamps(1,1),TimeStamps(1,end),
length(EEG1));

params.tapers = [5 9];
params.pad = 0;
params.Fs = srate;
params.fpass = [0 100];
params.err = [2 .05];
params.trialave = 0;

[EEG1] = cleaningscript(EEG1, params);

```

```

[EEG2] = cleaningscript(EEG2, params);

ntrials = size(IntStem,1);

lowpass1 = 6;
highpass1 = 11;
lowpass2 = 30;
highpass2 = 80;

for i = 2:ntrials
    for j = 1:(size(IntStem,2))-1
        Timestamps_new = Timestamps(Timestamps>IntStem(i,j) &
Timestamps<IntStem(i,j+1));
        EEG1_new = EEG1(Timestamps>IntStem(i,j) &
Timestamps<IntStem(i,j+1));
        EEG2_new = EEG2(Timestamps>IntStem(i,j) &
Timestamps<IntStem(i,j+1));
        EEG1_new = EEG1_new';
        EEG2_new = EEG2_new';
        EEG1_new = Detrend_LFP(EEG1_new);
        EEG2_new = Detrend_LFP(EEG2_new);
        EEG1_new = EEG1_new';
        EEG2_new = EEG2_new';

        params.fpass = [0 4];

[C,phi,S12,S1,S2,f,confC,phistd,Cerr]=coherencyc(EEG1_new,EEG2_new,pa
rams);
        C_Delta(i-1) = mean(C);

        params.fpass = [4 12];

[C,phi,S12,S1,S2,f,confC,phistd,Cerr]=coherencyc(EEG1_new,EEG2_new,pa
rams);
        C_Theta(i-1) = mean(C);

        params.fpass = [15 30];

[C,phi,S12,S1,S2,f,confC,phistd,Cerr]=coherencyc(EEG1_new,EEG2_new,pa
rams);
        C_Beta(i-1) = mean(C);

        params.fpass = [30 80];

```

```

[C,phi,S12,S1,S2,f,confC,phistd,Cerr]=coherencyc(EEG1_new,EEG2_new,pa
rams);
    C_Gamma(i-1) = mean(C);

    muDelta(:,j) = mean(C_Delta);
    muTheta(:,j) = mean(C_Theta);
    muBeta(:,j) = mean(C_Beta);
    muGamma(:,j) = mean(C_Gamma);
end
end

Coherence.Delta = muDelta;
Coherence.Theta = muTheta;
Coherence.Beta = muBeta;
Coherence.Gamma = muGamma;

for i = 2:ntrials;
    for j = 1:(size(IntStem,2))-1
        ts_new = Timestamps(Timestamps>IntStem(i,j) &
Timestamps<IntStem(i,j+1));
        eegtheta_new = EEG1(Timestamps>IntStem(i,j) &
Timestamps<IntStem(i,j+1));
        eeggamma_new = EEG2(Timestamps>IntStem(i,j) &
Timestamps<IntStem(i,j+1));
        eegtheta_new = eegtheta_new';
        eeggamma_new = eeggamma_new';
        eegtheta_new = Detrend_LFP(eegtheta_new);
        eeggamma_new = Detrend_LFP(eeggamma_new);
        eegtheta_new = eegtheta_new';
        eeggamma_new = eeggamma_new';

        data =
makedatafile(ts_new,eegtheta_new,eeggamma_new,lowpass1,highpass1,lowp
ass2,highpass2);

        M(i,j) = modindex(data,'n',18);
        MI(i,j) = M(i,j).MI;
    end
end

MI(1,:) = [];
MI = mean(MI,1);

for i = 2:ntrials

```

```

    for j = 1:(size(IntStem,2))-1
        Timestamps_new = Timestamps(Timestamps>IntStem(i,j) &
Timestamps<IntStem(i,j+1));
        EEG1_new = EEG1(Timestamps>IntStem(i,j) &
Timestamps<IntStem(i,j+1));
        EEG2_new = EEG2(Timestamps>IntStem(i,j) &
Timestamps<IntStem(i,j+1));
        EEG1_new = EEG1_new';
        EEG2_new = EEG2_new';
        EEG1_new = Detrend_LFP(EEG1_new);
        EEG2_new = Detrend_LFP(EEG2_new);
        EEG1_new = EEG1_new';
        EEG2_new = EEG2_new';

        params.fpass = [0 4];
        [S_Hipp,f_Hipp,Serr_Hipp]=mtspectrumc(EEG1_new,params);
        [S_PFC,f_PFC,Serr_PFC]=mtspectrumc(EEG2_new,params);
        S_DeltaHipp(i-1) = mean(S_Hipp);
        S_DeltaPFC(i-1) = mean(S_PFC);

        params.fpass = [4 12];
        [S_Hipp,f_Hipp,Serr_Hipp]=mtspectrumc(EEG1_new,params);
        [S_PFC,f_PFC,Serr_PFC]=mtspectrumc(EEG2_new,params);
        S_ThetaHipp(i-1) = mean(S_Hipp);
        S_ThetaPFC(i-1) = mean(S_PFC);

        params.fpass = [15 30];
        [S_Hipp,f_Hipp,Serr_Hipp]=mtspectrumc(EEG1_new,params);
        [S_PFC,f_PFC,Serr_PFC]=mtspectrumc(EEG2_new,params);
        S_BetaHipp(i-1) = mean(S_Hipp);
        S_BetaPFC(i-1) = mean(S_PFC);

        params.fpass = [30 80];
        [S_Hipp,f_Hipp,Serr_Hipp]=mtspectrumc(EEG1_new,params);
        [S_PFC,f_PFC,Serr_PFC]=mtspectrumc(EEG2_new,params);
        S_GammaHipp(i-1) = mean(S_Hipp);
        S_GammaPFC(i-1) = mean(S_PFC);

        muDelta(1,j) = mean(S_DeltaHipp);
        muDelta(2,j) = mean(S_DeltaPFC);
        muTheta(1,j) = mean(S_ThetaHipp);
        muTheta(2,j) = mean(S_ThetaPFC);
        muBeta(1,j) = mean(S_BetaHipp);
        muBeta(2,j) = mean(S_BetaPFC);
        muGamma(1,j) = mean(S_GammaHipp);
        muGamma(2,j) = mean(S_GammaPFC);

```

Appendix B

INSTITUTIONAL ANIMAL CARE AND USE COMMITTEE APPROVAL FORM

University of Delaware
Institutional Animal Care and Use Committee
Annual Review

(Please complete below using Arial, size 12 Font.)



Title of Protocol: Electrophysiological correlates of spatial memory	
AUP Number: 1177-2009-1	← (4 digits only)
Principal Investigator: Amy Griffin	
Common Name: Long Evans Hooded Rats	
Genus Species: <i>Rattus norvegicus</i>	
Category Assigned: (please mark one) <input type="checkbox"/> A. None to slight or momentary pain or distress <input checked="" type="checkbox"/> B. Pain or distress will be alleviated by drugs or other means <input type="checkbox"/> C. Pain or distress will not be alleviated	
Official Use Only	
IACUC Approval Signature: <u>Steven D. Bran</u>	
Date of Approval: <u>Nov. 10, 2009</u>	